Analysis of Synchronization and Accuracy of Synchrophasor Measurements

by

Qing Zhang

A Dissertation Presented in Partial Fulfillment
of the Requirements for the Degree
Doctor of Philosophy

Approved AUGUST 2012 by the
Graduate Supervisory Committee:

Gerald Heydt, Co-chair
Vijay Vittal, Co-chair
Raja Ayyanar
Jennie Si

ARIZONA STATE UNIVERSITY

December 2012

ABSTRACT

In electric power systems, phasor measurement units (PMUs) are capable of providing synchronized voltage and current phasor measurements which are superior to conventional measurements collected by the supervisory control and data acquisition (SCADA) system in terms of resolution and accuracy. These measurements are known as synchrophasor measurements. Considerable research work has been done on the applications of PMU measurements based on the assumption that a high level of accuracy is obtained in the field. The study in this dissertation is conducted to address the basic issue concerning the accuracy of actual PMU measurements in the field.

Synchronization is one of the important features of PMU measurements. However, the study presented in this dissertation reveals that the problem of faulty synchronization between measurements with the same time stamps from different PMUs exists. A Kalman filter model is proposed to analyze and calculate the time skew error caused by faulty synchronization.

In order to achieve a high level of accuracy of PMU measurements, innovative methods are proposed to detect and identify system state changes or bad data which are reflected by changes in the measurements. This procedure is applied as a key step in adaptive Kalman filtering of PMU measurements to overcome the insensitivity of a conventional Kalman filter.

Calibration of PMU measurements is implemented in specific PMU installation scenarios using transmission line (TL) parameters from operation planning data. The voltage and current correction factors calculated from the calibration

procedure indicate the possible errors in PMU measurements. Correction factors can be applied in on-line calibration of PMU measurements.

A study is conducted to address an important issue when integrating PMU measurements into state estimation. The reporting rate of PMU measurements is much higher than that of the measurements collected by the SCADA. The question of how to buffer PMU measurements is raised. The impact of PMU measurement buffer length on state estimation is discussed. A method based on hypothesis testing is proposed to determine the optimal buffer length of PMU measurements considering the two conflicting features of PMU measurements, i. e. uncertainty and variability. Results are presented for actual PMU synchrophasor measurements.

DEDICATION

This dissertation is dedicated to my parents for their endless love and support through all these years.

ACKNOWLEDGMENTS

Firstly, I would like to express my grateful thanks to my advisors, Dr. Gerald Heydt and Dr. Vijay Vittal for their guidance, patience and encouragement throughout this work. Their expertise and insight have been influential in performing this research work. I am grateful to Dr. Raja Ayyanar and Dr. Jennie Si for serving as my committee members.

I would also like to express my gratitude to the Salt River Project (SRP) for providing me an opportunity to perform this research work. My specific thanks go to Dr. Naim Logic and Mr. Steve Sturgill for their valuable suggestions and comments.

I would like to thank Dr. Yacine Chakhchoukh for his valuable comments and suggestions.

Furthermore, I would like to express my special thanks to Dr. Chen Chen, my advisor in Shanghai Jiao Tong University, for her encouragements and support of my study abroad.

Last but not least, I would like to thank all my friends in the area of electric power and energy systems for their support when I needed it the most.

TABLE OF CONTENTS

Page

CHAPTER Page

CHAPTER Page

LIST OF TABLES

Table Page

Table Page

LIST OF FIGURES

Figure Page

Figure Page

Figure Page

NOMENCLATURE

A_{af}	Angle difference across a TL based on calibrated PMU measurements
A_{bf}	Angle difference across a TL based on raw PMU measurements
A_i	A Boolean number to record the change observed from PMU measurements
a_{ij}	Coefficient of the voltage phase angle change at one end of a branch
$Angle(\cdot)$	Calculation of phase angle of a complex number
A_{win}	Angle difference across a TL when using CFs from the previous time window to calibrate PMU measurements
B	Shunt susceptance of a transmission line
B	The susceptance matrix
b_{ij}	Coefficient of the voltage phase angle change at the other end of a branch
B_{sub}	Partial of the susceptance matrix
C	Covariance matrix
CF	Correction factor
C_{ii}	The i^{th} diagonal element of C
c_{ij}	Coefficient of the voltage magnitude change at one end of a branch
CT	Current transformer
d_{ij}	Coefficient of the voltage magnitude change at the other end of a branch
e	The measurement error vector
GPS	Global positioning system
H_0	The null hypothesis
H_1	The alternative hypothesis
h_i	Testing results of hypothesis testing

H_k	Observation matrix
I_{B1}	Current through shunt susceptance of a transmission line
I_{B2}	Current through shunt susceptance of a transmission line
I_{From}	Ideal PMU current measurement at one end of a transmission line
I_{From_M}	Raw PMU current measurement at one end of a transmission line
I_{line}	Current through serial impedance of a transmission line
$Im(\cdot)$	Calculation of imaginary part a complex number
I_{To}	Ideal PMU current measurement at the other end of a transmission line
I_{To_M}	Raw PMU current measurement at the other end of a transmission line
J	Jacobian matrix
l	The length of a transmission line
M	Ideal PMU measurement vector
$Mag(\cdot)$	Calculation of magnitude of a complex number
M_{raw}	Raw PMU measurement vector
n_{bfl}	The buffer length obtained in the second step of hypothesis testing procedure
N_{bl}	The length of a memory buffer
n_{br}	The number of branches in a network
n_{HT}	The number of measurements considered in hypothesis testing
n_{bus}	The number of buses in a network
N_{meas}	The total number of PMU measurements in processing
n_{non}	The number of non-zero injection buses
N_{op_bl}	Optimal buffer length of PMU measurements for state estimation

n_{PMU}	The number of PMUs installed in a network
N_{rr}	Reporting rate of PMU measurements
N_{subset}	The number of the subsets with the length of N_{bl}
n_{subset}	The number of subsets in hypothesis testing
P_{From}	Brach active power flow measured at the 'From' end
P_{ij}	DC active power on the TL connecting bus *i* and *j*
P_k	Error covariance matrix in Kalman filter
P_{mis}	Active power mismatch
PMU	Phasor measurement unit
PPS	Pulse per second
PT	Potential transformer
PTDF	Power transfer distribution factor
P_{To}	Brach active power flow measured at the 'To' end
Q_{From}	Brach reactive power flow measured at the 'From' end
Q_k	Covariance matrix for v_k
Q_{mis}	Reactive power mismatch
Q_{To}	Brach reactive power flow measured at the 'To' end
R	An open-source software for statistical computing and graphics
R	Resistance of a transmission line
r	The residual vector
$r_{0.95}$	The value of r_{index} corresponding to the confidence level 0.95 in the cumulative distribution curve
$Re(\cdot)$	Calculation of real part of a complex number

r_{index}	The Euclidean norm of r
R_k	Covariance matrix for w_k
RTU	Remote terminal unit
SCADA	Supervisory control and data acquisition
t_{HT}	The time duration of PMU measurements considered in hypothesis testing
T_{I_From}	Correction factor for I_{From_M}
T_{I_To}	Correction factor for I_{To_M}
T_{inv}	Vector of inverse of correction factor
TL	Transmission line
TS_{err}	Time skew error
T_{V_From}	Correction factor for V_{From_M}
T_{V_To}	Correction factor for V_{To_M}
TVE	Total vector error
V_1	Voltage measurement from one of the two PMUs installed at the same bus
V_2	Voltage measurement from another one of the two PMUs installed at the same bus
V_{a12}	Relative voltage angle based on measurements from two PMUs
V_{From}	Ideal PMU voltage measurement at one end of a transmission line
V_{From_M}	Raw PMU voltage measurement at one end of a transmission line
v_i	Voltage magnitude at bus i
V_i	Voltage phasor at bus i
V_j	Voltage phasor at bus j
v_k	The measurement noise

V_{To}	Ideal PMU voltage measurement at the other end of a transmission line
V_{To_M}	Raw PMU voltage measurement at the other end of a transmission line
w_k	The process noise
WLS	Weighted least square
X	Phasor
X	Reactance of a transmission line
X	The state vector in a sate estimation
X_i	Imaginary part of a phasor
x_{ind}	The normalized Euclidean norm of the estimation error
x_{ind_a}	x_{ind} evaluated on the voltage angles
x_{ind_m}	x_{ind} evaluated on the voltage magnitudes
$X_i(n)$	Measured value of imaginary part of a phasor
x_{ik}	The reactance of the TL connecting bus i and k
x_k	State vector
X_m	Amplitude of a sinusoidal quantity
X_r	Real part of a phasor
$X_r(n)$	Measured value of real part of a phasor
Y_{ij}	The admittance of the TL connecting bus i and j
y_{ij}	The magnitude of Y_{ij}
y	The shunt admittance per unit length
Y	The total admittance of a transmission line
Y'	The lumped shunt admittance in the long line model

Z	Impedance of a transmission line
Z	The measurement vector in a state estimation
Z_c	The characteristic impedance
$Z(1)…Z(n_{subset})$	Subsets of PMU measurements
z	The series impedance per unit length
z_k	The measurement vector
Z'	The lumped series impedance in the long line model
γ	The propagation constant
δ_i	Voltage phase angle at bus i
δ_j	Voltage phase angle at bus j
ΔP	The increment vector of active power injections
$\Delta P'_{ij}$	Equivalent branch active power change
$\Delta P_{ij,k}$	The change of active power on branch ij due to the change of active power injection at bus k
ΔP_k	The change of active power injection at bus k
ΔT_1	Time duration that elapses for an accurate clock when a time stamp is generated
ΔT_2	Time duration that elapses for an inaccurate clock when a time stamp is generated
$\Delta\delta$	The increment vector of bus voltage phase angles
$\Delta\delta'_{ij}$	Equivalent phase angle difference change across the transmission line
$\Delta\theta$(k)	Voltage angle change indicated by two subsequent measurements from one PMU
ε	Time duration error
$\eta_{l,k}$	The variation of the active power on the lth branch with respect to the power injection at bus k
θ_{ij}	The phase angle of Y_{ij}

θ_{PMU}	The relative voltage angles with respect to measurements from the reference PMU
μ_x	The mean of a series of samples
$\hat{\mu}_z$	The estimation ofμ_x
σ	Standard deviation
ϕ	Phase
ϕ_k	The state transition matrix in a Kalman filter
ω	Angular frequency
$\hat{x}$	An estimated vector

Chapter 1

PHASOR MEASUREMENT UNITS IN ELECTRIC POWER SYSTEMS

1.1 Introduction

Phasor measurement units (PMUs) have been widely installed in power systems in recent years. In many references, the accuracy of PMU measurements is assumed to be higher than that of conventional measurements, such as power injections via current and potential transformers, voltage magnitude measurements, current magnitude measurements, and branch power flows collected by the supervisory control and data acquisition (SCADA) system. One of the important features of PMU measurements is the synchronization indicated by the time stamps. The global positioning system (GPS) provides the one pulse per second (1 PPS) signal which is used for the same time sampling at different locations. The precision of the 1 PPS signal is within 1 microsecond. IEEE Std. C37.118 [1] lays the ground work to standardize the measurements from different vendors. Reference [2] introduces the revised version of the standard, and highlights the differences between the old and new requirements. PMUs have the capability to provide three phase detail (including their symmetrical components) down to a time resolution of 1/60 second in a 60 Hz system.

The accuracy of a synchrophasor is measured by the total vector error (TVE). A pure sinusoidal quantity is given by the following equation,

$$x(t) = X_m \cos(\omega t + \phi) \tag{1-1}$$

The sinusoid is commonly represented in terms of its root mean square values by a complex phasor,

$$X = X_r + jX_i = \frac{X_m}{\sqrt{2}} e^{j\phi} \tag{1-2}$$

where ϕ depends on the time starting point. The definition of TVE [1] is given by

$$TVE = \sqrt{\frac{(X_r(n) - X_r)^2 + (X_i(n) - X_i)^2}{X_r^2 + X_i^2}} \tag{1-3}$$

where $X_r(n)$ and $X_i(n)$ are the measured values from the measuring device, and X_r and X_i are the theoretical values of the input signal.

There are few references in the literature that address the issue of accuracy of *actual* PMU measurements: many research results are based on simulation with the assumption that PMU measurements are very accurate. The TVE is helpful in evaluating the performance of a PMU, but it is only available under a calibration and test environment. Under practical operating conditions, power system states are desired by control centers in order to capture the system conditions and ensure the security and reliability of the system. As a result, it is meaningful to evaluate the accuracy of raw, actual PMU measurements, identify the discrepancies, and propose correction methods.

In the mean time, some new issues are raised when integrating PMU measurements into practical applications. Due to the different reporting rates of PMU measurements and SCADA data, one important issue of how to determine the optimal buffer length of PMU measurements is addressed in this dissertation when integrating PMU measurements into state estimation.

1.2 Literature review

Considerable research has been done to address the issue of how to utilize the PMU measurements for improved monitoring, protection and control of power systems. A brief introduction of applications of synchronized phasor measurements in power systems is provided in [3]. In this subsection, a literature review of applications of PMU measurements in power systems is presented. The discussion is partitioned into four categories: a) state estimation, b) angle stability, c) voltage stability, and d) other applications.

a) State estimation

State estimation is a key function in the energy management system for the secure operation of power systems. It is commonly formulated as a weighted least square (WLS) problem to obtain the best estimate of system states based on a set of measurements [4]. The conventional measurements obtained from the SCADA system for the state estimator include branch flows, power injections and voltage and current magnitudes. Since the formulated functions for state estimation are nonlinear, linearization of the functions are used, and the WLS problem is solved by an iterative scheme. PMUs provide voltage and current phasors directly. If the observability and redundancy requirements are met by installing a sufficient number of PMUs to provide phasor measurements, it is possible to implement a linear state estimation. A two-level linear state estimator is presented in [5][6]. A state estimator exclusively based on PMU measurements can be applied in portions of practical systems when the requirements of observability and re-

dundancy are met for specific portions of the whole system. A practical example is provided in [7].

There are many issues regarding integration of PMU measurements into state estimation [8]. One of the important issues deals with optimal placement of PMUs to minimize the number of PMUs and maximize the measurement redundancy simultaneously. References on PMU placement problem include [9]-[14]. The reliability problem is also discussed under conditions including loss or failure of PMUs as well as line or transformer outages in [9]-[13].

Even though the availability of PMU measurements has gradually increased, the number of PMUs in practical systems is still not sufficient to implement a linear state estimator. As a result, a hybrid state estimator with conventional and PMU measurements as the inputs is an efficient approach to using PMU measurements, and is the necessary transition step to a complete linear state estimator. In [15], an alternative method is proposed to use PMU measurements as a post-processing step after traditional state estimation. A constrained formulation for hybrid state estimation is presented in [16] to improve the accuracy of state estimation. Inclusion of PMU current phasor measurements in a state estimator is presented in [17]. Bad data detection and network parameter error identification in state estimation with PMU measurements is discussed in [18] and [19] respectively. The effect of PMU measurements on the choice of the reference bus in state estimation is presented in [20]. A distributed state estimator using synchronized phasor measurements is presented in [21]-[22] where PMU measurements are applied to aggregate the results from subsystem state estimation.

b) Angle stability

As more PMUs are installed in power systems, real-time measurements become available for on-line dynamic monitoring. As an example, on-line monitoring of rotor angle stability based on PMU measurements is presented in [23]. The rotor angle and speed of synchronous generators are the most important variables for real-time monitoring and controlling transient stability. These two measurements are essential in developing a controller to enhance system stability and reliability. The extended Kalman filter is a Kalman filter that accommodates nonlinear models and plants, and may be applied to estimate the rotor angle and speed of a synchronous machine based on PMU measurements [24]. The unscented Kalman filter [25] which is a straightforward extension of the unscented transformation to recursive estimation is able to overcome the drawbacks of the extended Kalman filter, and this configuration is applied in [26]. PMU measurements are also used to construct simplified interarea models of large power systems for wide-area analysis and control [27].

Reference [28] presents a theoretical basis and signal-processing approach for electromechanical mode estimation using PMU measurements. A PMU data based method is proposed for online estimation of power system electromechanical modes in [29]. Empirical mode decomposition based on masking signal approach is applied to effectively handle the mode mixing problem with the help of real-time signals provided by PMUs [30].

In [31], PMU measurements are used to trigger one-shot control in response to loss of synchronism detection. An adaptive phasor power oscillation

damping controller is proposed using the time stamps of PMU measurements to compensate for time-varying latency [32]. A new nonlinear control of flexible ac transmission systems controllers with inputs including PMU measurements to damp interarea oscillations is introduced in [33].

c) Voltage stability

Real-time voltage instability risk indicators are required to solve voltage stability and security problems in power systems. A real-time voltage instability identification algorithm based on local phasor measurements is illustrated in [34]. The performance of the algorithm is evaluated by a detailed sensitivity analysis. Two wide-area voltage protection methods are presented in [35]. The Thévenin equivalent circuit seen by a specific high voltage bus is calculated in real-time to provide a voltage instability index in the first cited method. In the second method, an effective coordination among different voltage regulators according to their hierarchies is implemented. In [36], a new concept called a "coupled single-port circuit" is proposed to overcome the problems with impedance matching since power system loads are nonlinear and dynamic. A real-time voltage stability monitoring scheme is developed based on PMU measurements without estimating Thévenin parameters.

A method for quick estimation of the long-term voltage stability margin is developed based on an artificial neural network in [37]. The node voltage magnitudes and phase angles which can be provided by PMUs in real time are identified as the best predictors of voltage stability margin in that paper. An online voltage

security assessment scheme using PMU measurements and periodically updated decision trees to prevent voltage collapse after contingencies is presented in [38].

d) Other applications

The ultimate objectives of other applications of PMU measurements are to obtain improved stability and reliability of power systems. In this category, research work on applications of PMU measurements in model validation, line outage detection, fault detection and location, and power system protection are presented.

In [39], PMU measurements are used to validate models of fixed speed induction generator-based wind farms during frequency transients. In [40], three major tests were performed to validate system performance and modeling using measurements from wide-area measurement system. In [41], an algorithm is developed to detect a single line outage based on PMU measurements and pre-outage system topology information. Further research on detection of double line outages is presented in [42].

A series of research papers has been published on fault detection and fault location for transmission lines based on PMU measurements [43]-[47]. The basic principles and philosophy for wide-area protection schemes are described in [48]. A remote backup protection scheme is proposed for supervised zone-3 operation of distance relays [49]. The fault on a transmission line is detected from the residual vector of a synchrophasor state estimator. A wide area backup protection algorithm is proposed to identify the fault branch based on analyzing the fault steady state component of differential current in each protection correlation region

[50]. The protection correlation region is constructed based on network topology and placement of PMUs. An adaptive protection scheme based on PMU measurements for both transposed and untransposed parallel transmission lines is described in [51].

1.3 Motivation for the study

Synchronized PMU measurements are inherently superior to conventional measurements in terms of resolution and accuracy. This is the case since synchronized measurements can be used to obtain an accurate time synchronized snapshot of the system parameters and hence an accurate snapshot of state of the system. Asynchronous measurements do not afford the commonality of time, and the system parameters may be displaced in time thus creating an erroneous system state. Synchronization is an important feature of PMU measurements. However, most research that has been done on applications of PMU measurements in power systems is based on the assumption that the expected accuracy and synchronization is obtained in the field. In many cases, only simulated PMU measurements are used in test beds and in synthetic (i.e., computer simulated) studies. In order to achieve the expected goals to improve power system performance using PMU measurements, one basic issue that needs to be addressed is to assess the synchronization of these measurements and their accuracy.

PMUs can provide measurements at a reporting rate of up to 60 per second [1]. The reporting rate of PMUs is much higher than the conventional measurements from SCADA system. Signal processing technology can be applied to best condition PMU measurements for further applications. A Kalman filter [52] is

recommended to be used to remove noise from PMU measurements. One difficult issue that needs to be addressed is how to deal with the 'jumps' detected from PMU measurements. The 'jump' could be a bad datum or a real physical state change due to the complexity of power system operating conditions. Processing measurements from one PMU only would result in latency due to the insensitivity of a conventional Kalman filter. The correlations between measurements from different PMUs are helpful to determine the nature of the observed 'jump'. An adaptive Kalman filter could be developed with the 'jump' detection and identification strategy.

Due to the different reporting rates of conventional measurements and PMU measurements, one issue that needs to be addressed is how to perform state estimation using a combination of conventional and PMU measurements. The benefits that would be obtained by processing a buffer of PMU measurements instead of using a single PMU measurement need be carefully studied. Also the optimal buffer length of PMU measurements needs to be determined.

1.4 Dissertation organization

The main contents of this dissertation are partitioned into 8 chapters. The dissertation is structured as follows:

In Chapter 1, background, related literature review, and motivation for the study are presented.

In Chapter 2, a time skew problem is identified from actual PMU measurements tagged with the same time stamps. A Kalman filter model is proposed to compensate the time skew error.

In Chapter 3, a general idea of an adaptive Kalman filter is proposed to process PMU measurements which are a time series contaminated by noises. A question is raised about the 'jump' detection and identification between physical state changes and bad data.

In Chapter 4, a bad data detection and identification algorithm is proposed based on power transfer distribution factors (PTDFs). This method can be applied to a whole network or portion of a network when the requirements of redundancy of PMU measurements are satisfied. This method can be applied to provide trigger information in real-time processing of PMU measurements.

In Chapter 5, another bad data identification method based on specific PMU installation topology is proposed to perform sanity checks of accuracy of PMU measurements. This method can be applied in cases when the system state change identification process is unable to perform due to lack of redundancy of PMU measurements from the view of the whole network.

In Chapter 6, integration of measurements and planning TL parameters is applied to test the accuracy of raw PMU measurements. Large discrepancies are observed between the calculated TL parameters and planning TL parameters. A novel calibration method is proposed to match the PMU measurements and planning TL parameters. Correction factors are calculated which indicate the potential errors in current and voltage phasor measurements from PMUs.

In Chapter 7, a specific issue is studied when integrating PMU measurements into state estimation. A hybrid state estimation based on both conventional and PMU measurements is the choice before the ultimate transition to a linear

state estimation based on PMU measurements exclusively. Due to the different reporting rates of conventional and PMU measurements, research work is done to determine the optimal buffer length of PMU measurements to take full advantage of the information from PMU data.

Conclusions, contributions and suggestions for future work are presented in Chapter 8.

In Appendix A, the data sources of PMU measurements are provided. In Appendix B, a sample of Matlab codes is provided.

Chapter 2

THE TIME SKEW PROBLEM IN PMU MEASUREMENTS

2.1 Time skew in measured data

In this chapter, the faulty synchronization of PMU measurements is termed the '*time skew*' problem. The time skew problem is identified based on analysis of actual PMU measurements. Time skew exists between measurements from different PMUs even though they are tagged with the same time stamps. The origin of the time skew is due to the inaccuracy of the sampling clock associated with specific PMUs. As shown in Fig. 2.1, the two measurements from two different PMUs are tagged with the same timestamp, even though the two measurements are taken at different instants. This is just a simple illustration of the time skew problem. For practical PMUs in the field, they receive the 1 PPS signal from the GPS. A resynchronization of all sampling clocks is achieved every second due to the 1 PPS signal.

This time skew problem is identified, but solving this problem is not an easy task and might not be accomplished in a short term due to procedural constraints in the field. As a result, a method is presented to compensate the time skew error. Analysis shows that the time skew error for one specific PMU with time skew problem could be treated as a constant. Then during each one second interval, the time skew errors are compensated before PMU measurements are used in further applications. The recognition of the time skew problem is of great importance to applications of PMU measurements in power system monitoring, protection and control.

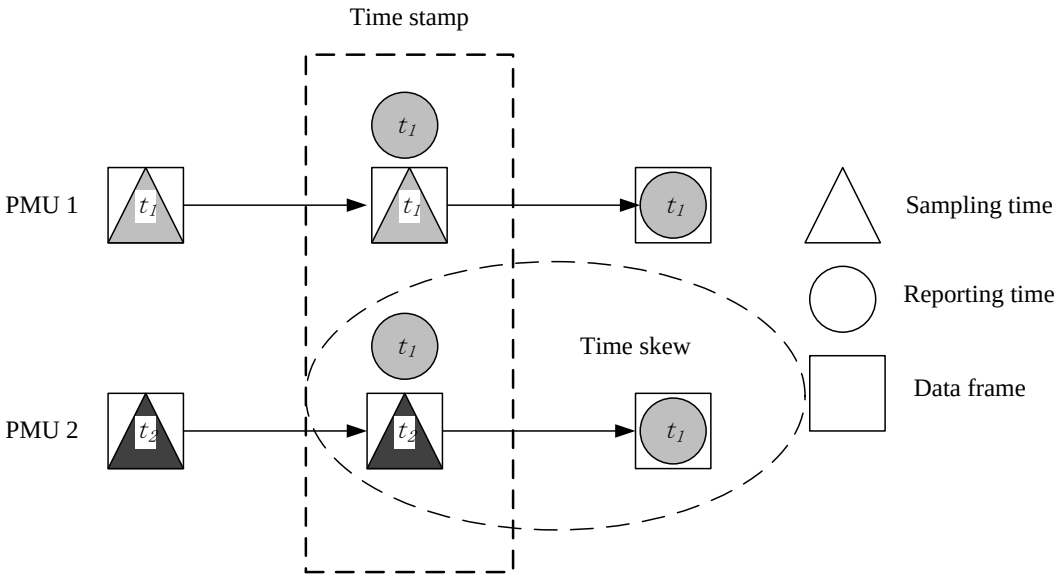

Fig. 2.1 Diagrammatic illustration of the time skew problem

2.2 Identification of the time skew problem

The existence of the time skew problem has long been recognized in traditional measurements collected by the SCADA system. Time synchronization is one of the most important features of the time-stamped PMU measurements. In this section, the identification of time skew between PMU measurements is presented.

In Fig. 2.2, the relative voltage phase angles calculated based on measurements from two actual PMUs which are installed at 230 kV buses are shown over a 3-minute period. One of the two PMUs is chosen as the reference. By observation, the relative voltage angle V_{a12} 'oscillates' in the range of (−1.5 −1.2) degrees. It is possible that the oscillation of V_{a12} is caused by the changing operating conditions in the practical system. This phenomenon is observed consistently over a long time period. Another possibility is that the 'oscillation' is an ab-

normal phenomenon. In the subsequent discussion, analysis is conducted to find out the reason for the observed oscillation.

The raw measurements from the reference PMU are shown by the curve in Fig. 2.3(a), and the raw measurements from the other PMU are shown by the curve in Fig. 2.3(b). The curve in Fig. 2.3(a) is relatively smooth, whereas 'jumps' are observed in the curve shown in Fig. 2.3(b). The jumps happen every second. Indeed, the analysis of the PMU signal in the frequency domain using the periodogram which is an estimate of the spectral density confirms this statement. The power spectral density is the discrete Fourier transform of the autocorrelation function of the signal and is estimated based on the periodogram smoothed using Daniell smoothers to obtain consistency [53]. This power spectral density estimate is convenient to detect the existing periodicities of the analyzed signal in the presence of short memory or uncorrelated noise. Detecting these periodicities is very important in order to remove them and obtain a stationary process. The spectral analysis is also helpful to model the state-space representation model used in the Kalman filtering and given in (2-13) and (2-14). Fig. 2.4 depicts the power spectral density estimate of the PMU obtained with the periodogram smoothed with Daniell smoothers and obtained using the statistical computing program R [54]. A peak is present at 1 Hz which corresponds to the 1 second periodicity.

All PMUs are receiving the 1 PPS from the GPS system, and sampling clocks are phase-locked to this time pulse. However, the sampling clocks might not be exactly synchronized during each one second interval due to the different

accuracy of the clocks, and time skew originates between measurements from different PMUs. In the following discussion, the origin of the time skew is analyzed and a method to compensate the time skew error is also presented.

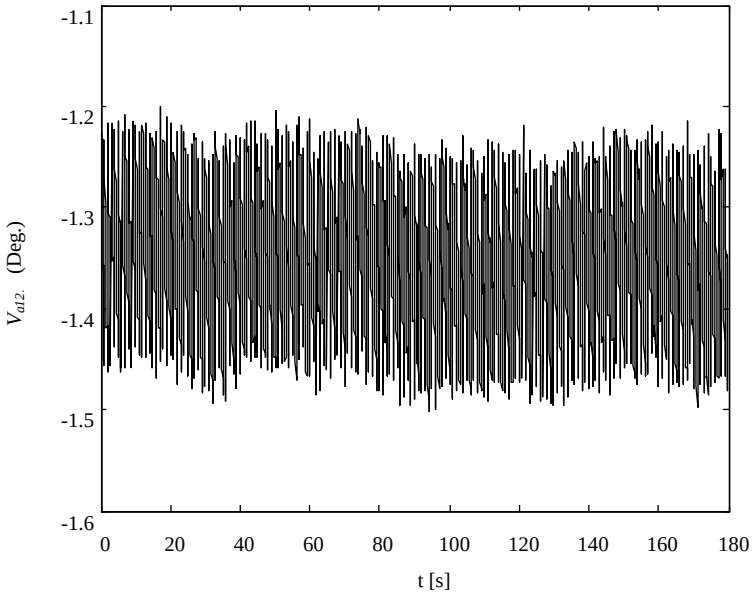

Fig. 2.2 Relative voltage angle based on measurements from PMUs in 3 minutes (PMU 2 and PMU 1, data file:#1-4)

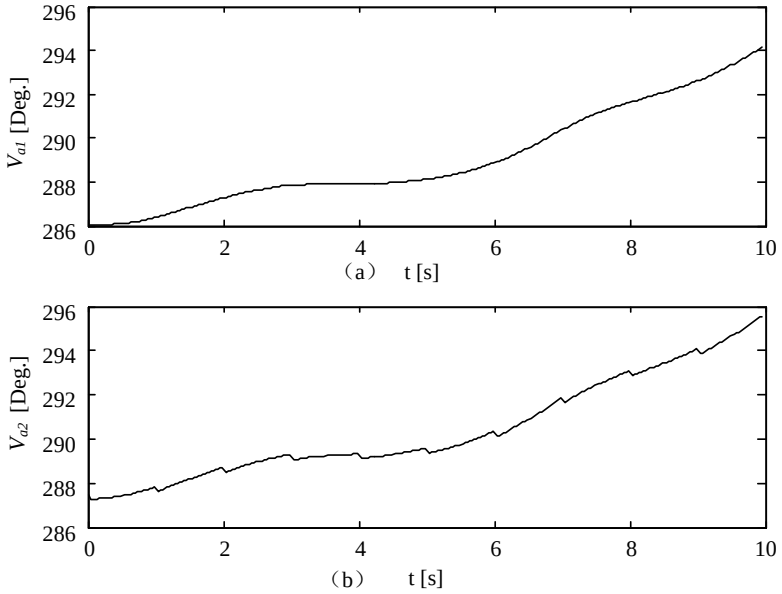

Fig. 2.3 Voltage angle measurements from two PMUs in the same time period (PMU 1 above, PMU 2 below, data file:#1-4)

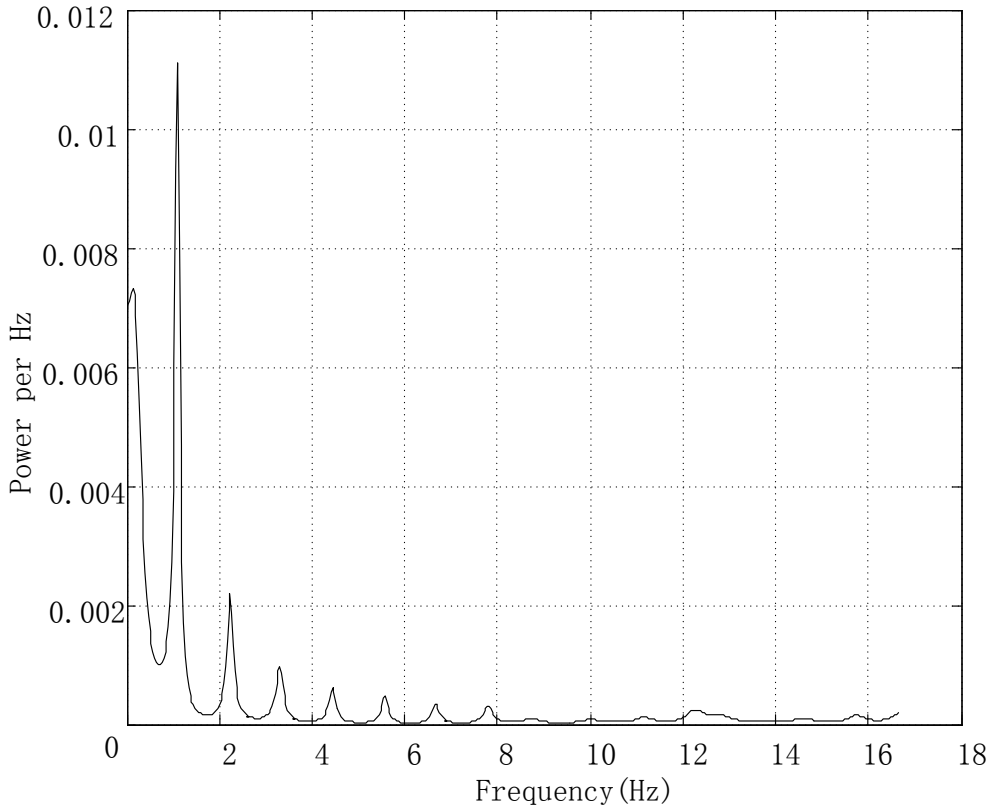

Fig. 2.4 Periodogram power spectral density estimate of relative voltage phase angles based on measurements from two PMUs in 3 minutes

2.3 Origin of the time skew error

In this section, a discussion of the origin of the time skew problem is presented. As stated above, measurements from different PMUs might not be synchronized as shown by the time stamps. When a sampling clock associated with a PMU provides accurate time, the measurement with time stamp is taken exactly at the specific instant shown by the time stamp. However, if a sampling clock associated with a PMU does not provide accurate time, the time skew problem occurs.

Assume the reporting rate of PMUs in a power system is 30 frames per second. That is, the measurements are reported every 1/30 second. Let ΔT_1 denote

the time duration that elapses for an accurate clock when a time stamp is generated, and ΔT_2 for a less accurate clock. Under the assumption, ΔT_1 equals to 1/30 second exactly, and ΔT_2 could be greater or less than 1/30 second. Let ε denote the time duration error. Fig. 2.5 and Fig. 2.6 illustrate the time skew between an accurate clock and a less accurate clock. As highlighted by the ellipses in the figures, the time skew increases in the one second interval. This assumes that the parameter ε is constant. The measurements from PMUs associated with a less accurate clock are actually not synchronized because they are not taken at the instants shown by the time stamps. As observed from Fig. 2.3, the 1 PPS signal plays a resetting role to make all the clocks to synchronize in the system again. This information is also shown in Fig. 2.5 and Fig. 2.6.

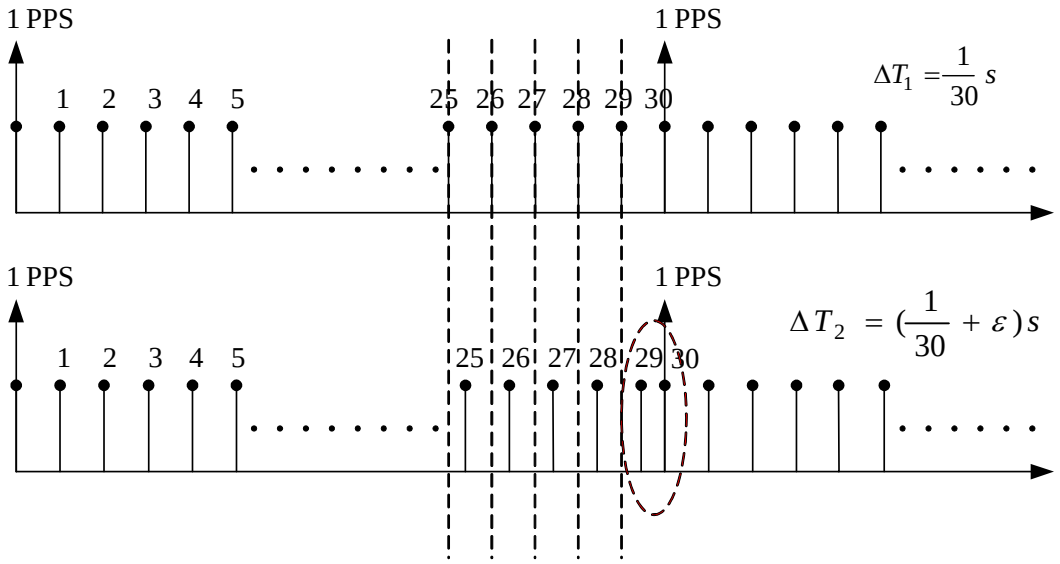

Fig. 2.5 Time skew originating from a less accurate clock when ΔT_2 is slightly greater than ΔT_1

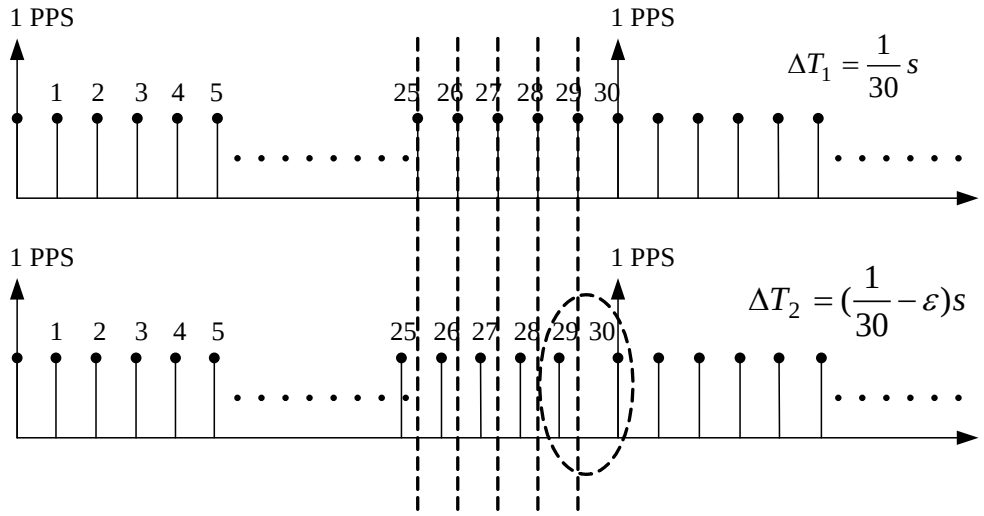

Fig. 2.6 Time skew originating from a less accurate clock when ΔT_2 is slightly less than ΔT_1

The question arises as to how to judge whether a clock is accurate or not. The voltage phase angle change is used to accomplish the goal. The voltage angle change is defined as

$$\Delta\theta(k) = \theta_{k\Delta T} - \theta_{(k-1)\Delta T} \tag{2-1}$$

where *k* is the sequence number count, and ΔT is the reporting interval. Consider the voltage phase angle change $\Delta\theta_1$ when the PMU is associated with an accurate clock in a one second interval with reporting rate of 30 per second. Since the clock is accurate, ΔT_1 = 1/30 second. The voltage phase angle change at each reporting interval is given by

$$
\begin{aligned}
&\Delta\theta_1(1) = \theta_1(\Delta T_1) - \theta_1(0) \\
&\Delta\theta_1(2) = \theta_1(2\Delta T_1) - \theta_1(\Delta T_1) \\
&\vdots \\
&\Delta\theta_1(29) = \theta_1(29\Delta T_1) - \theta_1(28\Delta T_1) \\
&\Delta\theta_1(30) = \theta_1(1) - \theta_1(29\Delta T_1)\ (1 pps\ signal)
\end{aligned}
\tag{2-2}
$$

Consider the voltage phase angle change $\Delta\theta_2$ when the PMU is associated with a less accurate clock in a one second interval with 30 measurements. Since the clock is less accurate, $\Delta T_2 = 1/30 \pm \varepsilon$. The voltage phase angle change is

$$
\begin{aligned}
\Delta\theta_2(1) &= \theta_2(\Delta T_2) - \theta_2(0) \\
&= \theta_1(1/30 \pm \varepsilon) - \theta_1(0) \\
\Delta\theta_2(2) &= \theta_2(2\Delta T_2) - \theta_2(\Delta T_2) \\
&= \theta_1(2/30 \pm 2\varepsilon) - \theta_1(1/30 \pm \varepsilon) \\
&\vdots \\
\Delta\theta_2(29) &= \theta_2(29\Delta T_2) - \theta_2(28\Delta T_2) \\
&= \theta_1(29/30 \pm 29\varepsilon) - \theta_1(28/30 \pm 28\varepsilon) \\
\Delta\theta_2(30) &= \theta_2(1) - \theta_2(29\Delta T_2) \\
&= \theta_2(1) - \theta_2(29/30 \pm 29\varepsilon)(1 pps\ signal)
\end{aligned}
\tag{2-3}
$$

Compare the 30th voltage phase angle change in (2-2) and (2-3). For an accurate clock, the time interval is still 1/30 second. But for a less accurate clock, the interval is $|1/30 \pm 29\,\varepsilon|$ which can be different from 1/30 second. As a result, a large voltage phase angle change is expected. The examples shown in Fig. 2.7 from actual measurements illustrate this point. The curve in Fig. 2.7(a) depicts the voltage phase angle change based on measurements from a PMU associated with a more accurate clock. It is observed that the voltage angle changes are relatively small numbers, and the absolute values of the angle changes are in a range of [0, 0.06] degree. As for the curve in Fig. 2.7(b), this plot depicts the voltage

phase angle change based on measurements from a PMU associated with a less accurate clock.

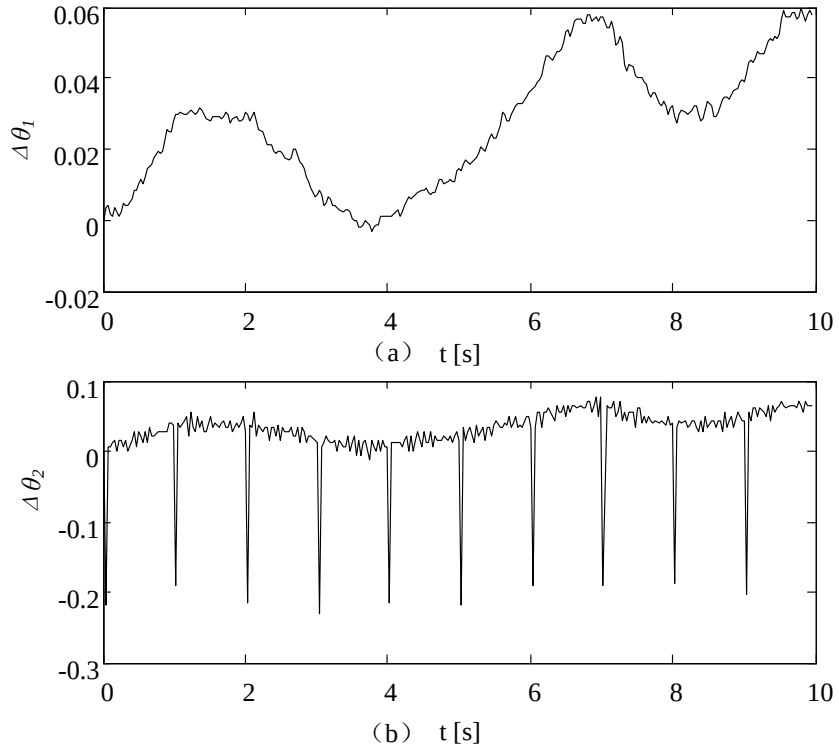

Fig. 2.7 Voltage angle changes from two PMUs in a time period of 10 s (PMU 1 above, PMU 2 below, data file: #1-4)

It is clearly seen that spikes occur every second corresponding to the large changes as stated in previous discussion. The absolute values of the spikes are about 0.2 degree. It should be noted that even though the 1 PPS signal plays the role of re-synchronizing all the sampling clocks, it is observed from actual measurements that the resynchronization takes place at one reporting step after the 1 PPS signal shown by the time stamp. In the subsequent discussion, a Kalman filter model is proposed to compensate the time skew error.

2.4 Compensation of time skew error using a Kalman filter

2.4.1 The Kalman filter model for time skew problem

The Kalman filter is a least square error estimator using measurements and system information to model the process dynamically [55]. It is a recursive optimal estimator based on the state space representation. The mathematical model of the discrete Kalman filter is presented briefly in the following. The discrete state space representation of the system is formulated as

$$x_{k+1} = \phi_k x_k + w_k \tag{2-4}$$

$$z_k = H_k x_k + v_k \tag{2-5}$$

where x_k is the state vector, ϕ_k is the state transition matrix, w_k is the process noise, z_k is the measurement vector, H_k is the observation matrix, and v_k is the measurement noise. The random variables w_k and v_k are assumed to be independent and normally distributed. The random variables are independent from each other as well. The covariance matrices for w_k and v_k are given by

$$E(w_k w_k^T) = R_k \tag{2-6}$$

$$E(v_k v_k^T) = Q_k \tag{2-7}$$

The equations that describe the Kalman filter estimator are divided into two steps: *time update* (*predictor*) *equations* and *measurement update* (*corrector*) *equations*. The computation procedure is as follows,

1) Project the state

$$\hat{x}_k = \phi_{k-1} \hat{x}_{k-1} \tag{2-8}$$

2) Project the error covariance matrix

$$P_k^- = \phi_{k-1} P_{k-1} \phi_{k-1}^T + Q_{k-1} \tag{2-9}$$

3) Compute the Kalman gain K_k

$$K_k = P_k^- H_k^T (H_k P_k^- H_k^T + R_k)^{-1} \tag{2-10}$$

4) Update estimate with measurement z_k

$$\hat{x}_k = \hat{x}_k^- + K_k (z_k - H_k \hat{x}_k^-) \tag{2-11}$$

5) Compute error covariance for the update estimate

$$P_k = (I - K_k H_k) P_k^- \tag{2-12}$$

It is noted that the knowledge, a reasonable assumption or estimation of the initial estimate error covariance P_0^- and a priori estimate $\hat{x}_0$ is needed.

The model to compensate the time skew error in one second interval is given by

$$x_{k+1} = \begin{bmatrix} 1 & 0 \\ 0 & 1 \end{bmatrix} x_k + w_k \tag{2-13}$$

$$z_k = \begin{bmatrix} 1 & i \end{bmatrix} x_k + v_k \tag{2-14}$$

where $x_k = \begin{bmatrix} \theta_{PMU} \\ TS_{err} \end{bmatrix}$, θ_{PMU} is the relative voltage angle when choosing one bus equipped with PMU without a time skew problem as the reference, and TS_{err} is the error caused by the time skew problem in each reporting step. The variable *i* in (2-14) is the step difference between present instant and the latest top of second. Suppose the reporting rate of PMUs in a practical system is N_{rr}, then the value of the variable *i* ranges from zero to N_{rr}-1.

The objective of the time skew correction procedure is to address the following two issues:

(a) ascertain whether the error due to the time skew problem is constant or not,

(b) determine the error identified in (a) above.

Since the off-line analysis is implemented, only measurements taken under relatively static operating conditions are involved. As stated previously, the initial estimate of the error covariance P_0^- and a priori estimate $\hat{x}_0$ are needed. For the first run of the computation procedure, the initial values are assigned. Then the computation procedure is run several times and the initial values are tuned according to the results from last run of the computation procedure.

2.4.2 Application of the Kalman filter model for practical measurements

In this section, an example is provided to compare the raw relative voltage angle measurements and the processed measurements using the proposed Kalman filter. In essence, the Kalman filter is used as a *dynamic state estimator*. Analysis is done to answer the two questions: a) ascertain whether the error due to the time skew problem is constant or not, and b) determine the error if it is constant.

The raw PMU relative voltage phase angle measurements are shown by the curve in Fig. 2.8(a), and the processed measurements are shown by the curve in Fig. 2.8(b). The time duration (start to end) is 3 minutes. There are 5400 measurements in total since the reporting rate in the system is 30 frames per second. By observation, the raw PMU relative voltage phase angle measurements are greater than -1.5 degrees and less than -1.2 degrees. By comparison, the processed measurements vary in a much smaller interval, which reflect the actual system operation condition. The straightforward conclusion is that the raw PMU

relative voltage phase angle measurements should be compensated for the error due to the time skew problem before they are used in further applications.

In Table 2.1 and Table 2.2, the time skew errors denoted by TS_{err} in one reporting step calculated based on measurements from different time durations for 10 PMUs which are denominated by identification numbers *PMUID* are listed. In Table 2.1, the results are calculated based on 6-minute measurements. 6-minute measurements are selected to guarantee that the system operating condition does not change much, since the focus of this chapter is to address the problem of time skew error. A series of TS_{err} for each PMU is obtained. The mean value of TS_{err} for each PMU is listed in the second column. The standard deviation of the TS_{err} is listed in the third second column. The percentage of the standard deviation with respect to TS_{err} is listed in the last column. The standard deviations are very small. Results based on analysis of PMU measurements for a longer duration are listed in Table 2.2. There are twenty four 6-minute measurement sets. First, the TS_{err} is calculated based on each measurement set. Then the mean value and standard deviation of the twenty four TS_{err} are calculated. The percentages of the standard deviation with respect to TS_{err} listed in Table 2.2 are also very small. Based on the analysis results shown in Tables 2.1 and 2.2, the questions posed in the previous subsection are answered: namely, can the time skew error for each PMU be treated as a constant, and can the time skew be calculated by the proposed method. The TS_{err} for a specific PMU with the time skew problem could be treated as a constant, and could be calculated by the proposed method.

Table 2.1 Time skew errors calculated based on 6-minute duration measurements

PMUID	TS_{err} (Degrees)	*Standard deviation of* TS_{err} *(*SD_TS_{err}*)* (Degrees)	SD_TS_{err}/TS_{err} *(%)*
2	0.008642358	0.000165698	1.92
3	0.007207332	0.000222037	3.08
4	0.007037759	0.000275179	3.91
5	0.005377695	0.000231127	4.30
6	0.007918075	0.000251130	3.17
8	0.009146446	0.000242653	2.65
9	0.004164572	0.000216751	5.20
10	0.004945508	0.000224501	4.54
11	0.005293479	0.000266943	5.04
12	0.006047007	0.000259488	4.29

Table 2.2 Time skew errors calculated based on 144 minutes measurements

PMU ID	TS_{err} (Degrees)	*Standard deviation of* TS_{err} *(*SD_TS_{err}*)* (Degrees)	SD_TS_{err}/TS_{err} *(%)*
2	0.008667357	0.000060329	0.69
3	0.007126107	0.000302416	4.24
4	0.007076260	0.000118066	1.67
5	0.005384481	0.000109332	2.03
6	0.007922148	0.000121784	1.54
8	0.009134131	0.000091560	1.00
9	0.004179683	0.000089345	2.13
10	0.005052859	0.000129770	2.57
11	0.005355541	0.000073464	1.37
12	0.006059347	0.000082086	1.35

The proposed method is easy to apply on practical PMU measurements because the computational cost is low. Also, the analysis results indicate that the

time skew error can be calculated off-line and be used to compensate the real-time PMU measurements with the time skew problem.

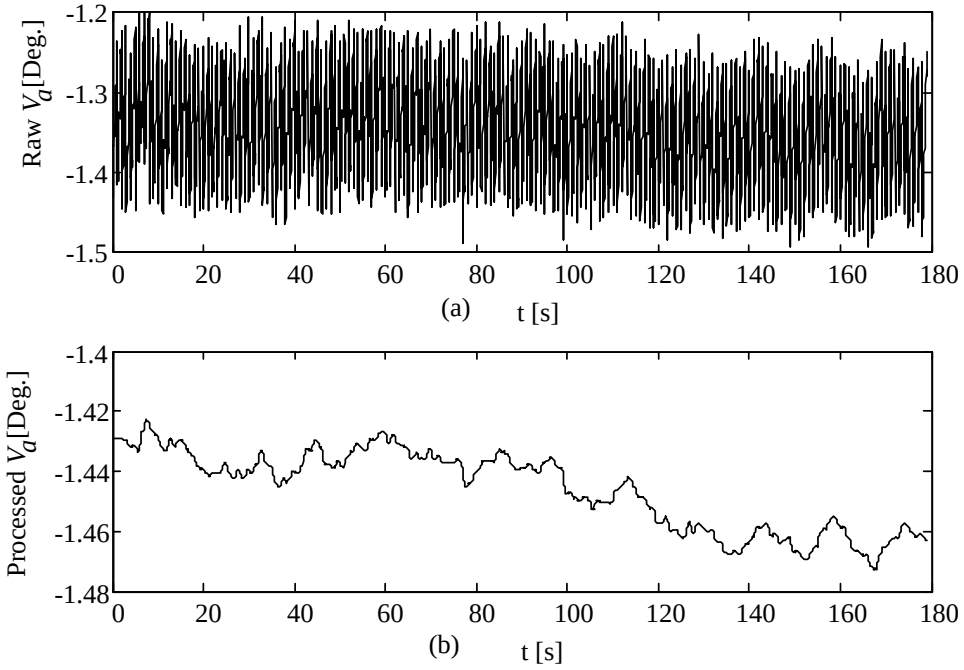

Fig. 2.8 Relative voltage phase angle without and with compensation for the time skew error in 3 minutes (PMU 1, PMU 2, data file: #1-4)

2.5 Conclusions

The research in this chapter deals with a specific issue concerning PMU measurements: time skew of measurements. The time skew problem is identified by analyzing the measurements from different PMUs in a practical system. The time skew existing between different PMUs means that the measurements are not exactly synchronized as shown by the time stamps. The origin of the time skew is discussed as well. A Kalman filter model is proposed to analyze and compensate the time skew error. It is concluded that the time skew error for a specific PMU could be treated as a constant. The calculated time skew error could be used to

compensate the raw PMU measurements before they are used in further power system applications.

The identification of the time skew problem of the actual PMU measurements indicates that validation of data quality of PMU measurements is needed. In the following Chapters 3 to 5, research on bad data identification and calibration of PMU measurements is presented.

Chapter 3

APPLICATION OF KALMAN FILTER ON PMU DATA

3.1 Problem statement

PMU measurements are a time sequence data series. There is measurement noise and possibility of bad data in the measurements. Data filtering is applied to remove the corrupted data points from the raw PMU measurements. In [56], singular value decomposition methods are used to reduce noise in PMU data. The objective is to obtain a more accurate estimate of the system states based on PMU measurements.

Even though the power system is never truly static, the power system states vary little when there is no large disturbance or change in operating conditions in the system. In this case, the relative phase angles based on PMU measurements are expected to be constant. A Kalman filter can suitably filter measurements from the PMUs in this case. In Chapter 2, a Kalman filter is applied to analyze and estimate the time skew error. Since the time skew error for a specific PMU is treated as a constant, the noise in PMU measurements still exists after the time skew error is compensated.

When processing PMU measurements using a Kalman filter, there are two conditions that need to be considered. One deals with bad data detection. The other one relates to the system state change detection. When a bad measurement is detected, the measurement should be replaced by an estimate of the system state or be simply discarded. When a system state change is detected, the measurement

should be retained. The question arises as to how to determine whether the 'abnormal' data observed are bad data or true system changes.

In this chapter, the possible bad data in PMU measurements are presented. The Kalman filter estimator is applied. Since the Kalman constant model does not perform well when step change occurs, an adaptive strategy is applied to make the Kalman filter robust to obtain the optimal estimate of the system state.

3.2 Possible bad data in PMU measurements

The possible bad data that appear in PMU measurements are depicted in Fig. 3.1. The two most frequently observed types of bad data from the true PMU measurements are spike and step changes. When there is only a spike, the Kalman filter performs well to remove the bad measurement and yields an optimal estimate of the system state. As stated previously, when a step change occurs, the regular Kalman filter is insensitive to the new state variation and begins to diverge. An adaptive strategy is provided in the following discussion to correct for this problem.

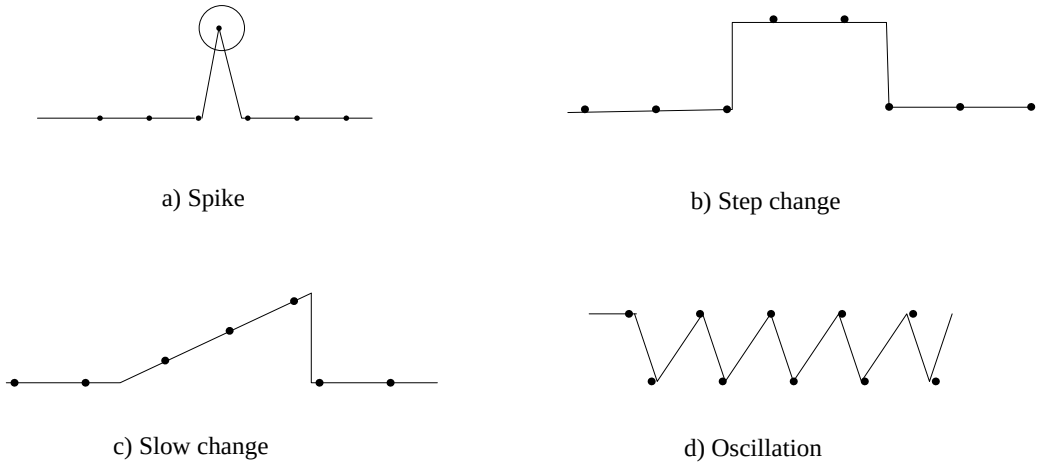

a) Spike

b) Step change

c) Slow change

d) Oscillation

Fig. 3.1 Types of bad data

3.3 The discrete time Kalman filter

The equations for the Kalman filter are provided in subsection 2.4.1 in Chapter 2. In this subsection, only the Kalman filter model used to filter the PMU measurements is provided. The bus voltage magnitude and phase angle are the state variables, and they vary little under relatively static operating conditions. The first order Kalman constant model used is listed below,

$$x_{k+1} = x_k + w_k \tag{3-1}$$

$$z_k = x_k + v_k \tag{3-2}$$

3.4 Adaptive Kalman filter

In the above two subsections, the basic ideas on the possible types of bad data in PMU measurements and the regular Kalman filter are provided. In this subsection, the concept and design of an adaptive Kalman filter is presented. The motivation for designing an adaptive Kalman filter is that a decision needs to be made to determine whether the detected abnormal data reflect real physical changes in the system. If the changes are real, the measurements should be retained. If the abnormal data are simply corrupted data, the bad measurements should be eliminated. Fig. 3.2 depicts the idea proposed for the detection of abnormal data when the system is operating at a normal steady state. Fig. 3.3 shows an example of change of bus phase angle. Under normal steady state conditions, the phase angle remains constant. After a period of abnormal operation, the data highlighted by the square box, the phase angle remains constant under another normal steady state. The focus of the adaptive filtering is during the period of abnormality in the data.

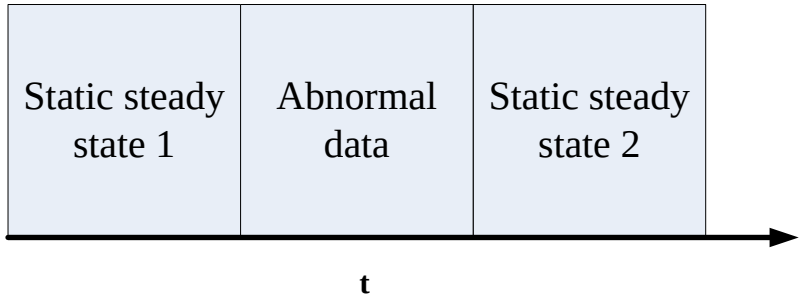

Fig. 3.2 Detection of abnormal data

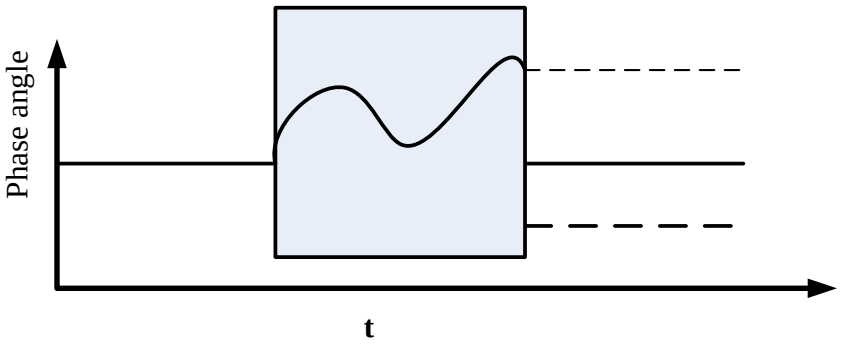

Fig. 3.3 Example of changes of phase angle

The procedure of adaptive data filtering is as follows:

a) Detection of abnormal data - A threshold needs to be set to trigger the alert. If no abnormal data are detected, continue processing. If abnormal data are detected, then go to step b).

b) Determination of the nature of abnormal data - This step deals with determining whether the abnormal data are results of a real physical change in the system. If yes, retain the measurements, and go to step e). If not, go to step c).

c) Filter the abnormal data using an adaptive filter. Detect the end edge of the abnormal data, then go to step d)

d) Output filtered measurements.

The procedure is depicted in Fig. 3.4.

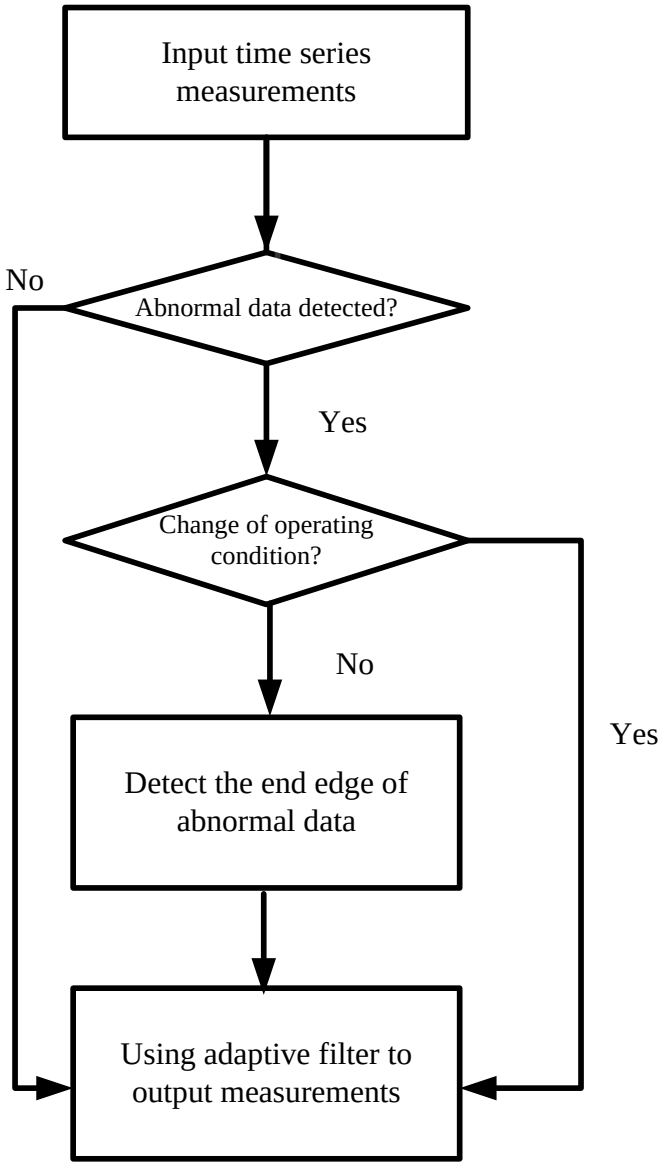

Fig. 3.4 Flow chart of adaptive data filtering

The critical step of the procedure is the determination of the nature of the abnormal data observed. One index from PMU measurement itself is the 'STAT word' in the data frame. This parameter, 'STAT' is a 2-byte word including bit flags which indicate the validity of the data and loss of synchronization. A quick

and initial decision could be made based on the STAT word with the PMU measurement. If the data are valid according to the STAT word and in the meantime the data are detected as abnormal data, bad data identification still needs to be implemented to decide whether the data should be retained or eliminated. Bad data detection and identification based on PMU placement is illustrated in detail in the subsequent chapters. The focus of this chapter is to provide the general idea of the adaptive Kalman filter.

3.5 Examples

In the subsequent discussion, a simple example is used to illustrate the insensitivity of a conventional Kalman filter to step change. Also, an example of an adaptive filter considering the STAT word applied to true PMU measurements is provided.

The first example is provided to show the performance of the regular Kalman filter when filtering a time sequence series with a step change. The step change is set to simulate a change in the power system state. As shown in Fig. 3.5, there are two curves depicting different signals. The first curve from the top shows the raw signal with a step change at the 60^{th} second. The second curve from the top is the raw signal filtered by the Kalman filter. By comparison with the raw signal, the step change is not retained. In this simulation case, the step change reflects a true variation of the state. Due to the insensitivity of the conventional Kalman filter to the state variation, the filtered signal diverges from the true state for a time period.

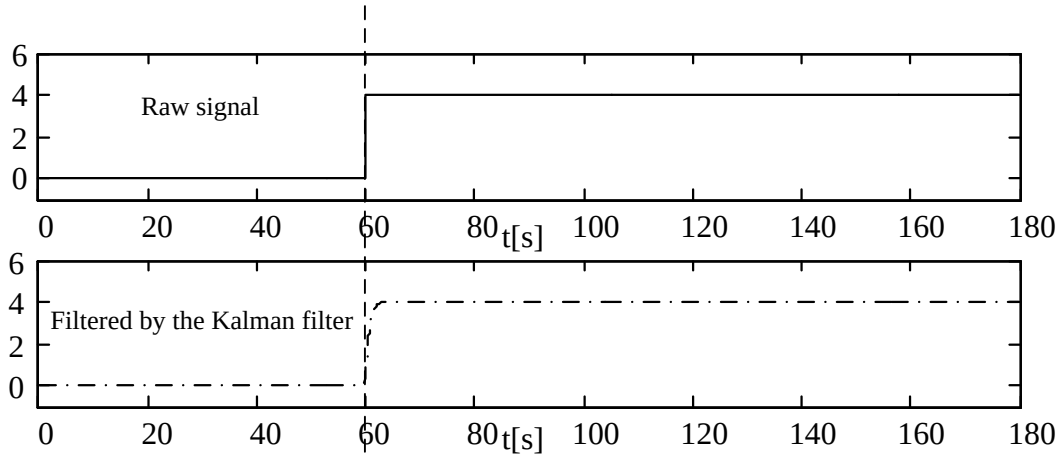

Fig. 3.5 Signal with step change filtered by a conventional Kalman filter

Fig. 3.6 depicts an example of the performance of the adaptive Kalman filter when filtering PMU measurements. The measurements are from a true PMU in a practical electric power system. There are obvious bad measurements in the raw measurements which appear in two subintervals. As shown by the second curve from the top, the Kalman filter performs poorly in eliminating these bad measurements. In the third curve from the top, the adaptive Kalman filter is designed to eliminate the bad measurements from raw data and performs well. It should be noted that only information from the STAT word is used when designing the adaptive Kalman filter. Another point that needs be noted is that the STAT information is not available for the PMU measurements in this example. As a result, pseudo-STAT information is provided manually. Another example is provided shown in Fig. 3.7. The STAT information is available together with the PMU measurements. There are bad measurements around the 60^{th} second and in the interval between around the 240^{th} second and the 350^{th} second. The adaptive Kalman filter based purely on the STAT information performs well to eliminate

the bad measurements and yield the estimate of the system state around the 60th second. For the bad measurements in the interval between around the 240th second and the 350th second, the output of the adaptive Kalman filter could not track the change in the system state. Once the status flag indicates that the PMU measurement is valid, the adaptive Kalman filter begins to track the system state again. There is another way to deal with bad PMU measurements. Under certain PMU installation scenario, measurements from other PMUs would help to identify and correct the bad data. Analysis of bad data identification based on PMU installation topology is provided in the next two chapters.

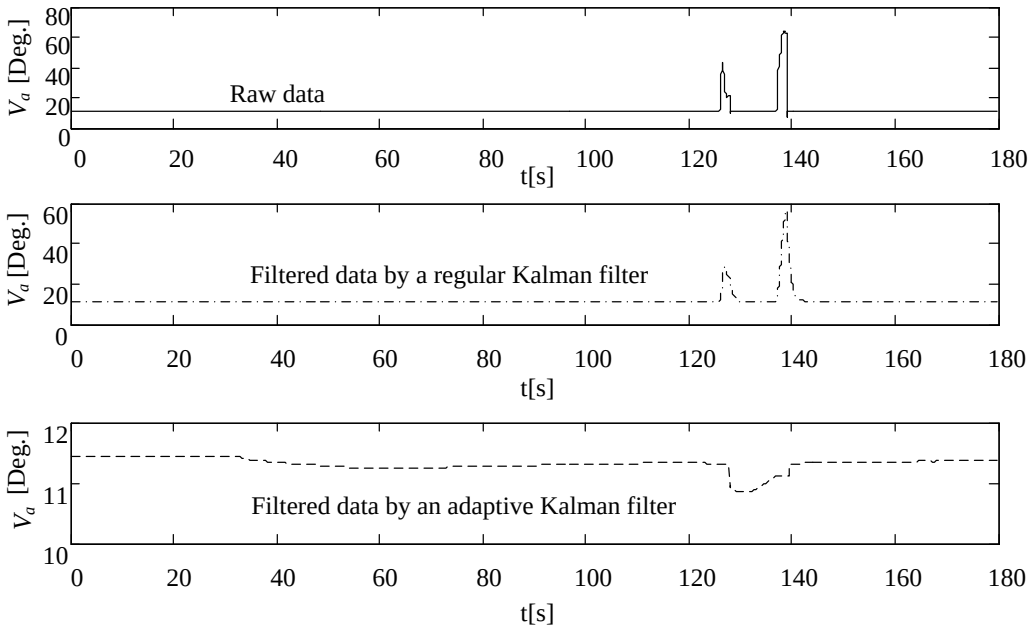

Fig. 3.6 PMU data filtered by different filters (PMU 13, data file: #1-2)

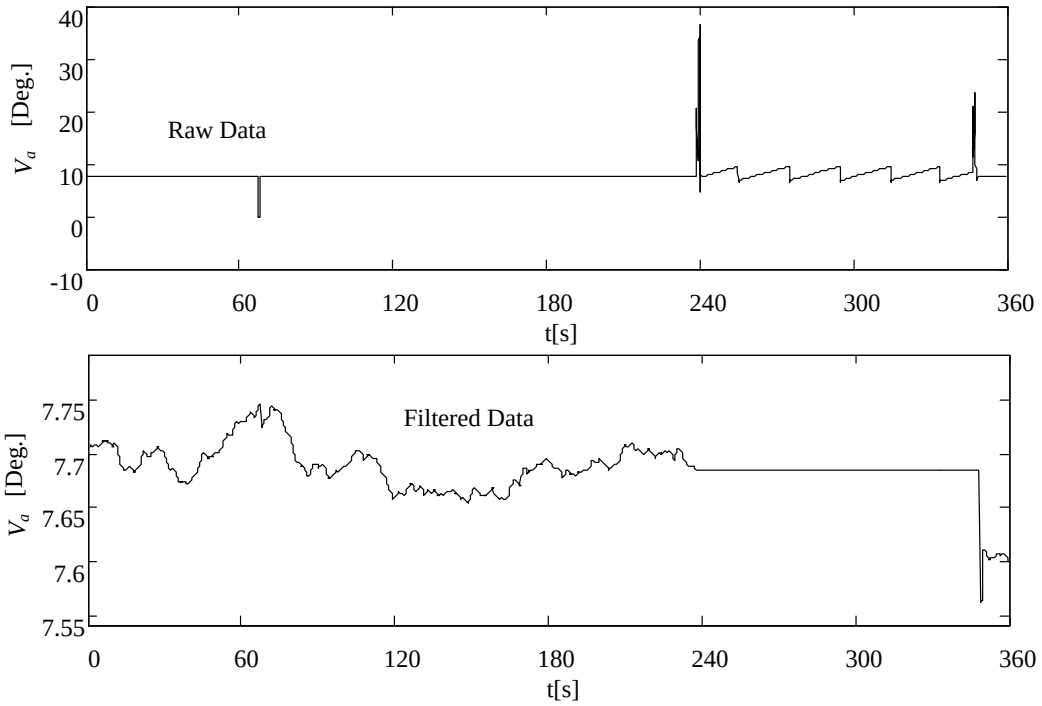

Fig. 3.7 PMU data filtered by an adaptive Kalman filter (PMU 13, data file:#4-436)

3.6 Conclusions

In this chapter, the general concept of an adaptive Kalman filter is provided. An example is presented to show the insensitivity of a conventional Kalman filter to the step change of the signal. As a result, an adaptive strategy is proposed to determine the nature of observed abnormal data. If bad data are identified, they should be eliminated. If the abnormal data reflect a physical change in the system, the measurements should be retained. In this chapter, only the information provided by the STAT word in the PMU data frame is used. In the following two chapters, the methodology of bad data identification based on PMU placement topology is provided.

Chapter 4

BAD PMU DATA DETECTION AND IDENTIFICATION BASED ON POWER TRANSFER DISTRIBUTION FACTORS

4.1 Problem statement

In Chapter 3, the general idea of an adaptive Kalman filter is presented. The key step in the procedure is to determine whether the abnormal data observed are real physical system state changes or not. If only measurements from an individual PMU are considered, it is difficult to track the system state change for the complexity of the system network. There are many factors that can cause the change of system states. As more PMUs populate power systems, certain installation topology of PMUs would help to track the system state changes. When the redundancy of PMU measurements is available, bad data detection and identification is implemented. In this chapter, a methodology of identifying bad data from PMU measurements based on power transfer distribution factor (PTDF) is presented. The effectiveness of this method is tested in test beds.

4.2 PTDF computation

The definition of PTDF is the relative active power change through a particular branch due to the change in active power injections. The change in active power on a particular branch due to change of injections at one or more buses can be calculated based on PTDF. PTDF is calculated based on direct current (DC) power flow equations. In this subsection, the calculation procedure of the PTDF is reviewed.

The formulation used in DC power flow calculation for an *n*-bus system is as follows,

$$\Delta P = -B\Delta\delta \tag{4-1}$$

where ΔP is the increment vector of active power injections, $\Delta\delta$ is the increment vector of bus voltage phase angles, and B is the susceptance matrix. The dimension of B is *n* by *n*. The elements are calculated by the following formulae. The off-diagonal elements are calculated by

$$B_{ik} = \begin{cases} \dfrac{1}{x_{ik}} & \textit{when bus k is connected with bus i} \\ 0 & \textit{when bus k is not connected with bus i} \end{cases} \tag{4-2}$$

where x_{ik} is the reactance of the transmission line connecting bus i and k. The diagonal elements are calculated by

$$B_{ii} = -\sum_{k=1,k\neq i}^{n} B_{ik} \tag{4-3}$$

From (4-1), the bus voltage phase angle changes due to the change of power injections are obtained by

$$\Delta\delta = -X\Delta P \tag{4-4}$$

When the slack bus is not included in the subnetwork of interest, the X matrix is obtained by

$$X = B^{-1}. \tag{4-5}$$

If all buses in a system are considered, and also the reference bus is considered (usually the ground bus), then B is singular. To avoid singularity, the row and column corresponding to the slack bus are eliminated from the susceptance matrix.

The remaining matrix is denoted by B_{sub} which is a (n-1) by (n-1) matrix. Without loss of generality, assume the slack bus is bus one. Then the X matrix is obtained by

$$X = \left[\begin{array}{c|ccc} 0 & 0 & \cdots & 0 \quad 0 \\ \hline 0 & & & \\ \vdots & & B_{sub}^{-1} & \\ 0 & & & \\ 0 & & & \end{array}\right]_{n\times n} \tag{4-6}$$

For the l^{th} branch, the two ends of the branch are bus i and bus j. The DC active power on the l^{th} branch is given by

$$P_{ij} = \frac{\delta_i - \delta_j}{x_{ij}} \tag{4-7}$$

where δ_i and δ_j represent the voltage phase angle at bus i and bus j respectively.

Consider the variation of the active power on the l^{th} branch with respect to the power injection at bus k. The PTDF denoted by $\eta_{l,k}$ is calculated by

$$\eta_{l,k} = \frac{\Delta P_{ij}}{\Delta P_k} \tag{4-8}$$

Substituting (4-7) into (4-8) yields,

$$\eta_{l,k} = \frac{\Delta\delta_i - \Delta\delta_j}{x_{ij}\Delta P_k} = \frac{1}{x_{ij}}\left(\frac{\Delta\delta_i}{\Delta P_k} - \frac{\Delta\delta_j}{\Delta P_k}\right) \tag{4-9}$$

From (4-4), $\frac{\Delta\delta_i}{\Delta P_k}$ and $\frac{\Delta\delta_j}{\Delta P_k}$ are the ik^{th} and jk^{th} elements in the X matrix. As a result, (4-9) can be rewritten as

$$\eta_{l,k} = \frac{1}{x_{ij}}(X_{ik} - X_{jk}) \tag{4-10}$$

If there is no topology change in the network under study, the susceptance matrix remains constant. Thus, the PTDF matrix also remains constant and needs to be calculated only once. In the following discussion, the bad PMU data detection and identification is implemented based on PTDF deduced in this subsection.

4.3 Methodology of bad PMU data identification based on PTDFs

In the previous subsection, the deduction and calculation procedure of the PTDF is provided. In this subsection, the methodology of bad PMU data identification based on PTDF is illustrated.

When a PMU is installed on a transmission line, both the voltage and current phasors are available. It is convenient to calculate the active power on the branch. If the operating condition in the system changes, the variation of the active power flow on a branch is observed in real time through the PMU measurements. For a network without change of topology, the PTDF matrix remains constant and can be calculated off-line. As a result, the PTDF matrix can be readily used for on-line analysis.

According to (4-8), the change of active power on a branch due to the change of active power injection at a specific bus is given by

$$\Delta P_{ij,k} = \eta_{l,k} \Delta P_k \tag{4-11}$$

Due to the complexity of power systems, there are rare cases when only one active power injection change occurs. Considering all the changes of the power injections, the change of active power on a specific branch is obtained by

$$\Delta P_{ij} = \sum_{k=1}^{n} \eta_{l,k} \Delta P_k \tag{4-12}$$

As indicated by (4-10), $\eta_{l,k}$ remains constant if there are no topology changes in the system. The relationship between $\Delta P_{ij,k}$ and ΔP_k is linear. Based on the superposition principle, the change of active power on a specific branch would be the summation of changes due to the changes of the non-zero power injections.

Now consider a power system network with n_{bus} buses and n_{br} branches. The number of non-zero injection buses is denoted by n_{non}, and the number of branches with PMU installed is denoted by n_{PMU}. For each PMU, an equation is obtained according to (4-12). Since the PTDF matrix can be readily used when there is no topology change in the network, the coefficients in the equations are also available. The injections at the n_{bus} buses are treated as unknowns. For zero injection buses, the change of active power injections are also zeros. As a result, there are n_{PMU} equations with n_{non} unknowns for the problem under study. When n_{PMU} equals n_{non}, analysis based on PMU measurements only can be conducted to locate the buses with power injection changes and calculate the amount of changes. However, without some level of redundancy, it is not possible to conduct analysis on bad data detection and identification. The bad data in PMU measurements would result in incorrect calculation of the changes of power injections. When n_{PMU} is greater than n_{non}, the optimal estimation of the changes of power injections is obtained by a least squares estimator. With certain level of redundancy, bad data analysis can be performed.

In the subsequent discussion, assume n_{PMU} is greater than n_{non} for the network under study. The equations are rewritten in matrix format as

$$z = Hx \tag{4-13}$$

where z is the branch active power change vector with dimension as n_{PMU} by 1, x is the bus active power injection change vector with dimension as n_{non} by 1, and H is formed by elements from the PTDF matrix.

The optimal estimation in the sense of least squares is obtained by

$$\hat{x} = (H^T H)^{-1} H^T z \tag{4-14}$$

where $\hat{x}$ is the estimated vector of bus active power injection. Substitute $\hat{x}$ into (4-13), and the residual vector r is calculated by

$$r = z - H\hat{x} \tag{4-15}$$

Set a threshold ε to check all elements in the residual vector. Analyzing the residual vector would help fulfill the following objectives:

a. When all elements in the residual vector are smaller than the threshold, the system state changes observed from PMU measurements in the network reflect physical changes. The information is applied in the adaptive Kalman filter presented in Chapter 3.

b. When there are elements in the residual vector greater than the threshold, an identification procedure is triggered to find the source of bad data which are not indicated by the STAT word in the PMU data frame.

c. When data from specific PMUs are identified as invalid measurements according to the STAT word, the phasor information can be estimated by the other PMU measurements if the required level of redundancy is satisfied.

In this chapter, the focus is on bad data identification based on the PTDF matrix. A flow chart as shown by Fig. 4.1 is provided to illustrate how the bad data identification procedure is reduced to an algorithm.

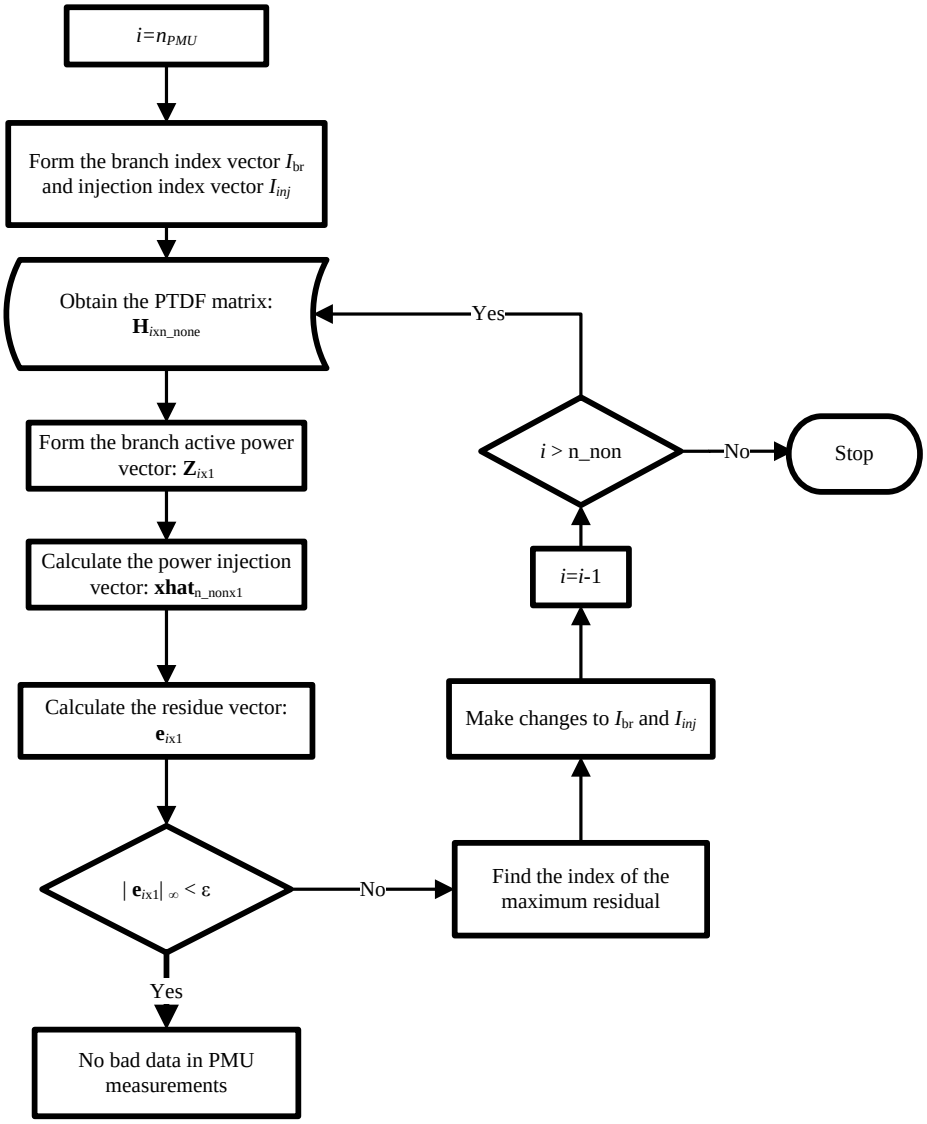

Fig. 4.1 Bad PMU data identification based on PTDF

In the subsequent discussion, test cases are provided to test the effectiveness of the bad data detection and identification procedure. As more PMUs are installed in practical power systems, the procedure can be easily and conveniently implemented if the required level of redundancy is satisfied.

4.4 Test cases

In this subsection, test cases are provided. The 9-bus system is used to test the bad data detection and identification procedure when the whole system is under study. The 14-bus system is used to test the bad data identification procedure when only partial system is under study. It is should be noted that the placement of PMUs in the test systems is determined to satisfy the required level of redundancy. Also only one PMU is installed on each branch. For the application in practical systems, the area that satisfies the requirement of the bad data detection and identification procedure is identified first. In addition there are many cases where PMUs are installed at both ends of a branch.

4.4.1 9-bus test system [57]

The one-line diagram of the 9-bus system is shown in Fig. 4.2. There are 9 buses, and 9 branches. Bus 1 is the slack bus. The non-zero injection buses include bus 2, bus 3, 5, 7 and 9. Suppose 8 PMUs are installed in the system indicated by the black dots. As a result, 8 equations are obtained with 5 unknowns. The number of PMUs is greater than the number of non-zero injections. The bad data detection and identification procedure can be implemented in the system.

First, the system power flow in the base case is calculated. The active power injections are listed in Table 4.1. Then in the new case, power injection at

bus 5 is increased by 10 MW, and power injection at bus 7 is decreased by 10 MW. The comparison of active power injections at bus 5 and 7 is listed in Table 4.2. The power injections at bus 2, 3, and 9 remain the same. The two cases are referred to as the 'base case' and the 'new case' respectively. System states change when the operating condition changes. The objective is to capture the system state change by PMU measurements. Also bad data detection and identification procedure is performed to check whether all PMU measurements are valid or not.

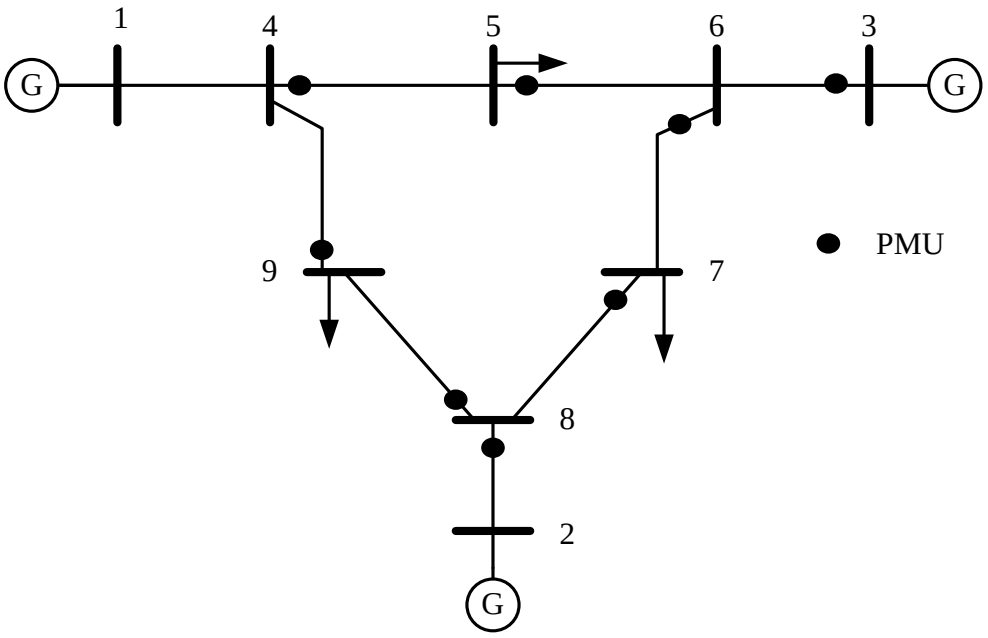

Fig. 4.2 One-line diagram of 9-bus system

Table 4.1 Non-zero power injections of 9-bus system in the base case

Bus Index	P_g (MW)	P_d (MW)	P_{inj} (MW)
2	163	0	163
3	85	0	85
5	0	90	-90
7	0	100	-100
9	0	125	-125

Table 4.2 Comparison of power injections at bus 5 and 7 (9 bus test bed)

Bus Index	Base case	New Case
	P_{inj} (MW)	P_{inj} (MW)
5	-90	-100
7	-100	-90

From Fig. 4.1, the required PTDF matrix is formed based on the system topology. The branch active power change vector is formed from PMU measurements. In Table 4.3, the active powers of branches with PMU installed are listed. The change of the branch active powers is obtained. In Table 4.4, the calculated power injection change vector is listed in the third column. By comparing the calculation results of the power injection changes with the true values listed in the second column, the differences are within the tolerance range of 0.2 MW. In this case, it is concluded that there are no bad data in the PMU measurements. The observed state changes reflect the true physical change in the system.

Table 4.3 Active powers of branches in the base case and new case (9 bus test bed)

Branch index (From bus – To bus)	Base case	New Case	ΔP_{ij} (MW)
	P_{ij} (MW)	P_{ij} (MW)	
2 (4-5)	30.728	34.965	4.237
3 (5-6)	-59.445	-65.261	-5.815
4 (3-6)	85.000	85.000	0.000
5 (6-7)	24.106	17.984	-6.122
6 (7-8)	-75.989	-72.081	3.909
7 (8-2)	-163.000	-163.000	-5.68e-14
8 (8-9)	86.504	90.464	3.960
9 (9-4)	-40.960	-37.230	3.730

Table 4.4 Comparison of calculated injection change vector and the true values (9 bus test bed)

Bus Index	True values	Calculated results (without bad data)	$\lvert\Delta P_{inj\_true}-\Delta P_{inj\_cal}\rvert$ (MW)
	ΔP_{inj_true} (MW)	ΔP_{inj_cal} (MW)	
2	0	0.013	0.013
3	0	-0.099	0.099
5	-10	-10.153	0.153
7	10	9.949	0.051
9	0	-0.198	0.198

Now consider that bad measurements exist in measurements from the 8 PMUs. Assume bad data from the PMU on branch (7-8) result in 1 MW error in $\Delta P_{ij(7-8)}$. The power injection change vector x is calculated based on branch active power change vector. Then the residual vector is calculated and listed in Table 4.5. The largest difference is observed at branch (7-8). As a result, measurements from the PMU on the branch (7-8) are treated as bad data candidates. Remove elements in the PTDF matrix corresponding to the branch (7-8). Repeat the calculation following the procedure shown in Fig. 4.1. The calculated power injection change vector with bad data is listed in the third column of Table 4.6. By comparing with the true values, the largest difference is about 0.75 MW. After removing the bad data, the power injection vector is recalculated and is listed in the fourth column of Table 4.6. And the largest difference from the true value is about 0.2 MW.

The effectiveness of the bad data detection and identification procedure is tested in the 9-bus test system. It should be noted that since there are 5 non-zero injection buses, the minimum number of PMU required to satisfy the redundancy

requirement is 6. The redundancy analysis is helpful for future PMU installation. However, the focus of the study in this chapter is on bad data detection and identification. The locations of PMU installation have already been determined, if the bad data identification procedure is applied in practical systems.

Table 4.5 Residual vector of branch active powers (9 bus test bed)

Branch index (From bus – To bus)	P_{ij_meas} (MW) (with bad data)	P_{ij_cal} (MW)	$\|P_{ij\_meas}$-$P_{ij\_cal}\|$ (MW)
2 (4-5)	4.237	4.338	0.102
3 (5-6)	-5.815	-5.755	0.060
4 (3-6)	0	-0.128	0.128
5 (6-7)	-6.122	-5.883	0.239
6 (7-8)	**2.909**	3.371	**0.463**
7 (8-2)	-5.68e-14	-0.3839	0.383
8 (8-9)	3.96	3.755	0.205
9 (9-4)	3.730	3.824	0.094

Table 4.6 Comparison of the calculated power injection change vector and the true values (9 bus test bed)

Bus Index	True values	Calculated results (with bad data)	Calculated results (with bad data removed)
	ΔP_{inj_true} (MW)	ΔP_{inj_cal} (MW)	ΔP_{inj_cal} (MW)
2	0	0.383	0.011
3	0	-0.128	-0.099
5	-10	-10.094	-10.162
7	10	**9.255**	9.953
9	0	0.069	**-0.208**

4.4.2 14-bus test system [58]

In this subsection, the example of a 14-bus test system is provided to test the effectiveness of the bad data detection and identification procedure when only a portion of the network is under study. The diagram of the 14-bus test system is shown in Fig. 4.3. The highlighted area depicted by the dotted line is under study.

There are 7 buses and 8 branches. The boundary buses which are connected with other buses outside of the study area are bus 6 and 9. For the boundary buses, the active power flows on branches which are not inside the study area are combined and treated as power injections. The main purpose of presenting this example is to demonstrate the effectiveness of the bad data identification procedure when applied to a portion of a network which is highlighted by dashed line in Fig. 4.3.

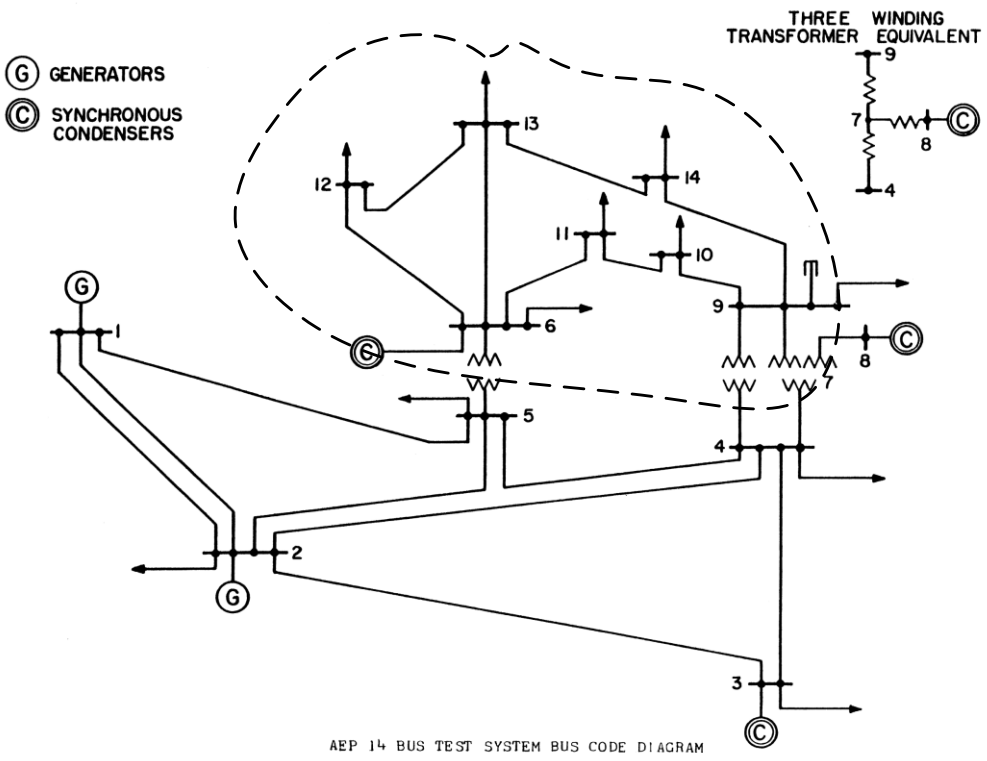

Fig. 4.3 14-bus system diagram [58]

For test purposes, the demand at bus 14 is decreased by 4.9 MW. The demands at the other buses remain the same. The active power flows on branch (6-5), (9-4) and (9-7) change due to the change of power injection at bus 14. As a result, for the area under study, power injection at bus 6 and 9 also change. In Table 4.7, the true values of elements in the injection change vector are listed in

the second column. The calculated values are listed in the third column. By comparison between the true values and the calculated ones, the differences are listed in the last column. The differences are small. It is concluded that the bad data detection and identification procedure is effective when applied in area portion of a network instead of a whole system.

Table 4.7 Comparison of calculated injection change vector and the true values (14 bus test bed)

Bus index	True values	Calculated results (without bad data)	$\lvert\Delta P_{inj\_true}-\Delta P_{inj\_cal}\rvert$ (MW)
	ΔP_{inj_true} (MW)	ΔP_{inj_cal} (MW)	
6	-2.237	-2.227	0.010
9	-2.792	-2.772	0.020
10	0	-0.016	0.016
11	0	-0.014	0.014
12	0	0.006	0.006
13	0	0.007	0.007
14	4.9	4.982	0.082

4.5 Conclusions

In this chapter, a bad data detection and identification procedure is developed based on the PTDF matrix. This procedure could be conveniently implemented in on-line analysis of PMU measurements. The procedure of bad data detection and identification helps to determine whether the system state changes reflected by PMU measurements are physical change or bad measurements. This procedure can be applied in the adaptive Kalman filter presented in the Chapter 3 to overcome the insensitivity of a regular Kalman filter. The effectiveness of the bad data detection and identification procedure is tested on the 9-bus and 14-bus systems. The 9-bus system is used as a test bed when the procedure is applied on

a whole system. The 14-bus system is used as a test bed when the procedure is applied on a portion of a whole system.

Chapter 5

BAD DATA DETECTION AND IDENTIFICATION BASED ON VOTING CRITERIA

5.1 The bad data detection and identification problem

In Chapter 4, a bad data detection and identification methodology is provided based on PTDFs. The assumption is that the number of PMUs installed in the network is sufficient to satisfy the redundancy requirement. In this chapter, a novel method is presented for bad data detection and identification of PMU measurements based on voting criteria. Under certain PMU installation scenarios, the topological relationship in the system could provide additional information that is helpful for bad data detection. This method could be applied under the condition that the redundancy requirement of PMU measurements is not satisfied to implement the bad data detection and identification procedure illustrated in Chapter 4. The proposed method is described in details in this chapter. Test cases are also provided to show the effectiveness of the method.

5.2 Physical topology of PMU installation

In electric power systems, the physical topology of PMU installation exists as shown in Fig. 5.1. There are two TLs with one common bus. Both ends of the TL have PMUs installed. Two PMUs are also installed at the common bus. The buses are labeled as bus *j*, bus *i*, and bus *k*, where the bus *i* is the common bus. The four PMUs are labeled as PMU 1 to PMU 4 from left to right.

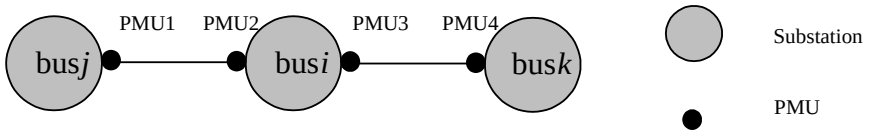

Fig. 5.1 Topology of two TLs with four PMUs

The PMUs can provide the voltage phasor measurements denoted by $v_i \angle \delta_i$ (i = 1, 2, 3, 4), where v_i is the voltage magnitude and δ_i is the voltage phase angle. The bus voltage magnitude varies relatively little to meet the requirements for assuring the safe and steady operation of the power systems. The bus voltage phase angle could vary when the system operating condition changes. In the subsequent discussion, the bus voltage phase angle is the system state of concern.

Suppose a change of bus voltage phase angle is observed. The change could be a bad measurement and the measurement should be discarded. However, if the change truly reflects the physical change of the system state, the measurement should be retained. For measurements from an individual PMU, it is difficult to determine whether a measurement is good or bad. The physical relationship between PMUs in the topology shown in Fig. 5.1 could provide useful information to evaluate the measurements from the four PMUs.

Variable A_i is a Boolean number to record the change observed from δ_i, where

$$A_i = \begin{cases} 1 \textit{ when a change is observed from } \delta_i \\ 0 \textit{ when no change is observed from } \delta_i \end{cases} \tag{5-1}$$

Consider the following cases:

Case a ($A_1 A_2 A_3 A_4$) = (0 0 0 0); No changes are observed from all the four PMUs. As a result, all the four bus voltage phase angle measurements are good.

Case b ($A_1 A_2 A_3 A_4$) = (1 0 0 0); A change is observed from δ_1, but no changes are observed from the other three PMUs. As a result, the possibility of δ_1 with error is high.

Case c ($A_1 A_2 A_3 A_4$) = (0 1 1 1); No change is observed from δ_1, but changes are observed from the other three PMUs. Similar to Case b, the possibility of δ_1 with error is high.

Table 5.1 lists all the possible cases when considering the changes of voltage phase angles observed from PMU measurements. The possible bad data source is also listed in the 3rd column. For cases 3, 4 and 5, it is difficult to determine the bad data source, but the bad data are identified. It is should be noted that, in real power systems, the possibility that there are bad measurements from two or more PMUs is small.

It is should be noted that the discussion above is the basic idea of how the physical relationship and placement of PMUs could help identify bad measurements. Considering the complexity of the power system network and the variation of operating conditions, it is possible there is no error in measurement from PMU 1 when ($A_1 A_2 A_3 A_4$) = (1 0 0 0).

Further details are needed to be considered when applying the idea to identify bad measurements based on the physical relationship between PMUs. First, a threshold needs to be set to define a change. The threshold should not be too conservative or too sensitive. Second, when changes of voltage phase angles

are observed from all the four PMUs, the reason for the change needs to be determined, i. e., actual change in the physical system or not.

Table 5.1 All possible cases of voltage phase angle changes observed from the four PMUs

Cases	*(A_1 A_2 A_3 A_4)*	*Possible error source*
1	(0 0 0 0) (1 1 1 1)	No error
2	(1 0 0 0) (0 1 1 1) (0 1 0 0) (1 0 1 1) (0 0 1 0) (1 1 0 1) (0 0 0 1) (1 1 1 0)	Error in PMU1 Error in PMU2 Error in PMU3 Error in PMU4
3	(0 0 1 1) (1 1 0 0)	Error in measurements
4	(0 1 0 1) (1 0 1 0)	Error in measurements
5	(1 0 0 1) (0 1 1 0)	Error in measurements

5.3 Identification of bad data based from power flow equations

In this subsection, a criterion based on the power flow equations is presented to evaluate and enhance the "accuracy" of PMU measurements based on physical topology. More accurate PMU measurements should be biased with heavy weights and less accurate PMU measurements should be biased with lower weights in further applications.

Fig. 5.2 shows the π-model of a medium length transmission line. Using the notation in the figure, $V_i = v_i \angle \delta_i$ and $V_j = v_j \angle \delta_j$, where v_i and v_j are the voltage magnitudes, δ_i and δ_j are the voltage phase angles. The admittance of the TL is denoted as Y_{ij} given by

$$Y_{ij} = y_{ij}\angle\theta_{ij} = \frac{1}{R + jX} \tag{5-2}$$

where R is the series resistance and X is the series reactance. This is a lumped parameter model.

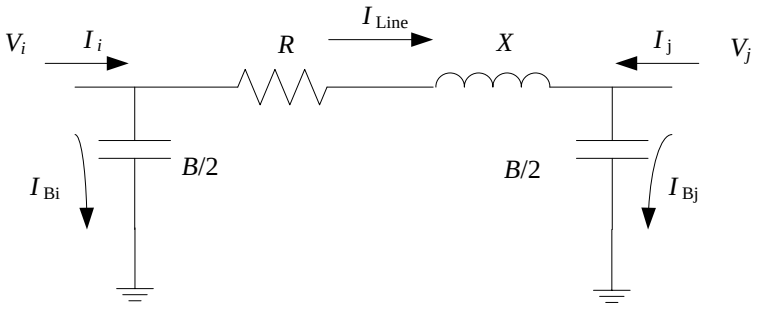

Fig. 5.2 Lumped π-model of a medium length transmission line

Based on Kirchhoff's circuit laws, the relationship between voltage, current and TL parameters is listed as follows,

$$I_{Line} = (V_i - V_j)Y_{ij} \tag{5-3}$$

The active power flow P_{ij} in the branch connected between bus i and j is written as

$$P_{ij} = \text{Re}(V_i I^*_{Line}) \tag{5-4}$$

where $Re(.)$ denotes the real part of a complex number, (*) denotes the complex conjugate of a complex number. Since the shunt resistance is neglected in the π-model, the real power P_{ij} could also be calculated by

$$P_{ij} = \text{Re}(V_i I_i^*) \tag{5-5}$$

Substituting (5-3) and the polar form of the bus voltages and admittance into (5-4), the real power flow P_{ij} is written as

$$P_{ij} = v_i^2 y_{ij} \cos\theta_{ij} - v_i v_j y_{ij} \cos(\delta_i - \delta_j - \theta_{ij}) \tag{5-6}$$

Using the Taylor series approximation around $\Delta\delta = 0$, ΔP_{ij} is written as

$$\Delta P_{ij} = \frac{\partial P_{ij}}{\partial \delta_i}\Delta\delta_i + \frac{\partial P_{ij}}{\partial \delta_j}\Delta\delta_j + \frac{\partial P_{ij}}{\partial v_i}\Delta v_i + \frac{\partial P_{ij}}{\partial v_j}\Delta v_j \tag{5-7}$$

Equation (5-7) is then written as

$$\Delta P_{ij} = a_{ij}\Delta\delta_i + b_{ij}\Delta\delta_j + c_{ij}\Delta v_i + d_{ij}\Delta v_j \tag{5-8}$$

where

$$a_{ij} = v_i v_j y_{ij} \sin(\delta_i - \delta_j - \theta_{ij}) \tag{5-9}$$

$$b_{ij} = -v_i v_j y_{ij} \sin(\delta_i - \delta_j - \theta_{ij}) \tag{5-10}$$

$$c_{ij} = 2v_i y_{ij} \cos\theta_{ij} - v_j y_{ij} \cos(\delta_i - \delta_j - \theta_{ij}) \tag{5-11}$$

$$d_{ij} = -v_i y_{ij} \cos(\delta_i - \delta_j - \theta_{ij}) \tag{5-12}$$

From (5-8) to (5-12),

$$\Delta P_{ij}^{'} = \Delta\delta^{'}{}_{ij} \tag{5-13}$$

where

$$\Delta\delta^{'}{}_{ij} = a_{ij}(\Delta\delta_i - \Delta\delta_j) \tag{5-14}$$

$$\Delta P_{ij}^{'} = \Delta P_{ij} - c_{ij}\Delta v_i - d_{ij}\Delta v_j \tag{5-15}$$

From (5-5), ΔP_{ij} could be directly calculated from the PMU measurements. The purpose is to check whether the observed voltage phase angle changes $\Delta\delta_i$ and $\Delta\delta_j$ are true or not. If both $\Delta\delta_i$ and $\Delta\delta_j$ are true, (5-13) holds. But if either $\Delta\delta_i$ or $\Delta\delta_j$ are corrupted, (5-13) does not hold.

As shown in Fig. 5.1, there are 3 buses and 4 PMUs. It is assumed that only one PMU measurement might be wrong, since the probability of two or more PMU measurements with errors is small. And the topology of the system does not change.

From Fig. 5.1, the following equations are obtained,

$$\begin{aligned}
\Delta P'_{ji} &= \Delta\delta'_{12} \\
\Delta P'_{ji} &= \Delta\delta'_{13} \\
\Delta P'_{ij} &= \Delta\delta'_{21} \\
\Delta P'_{ik} &= \Delta\delta'_{34} \\
\Delta P'_{ki} &= \Delta\delta'_{43} \\
\Delta P'_{ki} &= \Delta\delta'_{42}
\end{aligned} \tag{5-16}$$

The bad data detection and identification is based on a 'voting' criterion. If one of the equations in (5-16) does not hold, then both of the two voltage angle measurements involved get a vote for bad measurement. Check all the six equations in (5-16). The measurement with the largest number of votes would be considered as the candidate for a bad measurement. This makes sense considering the case that measurements from only one PMU are corrupted. Suppose there is an error in measurements from PMU 1 and measurements from the other three PMUs are good. As a result, the first three equations in (5-16) would not hold for the bad measurements from PMU 1. The last three equations in (5-16) hold. And the source of error could be identified. The error in other PMU measurements could be identified in a similar way.

5.4 Test case 1: no bad measurements

Data from 230 kV buses in a practical power system are used to test the effectiveness of the proposed method. In the practical power system, PMUs S19-S23, S23-S19, S23-S21, and S21-S19 are installed based on the topology shown in Fig. 5.1, and are labeled as PMU 1, 2, 3 and 4 respectively. Substation S19, S23, and S21 are denoted as substation *j*, *i* and *k* respectively. As discussed in the above subsection, the proposed method is used to identify bad data from PMU measurements.

The data are from different days and operating conditions which are indicated by the file IDs. The data file used is #1-4. Comparison between $\Delta P_{ij}^{'}$ and $\Delta \delta_{ij}^{'}$ in (5-13) is made. The calculation results of $\Delta P_{ij}^{'}$ and $\Delta \delta_{ij}^{'}$ in a time period of 3 minutes are shown in Fig. 5.3 and Fig. 5.4 respectively. Only measurements at the top of the seconds are used to avoid the impact of time skew between different PMUs.

From Fig. 5.3, it is observed that the active power variation is in a range of −0.5 MW to 0.5 MW. Fig. 5.5 shows the differences between $\Delta P_{ij}^{'}$ and $\Delta \delta_{ij}^{'}$. Thresholds of 1 MW and 5 MW are used to determine whether the differences are acceptable or not. If the absolute value of difference is in range [0, 1] MW, the PMU measurements involved get a good measurement ‘vote’. If the absolute value of difference is in range (0, 5] MW, the PMU measurements involved get a fair measurement ‘vote’. If the absolute value of difference is in range (5, ∞) MW, the PMU measurements involved get a bad measurement ‘vote’

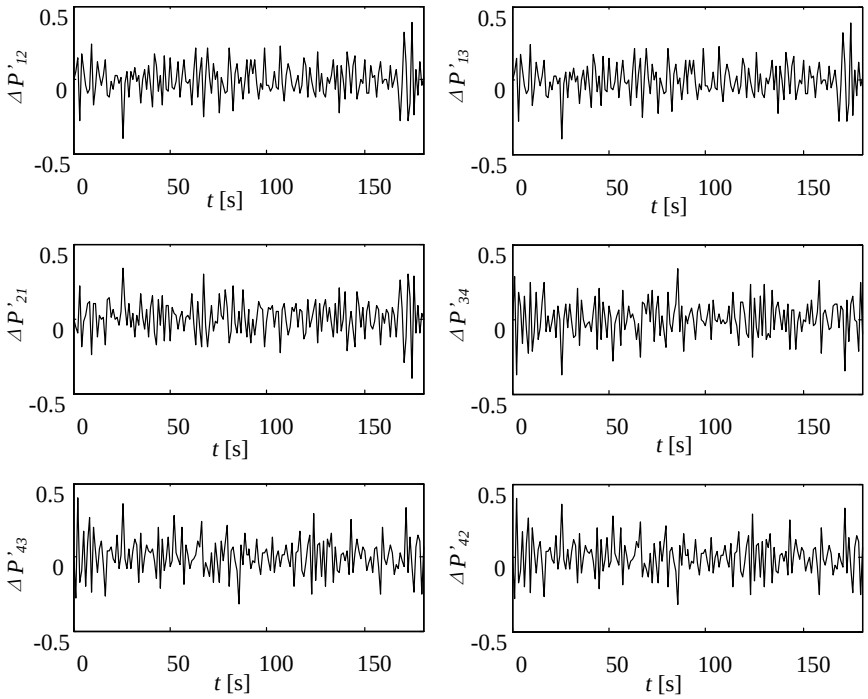

Fig. 5.3 $\Delta P_{ij}^{'}$ calculated from PMU measurements in topology S19-S23-S21 in a practical system (data file: #1-4)

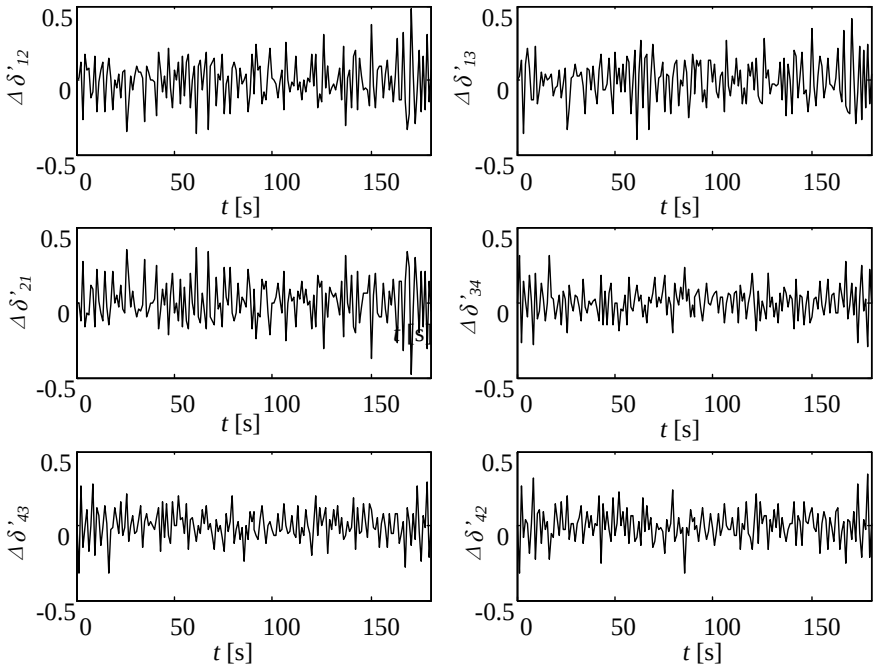

Fig. 5.4 $\Delta \delta_{ij}^{'}$ calculated from PMU measurements in topology S19-S23-S21 in a practical system (data file: #1-4)

From Fig. 5.5, all the differences are less than 1MW. As a result, it is concluded that all the measurements from the 4 PMUs in the data file are good measurements.

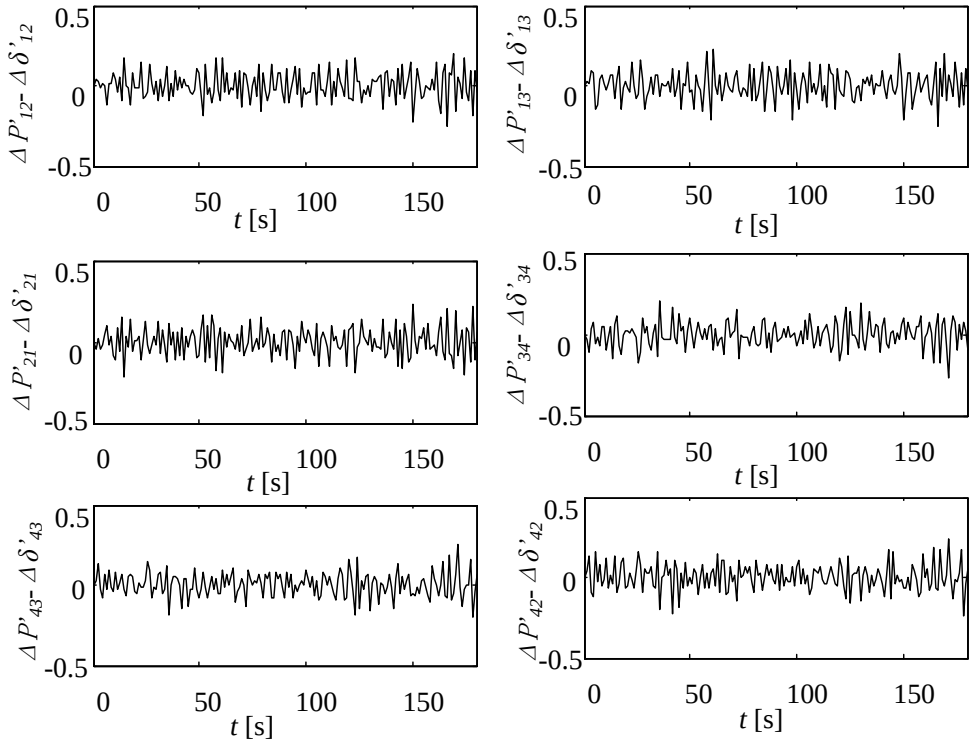

Fig. 5.5 Differences between $\Delta P_{ij}^{'}$ and $\Delta \delta_{ij}^{'}$ calculated from PMU measurements in topology S19-S23-S21 in a practical system (data file: #1-4)

5.5 Test case 2: identification of bad measurements

The data file used is #1-3 in this case study. Similar to case 1, Fig. 5.6 and Fig. 5.7 show the calculation results of $\Delta P_{ij}^{'}$ and $\Delta \delta_{ij}^{'}$. Fig. 5.8 shows the differences between $\Delta P_{ij}^{'}$ and $\Delta \delta_{ij}^{'}$. From Fig. 5.6, spikes are observed from all the curves of $\Delta P_{ij}^{'}$ at the 74th second. From Fig. 5.7, spikes are observed from all the curves of $\Delta \delta_{ij}^{'}$ at both the 74th and 152nd seconds. From Fig. 5.8, the measure-

ments from PMU 1 get three bad votes at the 152nd second for the differences are greater than 5 MW. It is concluded that the measurement at the 152nd second from PMU 1 is a bad measurement. Since spikes are observed at the 74th second from all curves of $\Delta P_{ij}^{'}$ and at both the 74th and 152nd seconds from curves of $\Delta \delta_{ij}^{'}$, Tables 5.2 and 5.3 list the specific values of $\Delta P_{ij}^{'}$ and $\Delta \delta_{ij}^{'}$ at the corresponding instant.

Table 5.2 $\Delta P_{ij}^{'}$ at the 74th and 152nd second in test case 2

Second	$\Delta P_{ji}^{'}$ (MW)	$\Delta P_{ij}^{'}$ (MW)	$\Delta P_{ik}^{'}$ (MW)	$\Delta P_{ki}^{'}$ (MW)
74th	1.8248	-1.8817	-0.7172	0.678
152nd	-0.0509	0.055	-0.0439	0.0231

Table 5.3 $\Delta \delta_{ij}^{'}$ at the 74th and 152nd second in test case 2

Second	$\Delta \delta_{12}^{'}$ (MW)	$\Delta \delta_{13}^{'}$ (MW)	$\Delta \delta_{21}^{'}$ (MW)	$\Delta \delta_{34}^{'}$ (MW)	$\Delta \delta_{43}^{'}$ (MW)	$\Delta \delta_{42}^{'}$ (MW)
74th	1.8584	1.8707	-1.859	-0.8257	0.8294	0.8209
152nd	12.4119	12.4332	-12.3994	-0.0311	0.0312	0

According to (5-16), the equations hold at the 74th second, but the first three equations do not hold at the 152nd second. Based on the voting criterion developed, the measurement from PMU 1 at the 152nd second is identified as a bad one.

Tables 5.4 and 5.5 list the raw voltage phase angle measurements from the 4 PMUs and the calculated phase angle changes around the 152nd second. It is not easy to identify the bad measurement from the raw phase angle measurements. From Table 5.5, there is about 0.2 degree error in δ_1.

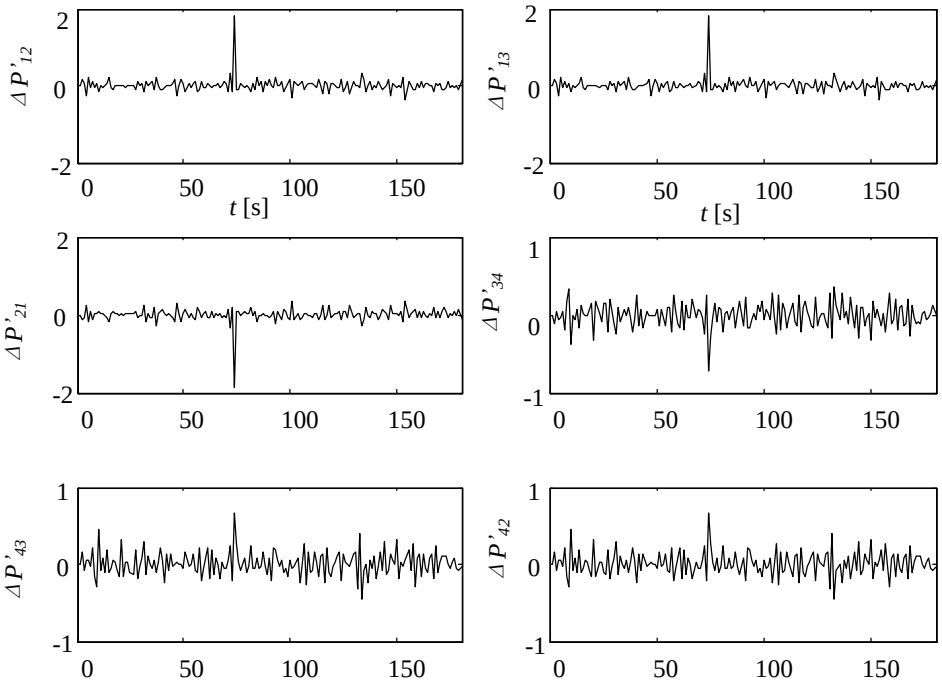

Fig. 5.6 $\Delta P_{ij}^{'}$ calculated from PMU measurements in topology S19-S23-S21 in a practical system (data file: #1-3)

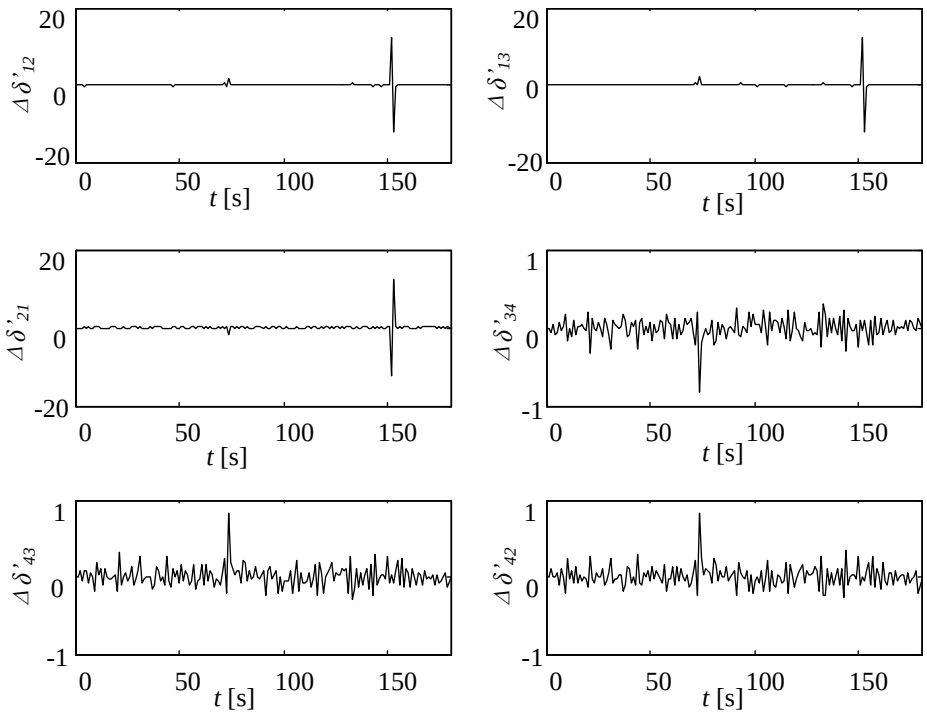

Fig. 5.7 $\Delta \delta_{ij}^{'}$ calculated from PMU measurements in topology S19-S23-S21 in a practical system (data file: #1-3)

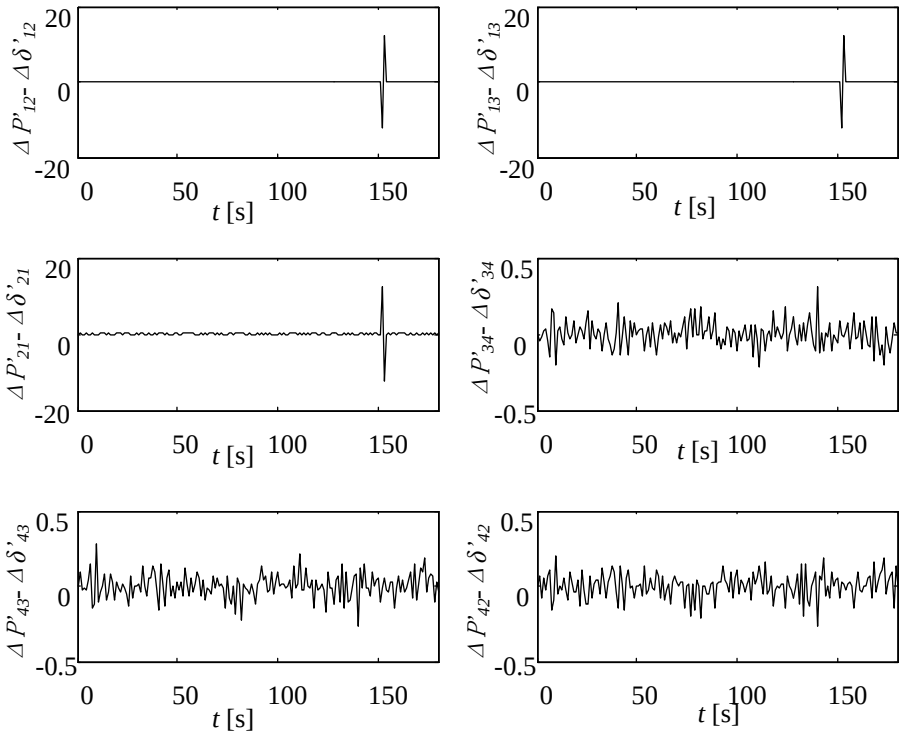

Fig. 5.8 Differences between $\Delta P_{ij}^{'}$ and $\Delta \delta_{ij}^{'}$ calculated from PMU measurements in topology S19-S23-S21 in a practical system (data file: #1-3)

Table 5.4 Raw voltage phase angle data from the 4 PMUs (data file: #1-3)

Second	δ_1 (Degrees)	δ_2 (Degrees)	δ_3 (Degrees)	δ_4 (Degrees)
150th	192.3771	192.4314	192.5104	193.3172
151st	185.729	185.7837	185.8619	186.6662
152nd	178.9147	178.7456	178.8229	179.6281
153rd	170.896	170.9468	171.0252	171.828

Table 5.5 Raw voltage phase angle changes from the 4 PMUs (data file: #1-3)

Second	$\Delta\delta_1$ (Degrees)	$\Delta\delta_2$ (Degrees)	$\Delta\delta_3$ (Degrees)	$\Delta\delta_4$ (Degrees)
150th	-6.1358	-6.1343	-6.1342	-6.1266
151st	-6.6481	-6.6477	-6.6485	-6.6510
152nd	-6.8143	-7.0381	-7.0390	-7.0381
153rd	-8.0187	-7.7988	-7.7977	-7.8001

5.6 Conclusions

In this chapter, a novel preprocessing method is presented to detect and identify bad measurements from PMUs which are closely related to the physical topology. For the specific PMU installation scenario, two transmission lines with a common bus are installed with 4 PMUs, two at the common bus and the other two at the other two ends. By deduction based on the lumped transmission line model, two deduced quantities, $\Delta P_{ij}^{'}$ and $\Delta \delta_{ij}^{'}$ should be equal. Several equations could be obtained in the specific PMU installation scenario. A voting procedure is developed to detect and identify bad data from the PMU measurements. Case studies based on real PMU data are presented to show the effectiveness of the proposed method. The preprocessing of PMU measurements would help to eliminate bad data.

Chapter 6

THE INTEGRATED CALIBRATION OF SYNCHRONIZED PHASOR MEASUREMENT DATA IN POWER TRANSMISSION SYSTEMS

6.1 Instrumentation accuracy

Measurements have become a key element of power system operation. Legacy systems are instrumented mainly utilizing potential and current transformers (PTs and CTs) and voltage, current, and power transducers. The accuracy of these measurements is largely determined by the accuracy of the sensory elements and the processing of the sensory data. As an example, the IEEE Standard 57.13-2008 [59] prescribes the accuracy (maximum error) of relaying class CTs as shown in Table 6.1and Table 6.2.

Table 6.1 Accuracy ratings for relaying class CTs [59]

Limits of ratio error relay class	*At rated current*	*At 20 times rated current*
C and T classification	3%	10%
X classification	1%	user defined

Table 6.2 Permissible error for power system instrument PTs [59]

Application	*Maximum error in ratio*	*Maximum error in phase*
Revenue metering	±0.1%	±0.9 mrad (3 min)
Other applications	±1.2%	±17.5 mrad (1 °)

Interestingly, the increase in the volume of measured data in power transmission systems may not be accompanied with an increase in accuracy and agreement of data from various sources. Anecdotally, power engineers indicate

that *planning data* and *operating data* often are disparate in the sense that impedance data, expected active and reactive power flows, and other key operating data may not agree as obtained from several different simultaneous measurements. The synchronization of measurements suggests that these data should agree quite well, but there are several factors that degrade agreement including:

- Faulty synchronization (e.g., errant clock signals)
- CT and PT calibration
- Misapplication of positive sequence data under unbalanced operation
- Bad data due to a range of issues including failure of the phase locked loop in the PMU to properly synchronize to the measured data
- Missing data / loss of the GPS signal at the PMU
- Incorrect CT or PT burden
- Effects of temperature
- Nonlinearities in the CT and PT and transducers
- Measurement noise.

In this chapter, integration of measurements and operations planning impedance data are applied to test the accuracy of raw PMU measurements. A novel calibration method is presented in order to match the PMU measurements and operations planning transmission line parameters. Different scenarios of PMU installation are studied. A real-time calibration process is proposed.

6.2 Integration of measurements and operations planning impedance data

The basic concept of integrating all available information to enhance power transmission operational measurements is exemplified by the inclusion of operations planning data into the measurement process.

A π-model of a long transmission line is shown in Fig. 6.1. The transmission line parameters are given by the following equations,

$$Z' = Z_c \sinh \gamma l = zl \frac{\sinh \gamma l}{l\sqrt{yz}} = Z \frac{\sinh \gamma l}{\gamma l} \tag{6-1}$$

$$\frac{Y'}{2} = \frac{1}{Z_c} \tanh(\frac{\gamma l}{2}) = \frac{yl}{2} \frac{\tanh(\gamma l / 2)}{(\gamma l / 2)} = \frac{Y}{2} \frac{\tanh(\gamma l / 2)}{(\gamma l / 2)} \tag{6-2}$$

$$Z_c = \sqrt{\frac{z}{y}} \tag{6-3}$$

$$\gamma = \sqrt{yz} \tag{6-4}$$

$$Z = zl \tag{6-5}$$

$$Y = yl \tag{6-6}$$

where z is the series impedance per unit length, y is the shunt admittance per unit length, l is the length of the transmission line, Z_c is called the characteristic impedance, γ is called the propagation constant, Z is the total impedance of the line, and Y is the total admittance of the line.

For small values of l, Z equals Z', and Y equals Y'. As a result, a lumped π-model shown in Fig. 6.2 could be used for a medium length TL. In the following study, a π-model (lumped) of a medium length TL with the associated planning data for the line can be utilized in conjunction with the measurement

system. It should be noted that for a long transmission line, a distributed parameter model should be used.

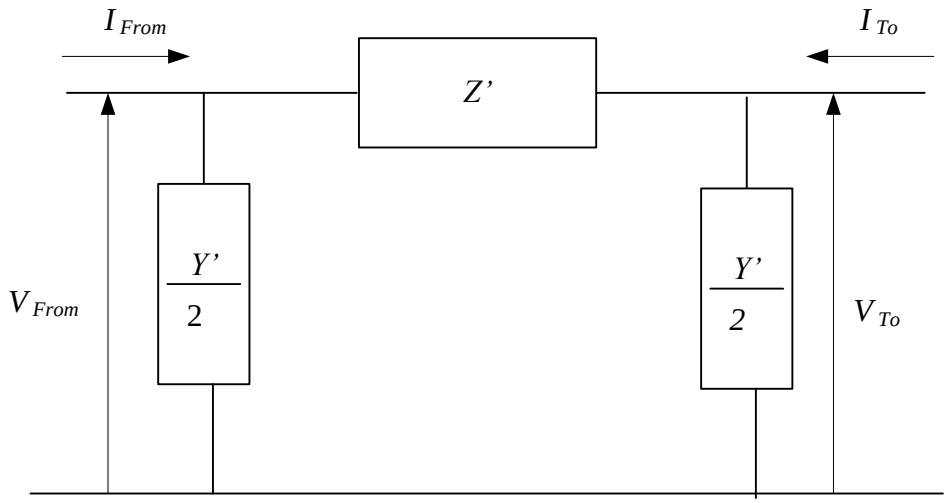

Fig. 6.1 π-model of a long transmission line with series line impedance and shunt admittances lumped

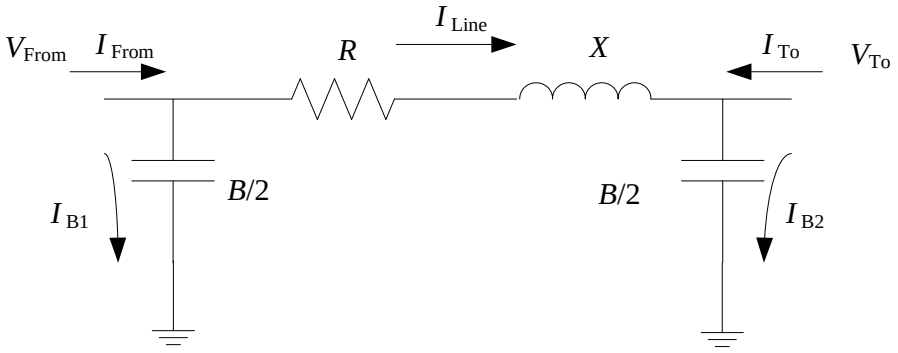

Fig. 6.2 π-model of a lumped transmission line

Based on the Kirchhoff's circuit laws, the relationships of voltage, current and TL parameters are listed as follows,

$$I_{Line} = \frac{V_{From} - V_{To}}{R + jX} \tag{6-7}$$

$$I_{From} = I_{Line} + I_{B1} \tag{6-8}$$

where $I_{B1} = V_{From} j\frac{B}{2}$. Also,

$$I_{To} = -(I_{Line} - I_{B2}) \tag{6-9}$$

where $I_{B2} = V_{To} j\frac{B}{2}$. From (6-7) - (6-9), $Z = R + jX$ and B could be calculated by the following formula,

$$Z = \frac{(V_{From} - V_{To})(V_{From} + V_{To})}{I_{From}V_{To} - I_{To}V_{From}} \tag{6-10}$$

$$j\frac{B}{2} = \frac{I_{From} + I_{To}}{V_{From} + V_{To}} \tag{6-11}$$

In order to calculate TL parameters, voltage and current at both ends of the TL are required. In the subsequent discussion, test cases based on different data files show that there are discrepancies between calculated TL constants evaluated from the raw PMU measurements as compared to those obtained from planning data. This was done for a test bed set of actual transmission lines under typical operating conditions. The data are from different days and operating conditions which are indicated by the file IDs. The TL names are denoted by the names of the two ends. The calculated impedances based on different time stamped data show substantial differences. For the TL S13 – S16, even negative resistances are calculated when using PMU data. This is unacceptable for practical TLs and indicates that there are errors in the voltage and current measurements from the

PMUs. The results for *R*, *X*, and *B*/2 calculations are shown in Table 6.3. Significant discrepancies are observed between the calculated impedance and the TL parameters from operations planning data. Also, the calculated impedances apparently vary as the operating conditions change.

At this point, *calibration* or *correction factors* (CFs) are introduced to calibrate each of the electrical current and voltage phasors measured. There could be errors both in magnitude and angle of synchrophasors. These CFs are complex quantities indicating correction of both magnitude and phase angle of the synchrophasor measurements. In the subsequent section, calculation and implementation of CFs are presented.

Table 6.3 Calculated impedance of TL S13 – S16

Data Source	*R* (Ω)	*X* (Ω)	*B*/2 (siemens)
*Power flow file	2.0367	17.7532	0.000117
#1-1	-7.2432	25.7345	0.000124
#1-2	-5.2347	30.0084	0.000123
#1-3	-15.5523	30.7044	0.000123
#2-1	-3.9426	21.5384	0.000125
#2-2	-4.0367	21.4644	0.000125
#3-1	-6.1083	23.0640	0.000124
#3-2	-9.2601	20.9250	0.000124

* TL parameters from operations planning data

6.3 Calibration using an integrated instrumentation approach

6.3.1 Calculation of correction factors

By comparing the impedances calculated from measurements and those obtained from the operations planning data, large discrepancies are observed for

all TLs with one PMU at each end. The mismatch relationship is expressed as inequalities,

$$I_{From\_M} \neq \frac{V_{From\_M} - V_{To\_M}}{R + jX} + V_{From\_M}\, jB_1 \tag{6-12}$$

$$I_{To\_M} \neq \frac{V_{To\_M} - V_{From\_M}}{R + jX} + V_{To\_M}\, jB_2 \tag{6-13}$$

where B_1 and B_2 denote the shunt susceptances at the FROM and TO ends of the TL respectively. The difference between the right and left hand sides of (6-12) and (6-13) are the mismatch. The subscript '*M*' indicates measurements from a PMU.

The inequalities (6-12) and (6-13) indicate that either there are errors in the PMU measurements or errors in the planning TL parameters or both. It is also possible that the circuit diagram assumed for the measurement and transmission line combination is erroneous. According to the results shown in Table 6.3, the calculated impedances change as the system operating conditions change. The differences between the calculated impedances based on different measurements made on different days are significant and deemed to be in disagreement.

In the following calibration process, the planning TL parameters are used. Using the notation in (6-12) and (6-13), four complex CFs are proposed to make the measurements match in the mean square sense after calibration. The CF is a complex number which indicates the errors in magnitude and phase angle of the voltage and current measurements from PMUs. By applying the CFs, the calibrated PMU measurements are obtained,

$$I_{From} = T_{I\_From} I_{From\_M} \tag{6-14}$$

$$I_{To} = T_{I\_To} I_{To\_M} \tag{6-15}$$

$$V_{From} = T_{V\_From} V_{From\_M} \tag{6-16}$$

$$V_{To} = T_{V\_To} V_{To\_M} \tag{6-17}$$

where T_{I_From}, T_{I_To}, T_{V_From} and T_{V_To} are the CFs, I_{From}, I_{To}, V_{From} and V_{To} are the calibrated PMU measurements. Equations (6-14) - (6-17) could be rewritten into the following form,

$$I_{From\_M} = T_{I\_From}^{-1} I_{From} \tag{6-18}$$

$$I_{To\_M} = T_{I\_To}^{-1} I_{To} \tag{6-19}$$

$$V_{From\_M} = T_{V\_From}^{-1} V_{From} \tag{6-20}$$

$$V_{To\_M} = T_{V\_To}^{-1} V_{To} \tag{6-21}$$

where $T_{I\_From}^{-1}$, $T_{I\_To}^{-1}$, $T_{V\_From}^{-1}$ and $T_{V\_To}^{-1}$ are the inverses of the CFs.

Based on Kirchhoff's circuit laws and complex power conservation laws, the following equations are used to solve for the CFs,

$$0 = I_{From} - \left(\frac{V_{From} - V_{To}}{R + jX} + V_{From} jB_1\right) \tag{6-22}$$

$$0 = I_{To} - \left(\frac{-V_{From} + V_{To}}{R + jX} + V_{To} jB_2\right) \tag{6-23}$$

$$0 = V_{From} I_{From}^{*} - V_{From} I_{Line}^{*} - V_{From} (V_{From} jB_1)^{*} \tag{6-24}$$

$$0 = V_{To} I_{To}^{*} - V_{To} (-I_{Line})^{*} - V_{To} (V_{To} jB_2)^{*} \tag{6-25}$$

where '*' indicates the complex conjugate of the corresponding element.

Equations (6-18) and (6-25) are written as the following function, where the inverses of CFs and the calibrated PMU measurements are the unknowns,

$$f_i(M, T_{inv}) = M_{rawi} \tag{6-26}$$

$$f_j(M, T_{inv}) = 0 \tag{6-27}$$

where $M = [\, I_{From},\ I_{To},\ V_{From},\ V_{To}\,]^t$, $T_{inv} = [\, T_{I\_From}^{-1},\ T_{I\_To}^{-1},\ T_{V\_From}^{-1},\ T_{V\_To}^{-1}\,]^t$, $M_{\text{raw}} = [\, I_{From\_M},\ I_{To\_M},\ V_{From\_M},\ V_{To\_M}\,]^t$, i = 1, 2, 3, 4, and j = 5, 6, 7, 8.

Equations (6-26) and (6-27) are denoted by a vector function F(X). The unknowns are $X = [\, x_1,\ \theta_1,\ x_2,\ \theta_2,\ \ldots,\ x_7,\ \theta_7,\ x_8,\ \theta_8\,]^t$, *where* $x_1 = Mag(I_{From})$, $\theta_1 = Angle(I_{From})$, $x_2 = Mag(I_{To})$, $\theta_2 = Angle(I_{To})$, $x_3 = Mag(V_{From})$, $= Angle(V_{From})$, $x_4 = Mag(V_{To})$, $\theta_4 = Angle(V_{To})$, $x_5 = Mag(T_{I\_From}^{-1})$, $\theta_5 = Angle(T_{I\_From}^{-1})$, $x_6 = Mag(T_{I\_To}^{-1})$, $\theta_6 = Angle(T_{I\_To}^{-1})$, $x_7 = Mag(T_{V\_From}^{-1})$, $\theta_7 = Angle(T_{V\_From}^{-1})$, $x_8 = Mag(T_{V\_To}^{-1})$, *and* $\theta_8 = Angle(T_{V\_To}^{-1})$. Define Mag(·) and Angle(·) as the functions to calculate the magnitude and angle of a complex number respectively, and denote angles in radians. The magnitude and angle of the unknowns in (6-26) and (6-27)are denoted with a subscript '*m*' and '*a*' respectively. Relating to I_{From} as an example, the parameter I_{From_m} is the magnitude of I_{From} and I_{From_a} is the angle of I_{From}.

In order to solve for the unknowns, $f_i(X)$ and $f_j(X)$ should be expanded into real and imaginary part respectively. There are 16 real valued functions. Define *Re*(·) and *Im*(·) as the real and imaginary part of a complex quantity. Then,

$$g_{2i-1}(X) = \mathrm{Re}(f_i(X)) = \mathrm{Re}(M_{rawi}) \tag{6-28}$$

$$g_{2i}(X) = \mathrm{Im}(f_i(X)) = \mathrm{Im}(M_{rawi}) \tag{6-29}$$

$$g_{2j-1}(X) = \mathrm{Re}(f_j(X)) = 0 \tag{6-30}$$

$$g_{2j}(X) = \mathrm{Im}(f_j(X)) = 0 \tag{6-31}$$

where i = 1, 2, 3, 4, and j = 5, 6, 7, 8.

The magnitudes of measurements from PMUs are assumed to be of high accuracy. As a result, the amplitude of CFs are expected to be unity. Only the constraints for the electrical current CFs are included. Two additional equations are added,

$$0 = Mag(T_{I\_From}^{-1}) - 1 \tag{6-32}$$

$$0 = Mag(T_{I\_To}^{-1}) - 1 \tag{6-33}$$

In summary, there are 16 real unknowns and 18 equations. It is an overdetermined problem. The equations are 'solved' by a least squares estimator. That is, the right and left hand side of the given 18 equations are made to agree in the least squares sense. Equations (6-28)- (6-33) are written in the following compact form,

$$Z = F(X) \tag{6-34}$$

where $Z = [Re(M_{raw1}), \cdots, Im(M_{raw4}), 0, \cdots, 0]^t$.

At this point, the Newton-Raphson method is used to solve (6-34), since these are nonlinear equations. The unknowns are solved by an iterative process: for iteration k+1, the results are updated by,

$$X_{k+1} = X_k - (J^T J)^{-1} J^T (F(X_k) - Z) \tag{6-35}$$

where J is the jacobian matrix of $F(X_k)$. The jacobian matrix in the $(k+1)^{th}$ iteration is given by

$$J = \frac{\partial F(X)}{\partial X} | X_k = \begin{bmatrix} \frac{\partial g_1}{\partial x_1} & \frac{\partial g_1}{\partial \theta_1} & \cdots & \frac{\partial g_1}{\partial x_8} & \frac{\partial g_1}{\partial \theta_8} \\ \frac{\partial g_2}{\partial x_1} & \frac{\partial g_2}{\partial \theta_1} & \cdots & \frac{\partial g_2}{\partial x_8} & \frac{\partial g_2}{\partial x_8} \\ \vdots & \vdots & \ddots & \vdots & \vdots \\ \frac{\partial g_{17}}{\partial x_1} & \frac{\partial g_{17}}{\partial \theta_1} & \cdots & \frac{\partial g_{17}}{\partial x_8} & \frac{\partial g_{17}}{\partial \theta_8} \\ \frac{\partial g_{18}}{\partial x_1} & \frac{\partial g_{18}}{\partial \theta_1} & \cdots & \frac{\partial g_{18}}{\partial x_8} & \frac{\partial g_{18}}{\partial \theta_8} \end{bmatrix} \tag{6-36}$$

The initial values of the calibrated PMU measurements are set to be equal to the raw PMU measurements. The initial values of elements in T_{inv} are set to be 1, i. e. [x_5^0, θ_5^0, x_6^0, θ_6^0, x_7^0, θ_7^0, x_8^0, θ_8^0] = [1 0 1 0 1 0 1 0]. After calculation, the calibrated PMU measurements and T_{inv} are obtained. The CFs are the inverses of T_{inv}.

In the discussion above, the basic idea of utilizing the least squares estimator and Newton-Raphson method to calculate the CFs is presented. The process considers only the case of one TL with one PMU at each end. Other equations could be developed in order to calculate CFs for additional PMU configurations. For example, if there are two PMUs at one substation, the voltage measurements made at a common bus utilizing different PMUs should be the same. Three cases are considered to test the proposed correction factors based on the availability of raw PMU measurements.

6.3.2 Description of cases under study

In the following discussion, three cases are considered. For the purpose of clear identification, the description of cases under study is listed in Table 6.4.

Table 6.4 Summary of cases under study

Case ID	Case description
Case 1	A single three phase transmission line with PMUs at both terminals, as shown in Fig. 6.3.
Case 2	Two transmission lines with four PMUs installed. Two PMUs are installed at the common bus, as shown in Fig. 6.5.
Case 3	One transmission lines with one PMU installed at one end, and with another PMU at the other end which could provide voltage phasor measurements, as shown in Fig. 6.9.

6.3.3 Case 1

In this case, both ends of the TL are installed with PMUs, as shown in Fig. 6.3. A practical example is given to show the effectiveness of CFs. The TL is denoted by S13 – S16.

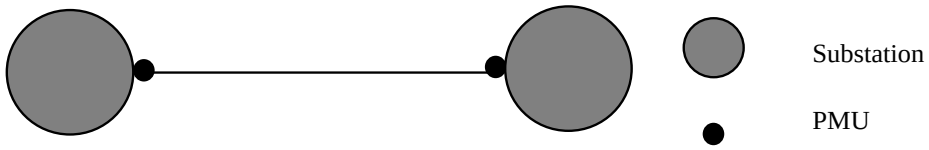

Fig. 6.3 Transmission line with two PMUs (Case 1)

In order to check the effectiveness of CFs, the following criteria are used: the active and reactive power mismatch are defined as,

$$P_{mis} = P_{From} + P_{To} - P_{loss} \tag{6-37}$$

$$Q_{mis} = Q_{From} + Q_{To} + V_{From} V_{From}^{*} B_1 + V_{To} V_{To}^{*} B_2 - Q_{loss} \tag{6-38}$$

where $P_{From} = Re(V_{From})$, $Q_{From} = Im(V_{From}\, I_{From}^{*}\, I_{From}^{*})$, $P_{To} = Re(V_{To})$, $Q_{To} = Im(V_{To}\, I_{To}^{*})$, $P_{loss} = I_{Line}\, I_{Line}^{*} R$, and $Q_{loss} = I_{Line}\, I_{Line}^{*} X$. Under ideal conditions

when the measurements and the TL parameters are accurate, P_{mis} and Q_{mis} should be zero. In the case where the CFs are not used, P_{mis} and Q_{mis} are nonzero. The absolute values of P_{mis} and Q_{mis} provide an effective approach to check whether the measurements are accurate or not. In Table 6.5, power mismatches of TL S13-S16 are listed. According to the criteria proposed in the above discussion, once the CFs are applied to the measurements, the calculated power mismatches should be zero. From Table 6.5, it is evident that the mismatches after calibration are zero. Fig. 6.4 shows the power mismatch with and without calibration. The upper plot is for active power and the lower plot for reactive power. The upper curves are the mismatches with calibration. By comparison, the calibrated measurements and the TL parameters match well.

It should be pointed out that all the CFs calculations are based on a single set of measurements at the same instant. The characteristics of CFs for a certain time duration are presented in the subsequent section.

Table 6.5 Comparison of power mismatch before and after calibration for Case 1 (TL S13 – S16)

Files ID	P_{mis_before} (MW)	Q_{mis_before} (MVAr)	P_{mis_after} (MW)	Q_{mis_after} (MVAr)
#1-1	-0.39822	-0.57087	3.6727e-10	6.9655e-10
#1-2	-0.31651	-0.58937	1.9001e-8	1.2559e-8
#1-3	-0.31908	-0.51865	-1.6938e-11	3.9069e-11
#2-5	-0.60784	-0.62742	-3.3945e-6	9.1588e-7

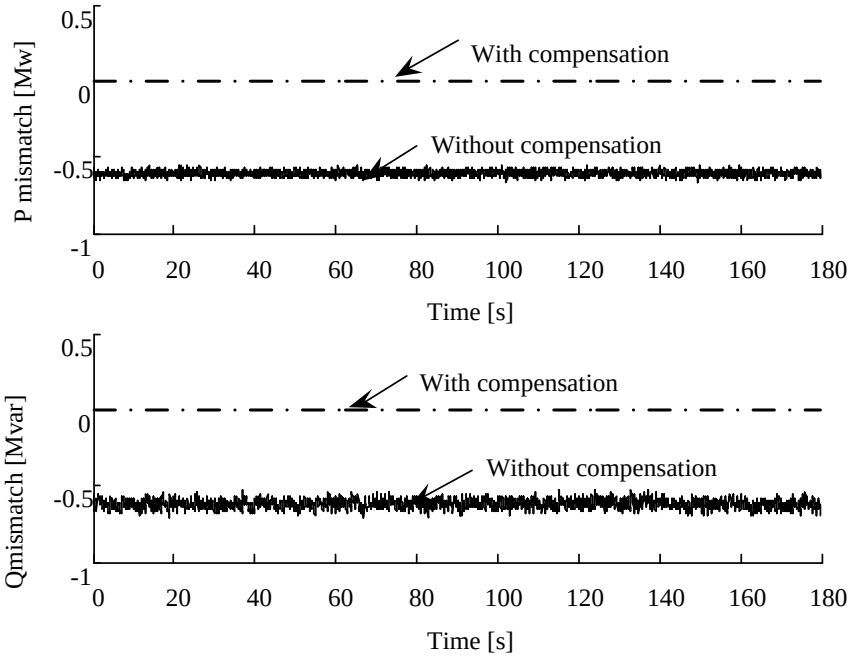

Fig. 6.4 Active and reactive power mismatch (TL S13 – S16 at 230 kV voltage level) in 3 minutes for Case 1 (data file #2-5)

6.3.4 Case 2

Fig. 6.5 shows another topology of a PMU installation. In Case 2, there are two TLs with four PMUs. The voltage measurements of the bus with two PMUs should be the same.

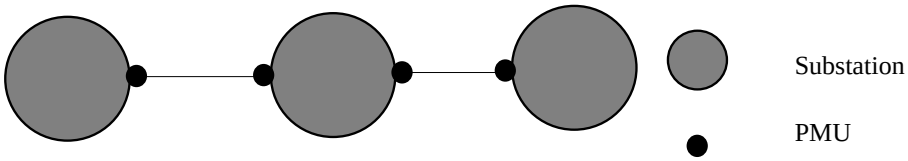

Fig. 6.5 Two transmission lines with four PMUs (Case 2)

In Case 2, except for the equations corresponding to (6-26) and (6-27) for each TL respectively, the analysis is similar. There is an added condition in Case 2 because of the common bus at which voltage is measured,

$$V_1 - V_2 = 0 \tag{6-39}$$

In (6-39), V_1 and V_2 are the calibrated voltage measurements of the two PMUs at the same bus. Similar to (6-26) and (6-27), expand (6-39) into real and imaginary parts; and then take the derivative with respect to the unknowns to form the jacobian matrix. For this case, there are 32 real unknowns, and the order of the jacobian matrix is 38 by 32.

In a practical example, consider two TLs denominated S19 – S23 and S21 – S23 respectively. Bus S24 is the location with two PMUs. Fig. 6.6 and Fig. 6.7 show the active and reactive power mismatches in an interval of 3 minutes for TL S19 – S23 and S21 – S23 respectively.

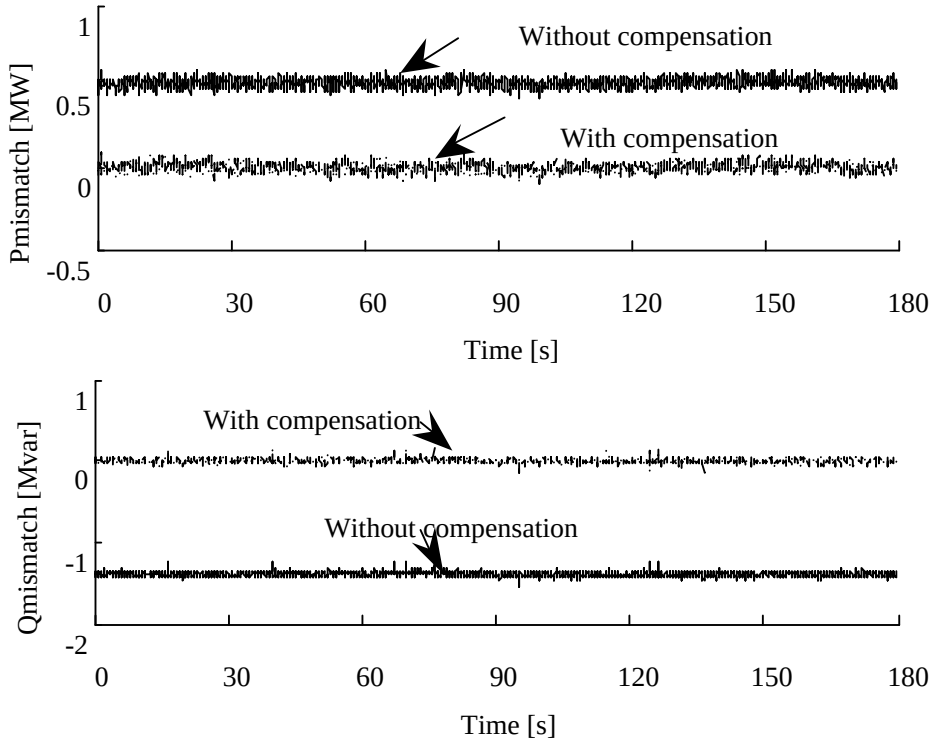

Fig. 6.6 Curves of power mismatch (TL S19 – S23) for Case 2 over 3 minutes (data file #1-4)

Table 6.6 provides the summary of the comparison of voltage differences from the two PMUs. The rated voltage at bus S23 is 230 kV. Without calibration, the voltage magnitude mismatches are in the range of 300 to 400 V and the voltage angle mismatches in the range of 0.1 degree. With calibration, the differences are negligible. Fig. 6.8 shows the voltage differences between the measurements with and without calibration. The upper trace in Fig. 6.8 shows the magnitude, and the lower graph shows the phase angle differences.

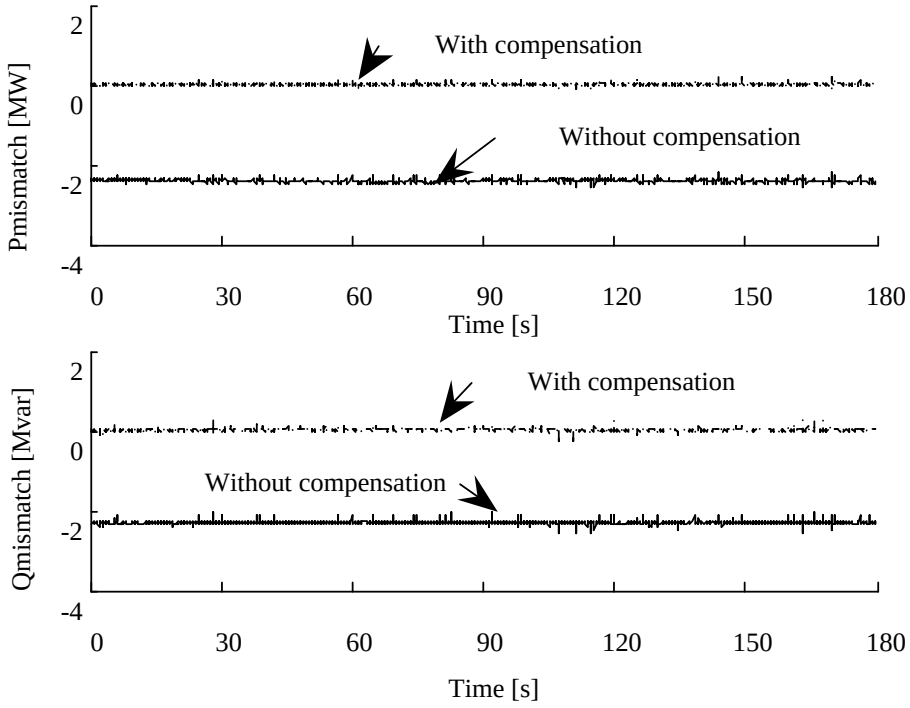

Fig. 6.7 Active and reactive power mismatch (in TL S21 – S23) for Case 2 with data taken over3 minutes (data file #1-4)

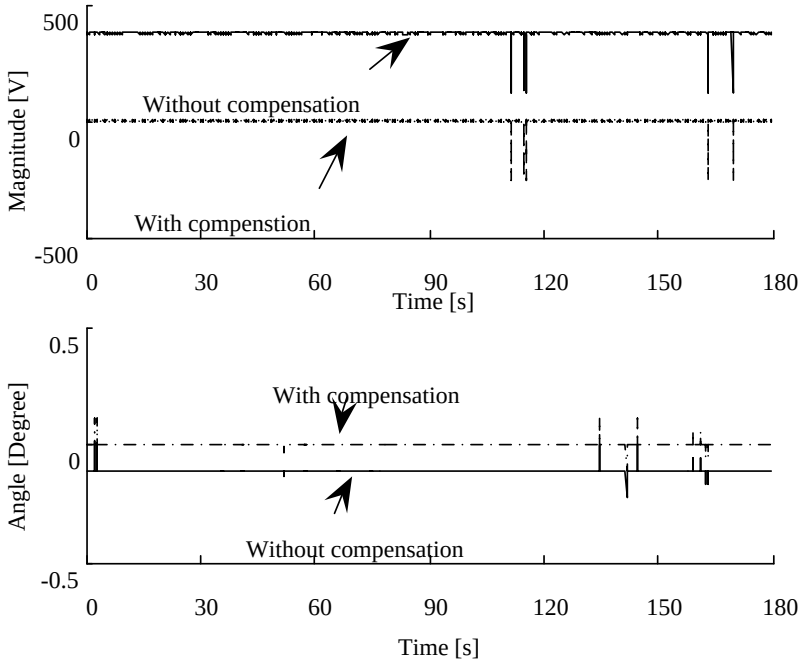

Fig. 6.8 Voltage measurement difference between two PMUs for Case 2 at bus S23 for a 3 minute interval (data file #1-4)

Table 6.6 Comparison of voltage measurements for case 2 at one bus from two PMUs (at Bus S23)

File ID	$V_{m\_Diff\_before}$ (V)	$V_{a\_Diff\_before}$ (Degrees)	$V_{m\_Diff\_after}$ (V)	$V_{a\_Diff\_after}$ (Degrees)
#1-1	299.979914	-0.082147	-7.3051e-11	1.2551e-11
#1-2	341.895865	-0.096967	0.000207	0.019939
#1-3	288.080683	-0.078402	-3.6481e-7	0.039437
#1-4	377.477521	-0.111347	-7.3450e-9	0.019719

6.3.5 Case 3

In Fig. 6.9, the TL shown has only one PMU located at one end. At the other end, there is no PMU for the TL, but the PMU at the other TL could provide a voltage measurement. There are three raw PMU measurements and 3 CFs. The electrical current at the end without PMU is treated as an unknown. In this con-

figuration, the total number of real unknowns is 14. The order of the jacobian matrix is 15 by 14.

In a practical example of Case 3, the TL S3 – S16 has one PMU at bus S3. Only the voltage measurement from PMU at Bus L is used in the calculation, and only the voltage CF is calculated. When calculating the power mismatch, the calculated current is used for bus L to obtain the injected power. Fig. 6.10 shows the active and reactive power mismatch during a certain period of 3 minutes.

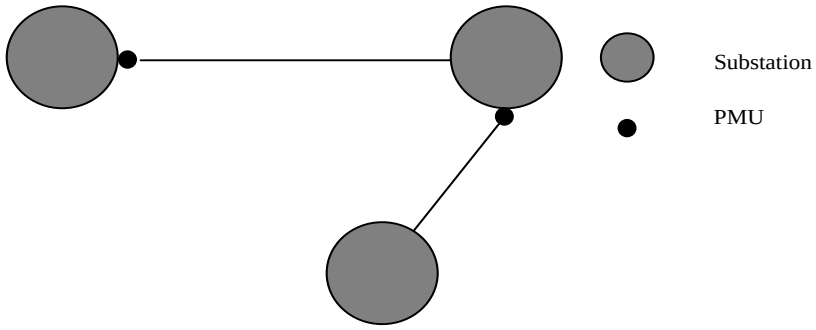

Fig. 6.9 One transmission line with one PMU (Case 3)

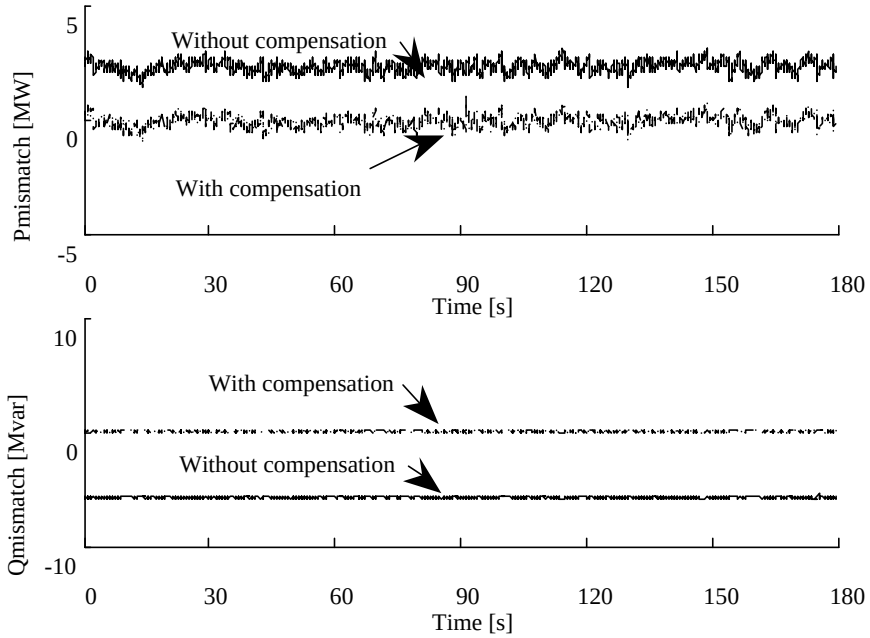

Fig. 6.10 Active and reactive power mismatch (TL S3 – S16) for Case 3 over 3 minutes (data file #2-5)

6.3.6 Other possible cases

There are a wide variety of possible PMU and bus configurations. As a final example, consider the configuration in which more than four PMUs are involved in the calibration process. As shown in Fig. 6.11, there are *N* TLs with 2(*N*-1) PMUs. For two PMUs at the same bus, (6-36) could be used to deal with the voltage measurements from the two PMUs at the same substation. All CFs can be calculated simultaneously. If there are more than two PMUs at one bus, as in the case of the radial structure shown in Fig. 6.12, a similar process could be applied to calibrate all the PMUs simultaneously. In summary, by applying CFs, the calibrated PMU measurements and the TL parameters match well. The power mismatches are zero in all three cases of different PMU installation.

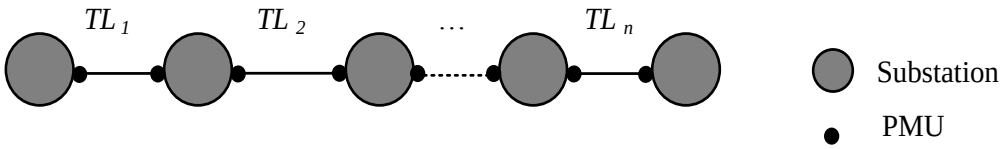

Fig. 6.11 *N* transmission lines with (2N-2) PMUs in chain structure

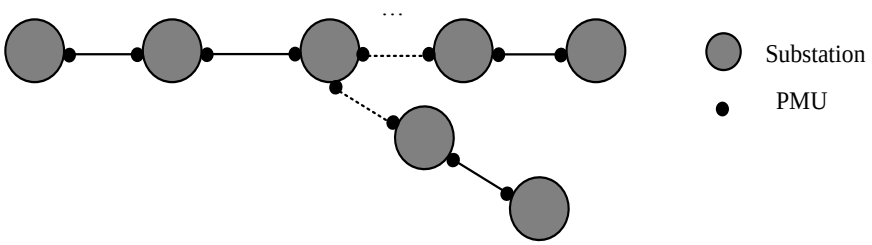

Fig. 6.12 Transmission lines with PMUs in a radial structure

6.4 Implementation of correction factors

6.4.1 Characteristics of correction factors

In this section, the characteristics of CFs are presented. All the calculations of CFs are based on the measurements at the same instant. It is meaningful

to explore the characteristics of CFs in order to calibrate the PMU measurements. The proposed idea calibrates the PMU measurements in real time using CFs based on previous measurements.

The magnitudes of both current and voltage CFs in a certain time period do not change. But the angles of the CFs are different for measurements taken at different instants. Fig. 6.13 shows the angles of current and voltage CFs in a period of 3 minutes. The total number of measurements is 5400. It is observed that the angles of CFs are not constant. By comparison, the angles of voltage CFs vary around a specific value, while the angles of electrical current CFs vary greatly. In Table 6.7 and Table 6.8, the mean values and standard deviations of the phase angles of CFs for measurements in different data files are listed.

Table 6.7 Mean values of phase angle of CFs (TL S13 – S16) in Case 1

File ID	$mean(T_{i1\_a})$ (Degrees)	$mean(T_{i2\_a})$ (Degrees)	$mean(T_{v1\_a})$ (Degrees)	$mean(T_{v1\_a})$ (Degrees)
#1-1	0.097409	-0.59271	0.121766	-0.12908
#1-2	1.081243	0.273868	0.130027	-0.13793
#1-3	-0.31134	-1.39308	0.141845	-0.14889
#2-5	0.023247	-0.4265	0.083277	-0.08949

Table 6.8 Standard deviations of phase angle of CFs (TL S13 – S16) in Case 1

File ID	$Std(T_{i1\_a})$ (Degrees)	$Std(T_{i2\_a})$ (Degrees)	$Std(T_{v1\_a})$ (Degrees)	$Std(T_{v1\_a})$ (Degrees)
#1-1	0.225921	0.213653	0.014263	0.014893
#1-2	0.289362	0.249809	0.00995	0.010552
#1-3	0.234668	0.216339	0.010629	0.011094
#2-5	0.229699	0.222982	0.008461	0.009135

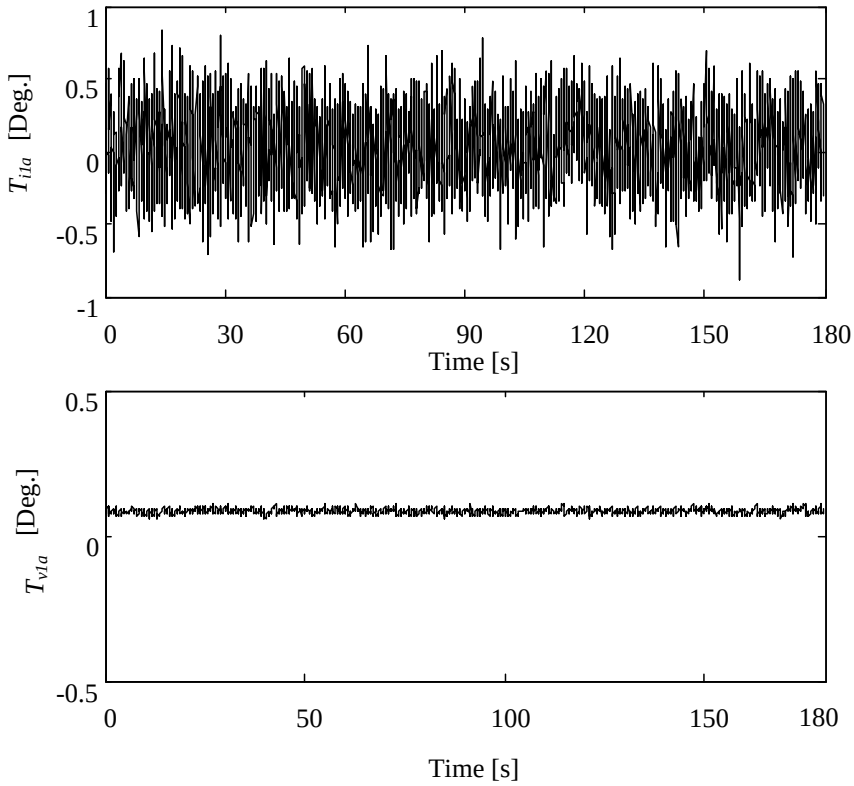

Fig. 6.13 Phase angles of current and voltage CFs for PMU 12 (data file #2-5)

As shown in Table 6.8, the standard deviations of voltage phase angle CFs are small, while the standard deviations of electrical current phase angle CFs are large. As a result, the calculated voltage CFs could be used to calibrate voltage measurements in the subsequent time period. For a TL, when the voltages at both ends and the TL constants are known, it is easy to calculate the required information, such as currents and power flow.

6.4.2 Implementation of correction factors

Fig. 6.14 shows a diagram which describes how CFs are applied. A time window is introduced which is the time duration for executing the calibration process using CFs. As the calibration process begins, voltage CFs based on raw PMU measurements in Window 0 are obtained. The mean voltage CFs of meas-

urements in Window 0 is used to calibrate measurements in Window 1. For measurements in Window 1, calibrated PMU measurements are obtained using the CFs from Window 0. Subsequently, CFs are also calculated from measurements in Window 1 in Window 2. The calibration process would continue using this sliding window approach.

In the practical case, the length of the time window is 2 seconds. There are 60 measurements in the time window. Comparison of the angle difference across the TL shows the implementation of CFs. Angle differences based on raw PMU measurements are denoted as A_{bf}. Angle differences based on calibrated PMU measurements using CFs at each instant are denoted as A_{af}. Angle differences based on calibrated PMU measurements using the CFs from previous time window are denoted as A_{win}. In Fig. 6.15, plots of A_{bf}, A_{af} and A_{win} are shown respectively. The plot of A_{af} is smoother than that of A_{bf} and A_{win}. The plot of A_{win} maintains the shape and changing trend of A_{bf}. In Fig. 6.16, plots of A_{bf}, A_{af} and A_{win} are shown in the same upper graph. The plot of A_{af} cannot be seen for it is covered (over-plotted) by that of A_{win}. Partial curves of A_{af} and A_{win} are magnified for a better display. The differences between A_{af} and A_{win} are shown in the lower graph. It is observed that the differences between A_{af} and A_{win} are in an acceptable range.

The proposed calibration process is meaningful for the applications of PMU measurements in power systems. The calibrated voltage phasor measurements provide a more accurate snapshot of the system state. Accurate measurements are the basis of applications which require high precision data, such as state

estimation and transient instability monitoring. The calibration process could be implemented in real-time.

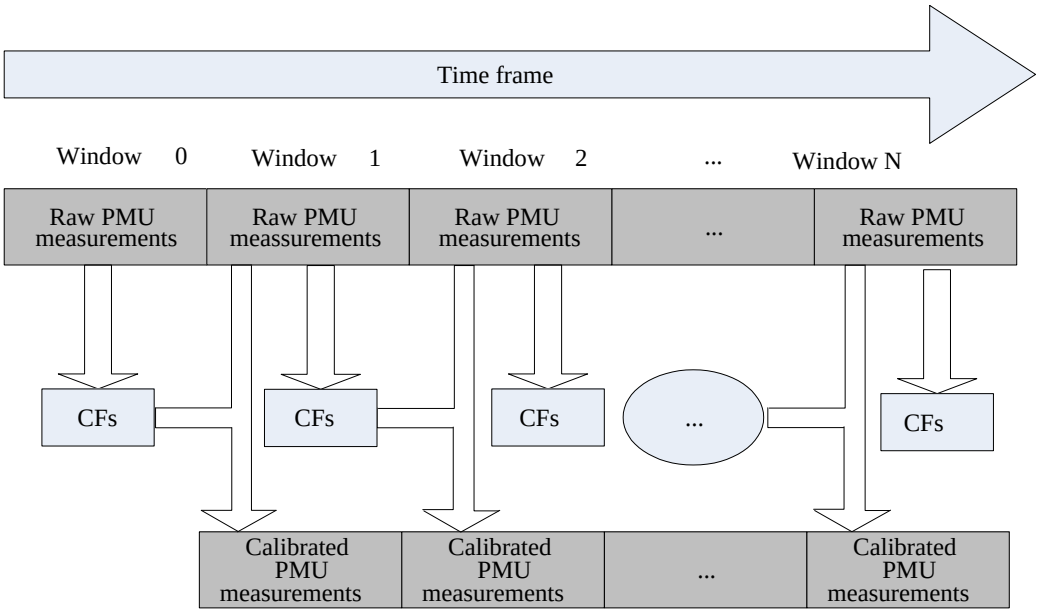

Fig. 6.14 Diagram showing implementation of correction factors

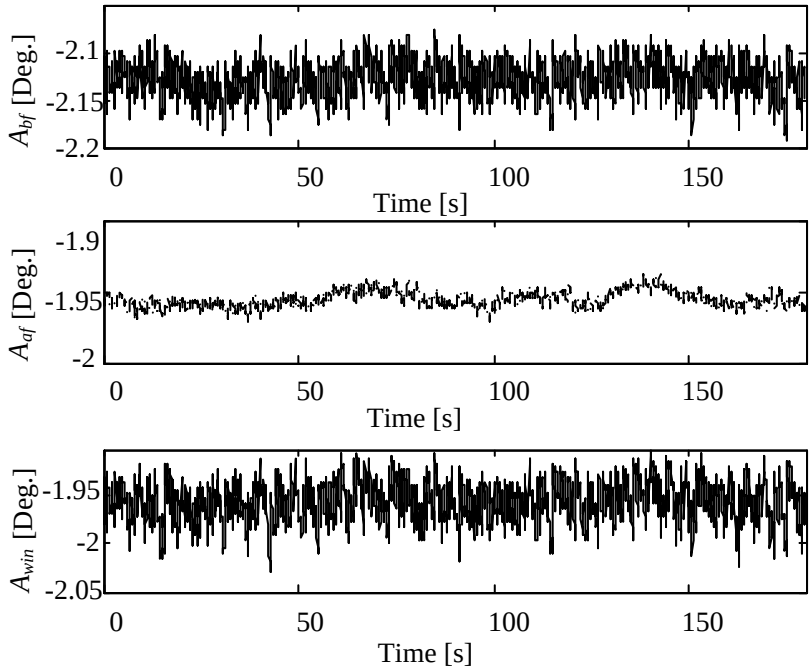

Fig. 6.15 Angle differences across TL S13 – S16 (data file #2-5) in Case 1

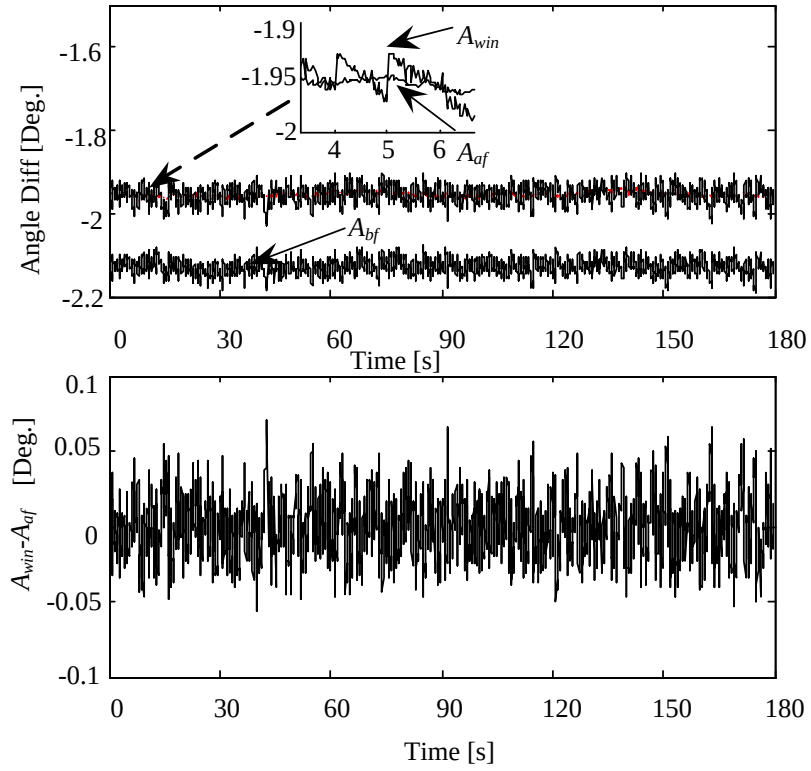

Fig. 6.16 Phase angle differences across TL S13 – S16 (data file #2-5) (above); difference between A_{win} and A_{af} (below) in Case 1

6.5 Conclusions

The research in this chapter deals with the error, accuracy and validation of PMU measurements from a practical electric power system. Data from operations planning cases are integrated with measurements taken during actual operation. In order to utilize PMU measurements in system control, validation of the data from PMUs is required. The calculated TL impedance based on the raw measurements from PMUs shows big difference from TL parameters from planning data. Correction factors are introduced to calibrate the current and voltage measurements. The CFs are complex quantities which indicate possible error in the magnitude and angle of the measurements. Three different cases are considered to calculate the CFs. By analyzing the characteristics of CFs, a novel cali-

bration process of PMU measurements is proposed which is applicable in real-time power system operation.

The accuracy of PMU measurements is an important issue in power system operation. Further work is needed to test the effectiveness of CFs at a system level rather than only considering a simple single TL model. More information is needed to accomplish this goal (e.g., active and reactive power measurements from SCADA system). Specific sources of errors in PMU measurements indicated by CFs need to be identified. Simulation of the instrumentation channel would be helpful to determine the possible errors introduced by the instrumentation channel.

Chapter 7

IMPACT OF PMU MEASUREMENT BUFFER LENGTH ON STATE ESTIMATION AND ITS OPTIMIZATION

7.1 The role of PMU measurements in state estimation

State estimation is a key function in the energy management system for the secure operation of power systems. State estimation is commonly formulated as a weighted least squares (WLS) problem to obtain the best estimate of system states based on a set of measurements and assumed system configuration [4]. The conventional measurements obtained from the SCADA system for the state estimator include branch flows, power injections and voltage and current magnitudes. A time skew problem has long been observed in SCADA data which are assumed to be taken from the same snapshot of a power system, and time skew in measurements has an impact on the accuracy of the state estimation [60]. PMUs could provide the voltage and current phasor with time stamps utilizing synchronized measurement technology. The synchronized PMU measurements are superior to the conventional measurements in terms of resolution and accuracy. Currently, incorporating PMU measurements into the traditional state estimator is being studied since the number of PMUs installed in various systems is not sufficient to solve the state estimation problem by exclusively using PMU measurements.

However, the PMU measurements are not free of measurement errors, time stamp error and noise. The major source of the errors in PMU measurements is due to the instrumentation channel, comprised of the instrument transformer, the A/D converters, and the communication channel which connects these com-

ponents. The error due to the instrumentation channel is systematic and could be corrected by the correction factors proposed in [61].

In order to effectuate the most likely state estimate, the measurement weights in state estimation are determined by the corresponding elements in the error covariance matrix. A tuning process to determine the weights for PMU measurements is provided in [62]. The method assumes that only one measurement from one PMU is processed together with other conventional measurements. In practical systems, the reporting rate of PMU measurements is much higher than that of convention measurements. If a buffer of PMU measurements is utilized (i.e., a memory buffer of length N_{bl}), the variance of the PMU measurements could be directly calculated. As for the noise in the PMU measurements which is a random process and needs to be modeled accordingly, noise is generally assumed to be normally distributed with zero mean. In this sense, more measurements should be included to yield best estimate of the 'true' value of the state when the system is static. However, power systems are never truly stationary or static. The more measurements that are included, the larger is the deviation that would result due to system dynamics. These competing aspects raise the question of how to choose the buffer length of the PMU measurements in preprocessing state estimation. The first aspect is referred to as uncertainty due to the noise in the measurements. The second aspect is referred to as variation of data due to the change in the system dynamic states. In this chapter, the importance of insuring a good tradeoff between these two aspects is illustrated and an approach is proposed

to determine the optimal buffer length. In the discussion that follows, it is assumed that the bad data have been removed from the raw PMU measurements.

7.2 Statistical description of the PMU measurements

The PMU measurements are not deterministic in nature for they are not exactly predicable. If the system is assumed to be static, only noise in the measurements is considered. The description of one measurement from one PMU, which measures directly the voltage magnitude or angle i.e., one state variable, at a certain instant t_1 is as follows,

$$Z_i(t_1) = X_i(t_1) + v_i(t_1) \tag{7-1}$$

where Z_i is a PMU measurement at bus i, X_i is the system state component at bus i (voltage magnitude or angle), and v_i is the PMU noise. The noise is assumed to be normally distributed with zero mean and standard deviation σ. In this model, the system state and the standard deviation σ of the noise are unknown. In order to estimate the system state, an ensemble of measurements from many 'identical' PMUs installed at the same substation at t_1 is required. In practical systems, such an ensemble of measurements is not usually available. In most cases, there is only one PMU installed at a substation.

The PMU measurements series is a set of random variables as described in (7-1). If a random process is ergodic, the time average is equivalent to the ensemble average. In this case, a single-sample time signal of the process could be used to estimate the system state utilizing straightforward statistical methods. Consider N measurements under static operating conditions. The mean $\hat{\mu}_z$ of the

random variable Z is usually estimated by the average of the sample, which is the maximum likelihood estimator of μ_x under the assumption of independently and identically distributed (i.i.d.) noise observations. Under this realistic assumption the estimator is asymptotically efficient and consistent [63]. The sample mean is

$$\hat{\mu}_z = \frac{1}{N}\sum_{i=1}^{N} Z_i \tag{7-2}$$

where $Z(t_i)$ is denoted as Z_i for compactness. The variance of the estimated mean is

$$\mathrm{var}(\hat{\mu}_z) = \frac{1}{N^2}\sum_{i=1}^{N} \mathrm{var}(Z_i) = \frac{\sigma^2}{N} \tag{7-3}$$

From (7-3), the variance of the estimated mean will usually decrease when more measurements are used.

Ergodicity and stationarity should be tested before a PMU measurement (which is a single-sample time signal in most cases) is used. In practice, power systems are never strictly static or stationary. The system states vary due to changing operating conditions. Consider the PMU measurements in one second. Suppose the reporting rate is n samples per second. The measurement series is denoted by $z = [z_1, z_2, \cdots, z_n]$. The following equations describe the measurements in a one second interval,

$$\begin{aligned} z_1 &= x_1 + v_1 \\ z_2 &= x_1 + \Delta x_2 + v_2 \\ &\cdots \\ z_n &= x_1 + \Delta x_n + v_n \end{aligned} \tag{7-4}$$

where x_1 is the system state at the top of the second, $\Delta x = [\Delta x_2, \Delta x_3, \cdots, \Delta x_n]^T$ is the change of the system state compared with x_1. The vector Δx is a random process. It is difficult to describe Δx in a probabilistic sense because the change of operating conditions is generally difficult to predict.

7.3 State estimation

Static state estimation is applied to process a set of measurements to obtain the best estimate of the system states in a least square sense. The equations relating the measurements *z* and the state vector *x* are

$$z = h(x) + e \tag{7-5}$$

where *z* is the measurement vector, *e* is the measurement error vector and $h(x)$ are functions of the system states *x*. The covariance matrix of *e* is denoted as *R*.

Since the stated formulation (7-5) is nonlinear, linearization of the function $h(x)$ is used and the resulting linear state estimation is formulated as a weighted least square (WLS) problem. This is solved by an iterative scheme changing the point of linearization as needed. In the k^{th} iteration, the WLS problem is solved by

$$\Delta\hat{x}_k = (H_k{}^T R^{-1} H_k)^{-1} H_k{}^T R^{-1} \Delta z_k \tag{7-6}$$

where $\Delta\hat{x}_k = \hat{x}_k - \hat{x}_{k\text{-}1}$, $\hat{x}_k$ being the estimated state vector, and $\hat{x}_{k\text{-}1}$ being the estimated state vector from previous iteration, H_k is the jacobian matrix, *R* is the covariance matrix of *e*, and $\Delta z_k = z - h(\hat{x}_{k\text{-}1})$. The residual vector *r* is defined as

$$r = z - h(\hat{x}) \tag{7-7}$$

where $\hat{x}$ is the final estimated state vector. The Euclidean norm of r is

$$r_{index} = \|r\| \tag{7-8}$$

For a synthetic test bed, the performance of state estimation can also be evaluated using the normalized norm of the state vector error defined by,

$$x_{ind} = \|\hat{x} - x\| / \sqrt{\dim(x)} \tag{7-9}$$

where x is the true state which is obtained by solving the power flow equations, $\hat{x}$ is the estimated state vector using noisy measurements, dim(x) is the dimension of vector x and x_{ind} is the normalized Euclidean norm of the estimation error. Normalizing gives a standard index valid for power systems of different size. The main reason to choose x_{ind} instead of r_{index} as a metric is that x_{ind} directly reflects the discrepancy between the estimated states and the true states. It should be noted that x_{ind} is only obtainable for a synthetic test bed. On the other hand, r_{index} can be used for both synthetic and real life power system measurements.

When incorporating PMU measurements into the state estimator, the different reporting rates of the conventional measurements and PMU measurements would raise the question as to how to synchronize and when to use the measurements. This issue includes the determination of the optimal buffer length of PMU measurements. Assume that in a practical system, the state estimator runs every 30 seconds. As shown in Fig. 7.1, assume that the reporting rate of the measurements from the remote terminal unit (RTU) is 1 per second. The reporting rate of the synchronized measurements is assumed to be 30 per second. The conventional measurements from the RTU in the last second of the cycle are used in the state

estimation. There are 30 measurements from the PMU in one second. The question as discussed above is how could the PMU measurements be integrated into the state estimation? The first question is the determination of the buffer length. The mean value of measurement data in the buffer is used in the state estimation. It should be noted here that even though the SCADA data are assumed to be taken from the same snapshot of the system, the time skew remains problematic [60].

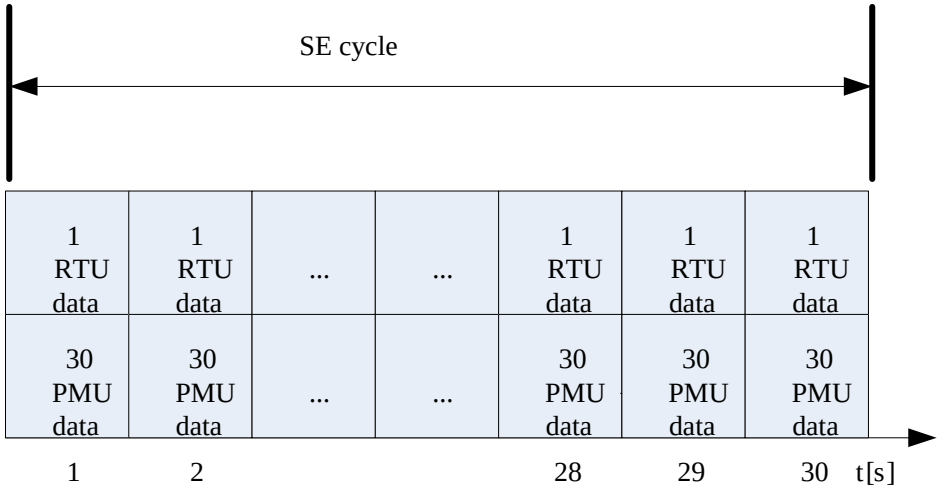

Fig. 7.1 Data stream of RTU data and PMU data in one state estimation cycle

7.4 Test bed simulations: PMU buffer length impact on state estimation

In this section, the two previously explained aspects of PMU measurements and their impact on the choice of buffer length are illustrated. These are: (1) the uncertainty due to measurement noise; and (2) the variation of data due to the change in the system states. The simulations are carried out on a test system which is derived from an actual power system. Heuristic evaluation is applied on the impact of different buffer lengths on state estimation results in the real life based test bed. Theoretical analysis is provided as well.

7.4.1 A real life based test bed description

For purposes of illustrating the time synchronization and buffer length design problems, consider a test system. In this test bed, Monte Carlo simulation is used to replicate actual system operation. The test bed includes 180 buses and 254 branches. The measurements used for state estimation include 475 branch flows, 198 injections, and 75 voltage magnitudes. The total number of the conventional measurements is 748. Plow flow solutions from PSAT [64] are used for the state estimation. Different numbers of PMUs are installed. This particular test system is derived from an actual power system, and it is believed that results obtained and conditions modeled are typical. The simulated PMU voltage measurements series is obtained by the following method:

a) Obtain the voltage angle solution from the power flow file.

b) Create a vector with dimension N_{meas}, where N_{meas} is the total number of PMU measurements.

c) Add normally distributed noise to the PMU measurements.

The variance of the noise is changed in different cases to assess its impact on the residual. It should be noted that the simulated N_{meas} measurements could be treated as a stationary random process under the assumption that the system is static. Also the simulated N_{meas} measurements could be treated as measurements provided by 'identical' PMUs at the same instant. The scalar r_{index} defined in (7-8) is used as an index to check the impact of different buffer length of PMU measurements on the state estimation. It is should be noted that there is no noise added

to the conventional measurements at first. The main purpose of study in this part is to show that processing a buffer of PMU measurements helps reduce the impact of noise uncertainty. For simplicity, the covariance matrix *R* used in the state estimation is an identity matrix. In other words, the weights for the PMU measurements and the conventional measurements are the same. It is straightforward to obtain the variance of a buffer of PMU measurements which is helpful in determining the weights of PMU measurements in the state estimation. In the next section, the optimal weights for both SCADA and PMUs will be considered in the WLS. N_{subset} could be treated as the number of Monte-Carlo replications. For different buffer length N_{bl}, N_{subset} should be the same. N_{meas} equals $N_{bl} * N_{subset}$. For a given buffer length N_{bl}, the mean value of the measurements in each subset is calculated. Then each of the mean values is used in the state estimation to obtain r_{index}.

As show in Fig. 7.2, the quantity r_{index} is also a random variable when assuming the measurements are provided by identical PMUs. In this case, N_{meas} is 300, N_{bl} is 3 and N_{subset} which is the number of the subsets is 100. In order to obtain the probability distribution function of the r_{index}, a large number of Monte Carlo simulations are conducted.

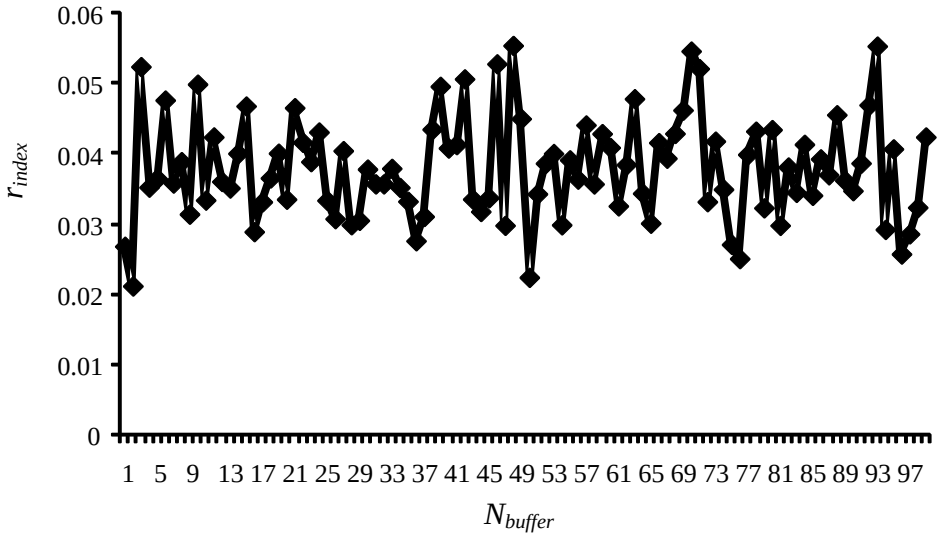

Fig. 7.2 The simulated r_{index} of the state estimation when N_{bl} = 3, σ = 1 degree

7.4.2 Reducing noise uncertainty in the measurements: practical illustration

In order to illustrate the impact of noise uncertainty on state estimation, the cumulative distribution of r_{index} is examined. As stated in the above subsection, r_{index} is also a random variable. Fig. 7.3 shows the cumulative distribution of r_{index} for two values of the buffer length. Assume the confidence level is set to be 0.95; the corresponding r_{index} for different buffer length is used as a metric to determine the optimal buffer length. This buffer length metric is denoted by $r_{0.95}$. The buffer length of the measurements from the 15 PMUs is changed at the same time. From Fig. 7.3, the probability of r_{index} being less than $2.252*10^{-3}$ is 0.95 when N_{bl} = 30. On the other hand, the probability of r_{index} being less than $2.252*10^{-3}$ is almost zero when N_{bl} = 3. The r_{index} corresponding to 0.95 confidence level is $5.241*10^{-3}$ when N_{bl} = 3. It is obvious that $r_{0.95}$ *decreases* as the buffer length *increases*. When the system is static, the larger the N_{bl} is, the better

the state estimation gets. The more data that are considered in the sample mean the better the state estimate of voltage magnitudes and angles. This can be assessed by (7-3). Since some measurements are provided with better accuracy, the state estimation is also impacted by a better precision. Fig. 7.4 shows the results from the simulation case for the same test bed. It is evident that if only the uncertainty due to noise in measurements is considered, a large buffer length would yield better (lower) r_{index} than a small buffer length.

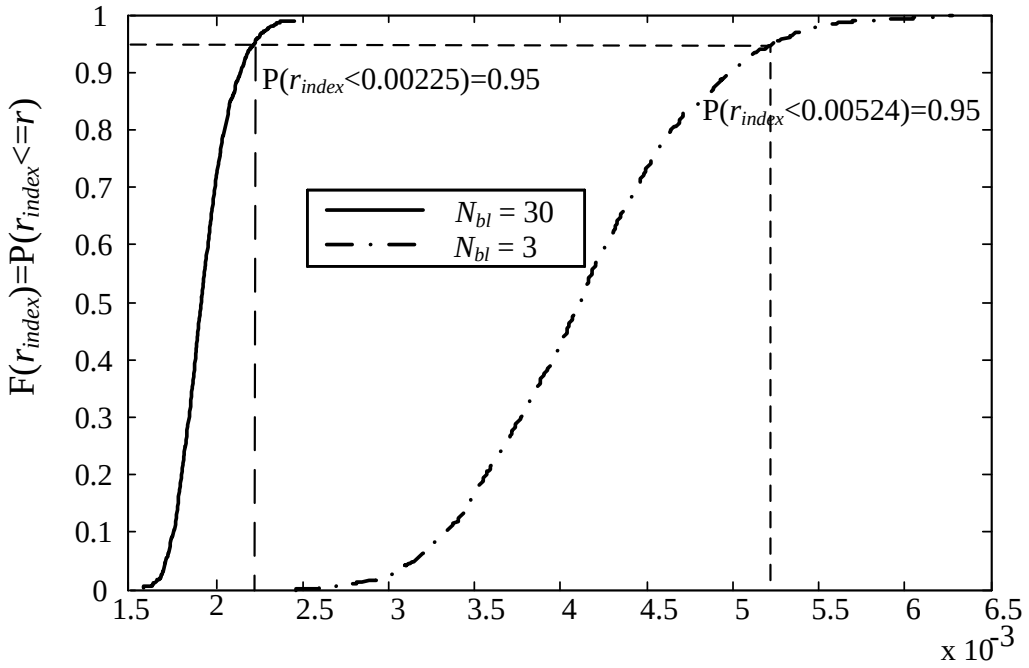

Fig. 7.3 The cumulative distribution of r_{index} when σ = 0.1, N_{bl} = 3, 30 in the real life based test bed

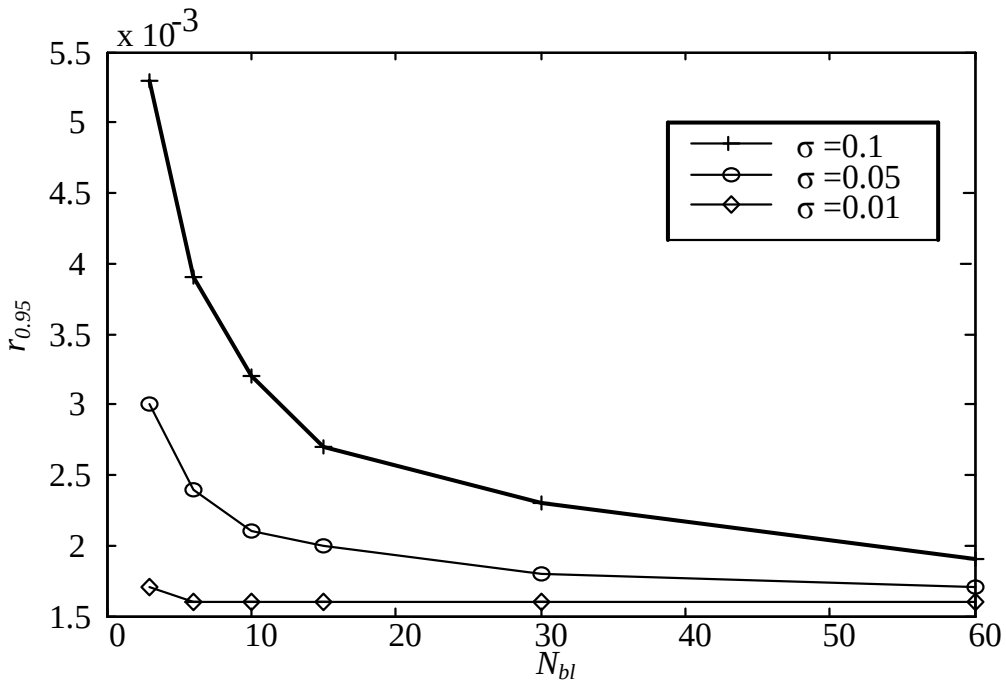

Fig. 7.4 Impact of buffer length on $r_{0.95}$ when σ = 0.1, 0.05, 0.01 in the real life based test bed

7.4.3 Reducing noise uncertainty in the measurements: Analytical illustration

The first aspect which is uncertainty due to the noise in PMU measurements is illustrated and the way to improve the estimate of the electrical power state vector when the system is considered static by exploiting PMU measurements is shown. Different parameters that influence the buffer length impact on state estimation are considered as well. These parameters are: the number of installed PMUs, their placement, and ratio between SCADA and PMU error standard deviations. In some cases, redundancy can also affect the buffer length impact as well.

Consider the previously described real life test bed. If the state vector x contained both voltages magnitudes and angles, considering two norms would

have been recommended, one representing the angles errors and the other for the voltage magnitude errors. Each PMU delivers several measurements in time which are considered to be i.i.d. Gaussian. Furthermore, Monte Carlo simulations are carried out where the estimation is replicated 500 times and the mean of the norm of the error is shown,

$$x_{ind}^{M} = \frac{1}{500}\sum_{k=1}^{500} x_{ind}^{[k]} \tag{7-10}$$

where $x_{ind}^{[k]}$ the error norm obtained at the k^{th} Monte-Carlo run. The quantity x_{ind_m} is the index evaluated on the voltage magnitude states, and x_{ind_a} is its angle counterpart. The error standard deviations used for PMU voltage angle and magnitude are $2*10^{-2}$ degrees and 10^{-2} pu, and for SCADA power and voltage magnitude $1.5*10^{-2}$ pu and 10^{-2} pu respectively. It should be noted that in practice, the error variance of the PMUs is due not only to the sensors but also to the communication process.

In order to assess the impact of the installed number of PMUs, measurements from 20, 30 and 60 PMUs are integrated into state estimation together with the 748 conventional measurements. The 30 PMUs are placed at different locations than the 20 PMUs. The 60 PMUs include the first 20 PMUs but not the 30 PMUs. Fig. 7.5 illustrates the impact of PMUs placement on the buffer length based state estimation. In some cases, increasing the buffer length changes the performance obtained with different PMU placements. In the upper Fig. 7.5, the 30 PMUs based SE results with a different PMU placement offer a slightly better performance than the 60 PMUs for large buffer lengths. For small buffer lengths

the opposite is true. It seems that the optimal PMU placement depends in some cases on the buffer length used.

It is also convenient to consider the plots obtained when evaluating the normalized index on the state errors directly improved by the PMUs or on buses where PMUs are installed. x_{ind_m}(PMU) is the index evaluated on the voltage magnitude states related only to PMUs; x_{ind_a}(PMU) is its angle counterpart. The obtained curves are shown in Fig. 7.6. In the case, where the PMUs are very precise even for N_{bl} = 1, i.e., their variance is very small if compared to the SCADA errors variance, the state variables linked to the PMUs measurements are already very precise. Although increasing the buffer length improves these PMU state variables estimation, as illustrated in the lower Fig. 7.6, this improvement is still negligible if compared to the other state errors that are not improved significantly. The same remark holds for small numbers of PMUs installed in the system. This statement explains the non-decreasing curve in the lower Fig. 7.5.

Consider the impact of the ratio of the SCADA and PMU standard deviation. If the previous SCADA error variances are fixed, 120 PMUs are considered for which voltage angle and magnitude standard deviations are respectively: (10^{-2} and $5*10^{-3}$ degrees), and ($5*10^{-3}$ and $5*10^{-3}$ pu). The curves obtained are shown in Fig. 7.7. The buffer length impact will be maximized in a certain interval based on the ratio between the noise SCADA and PMUs variances as illustrated in Fig. 7.7.

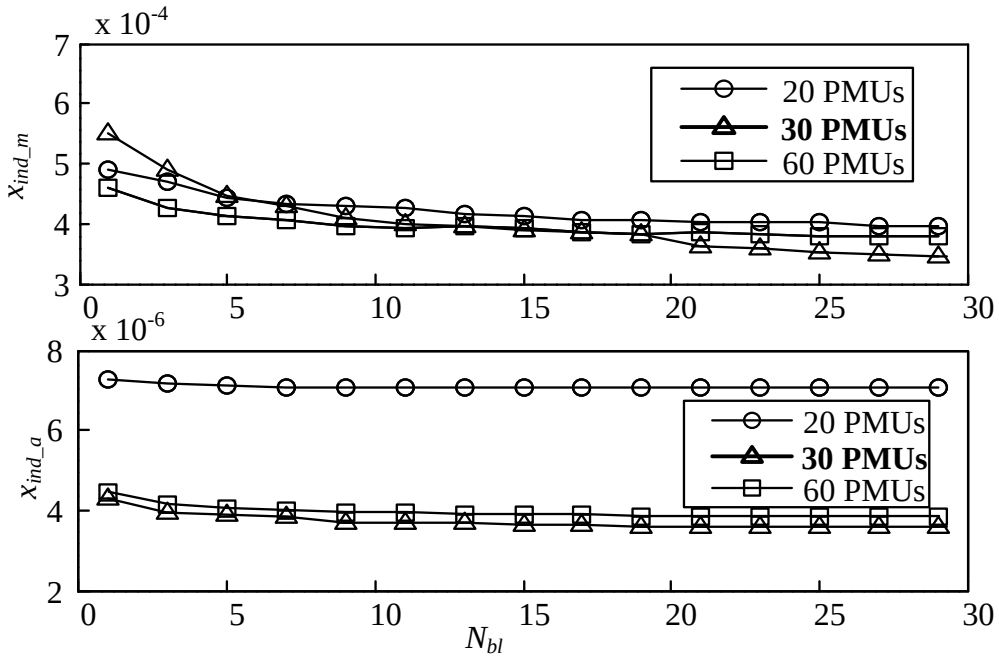

Fig. 7.5 Impact of the buffer length on state estimation error x_{ind}^{M} considering different PMU placements in the real life based test bed

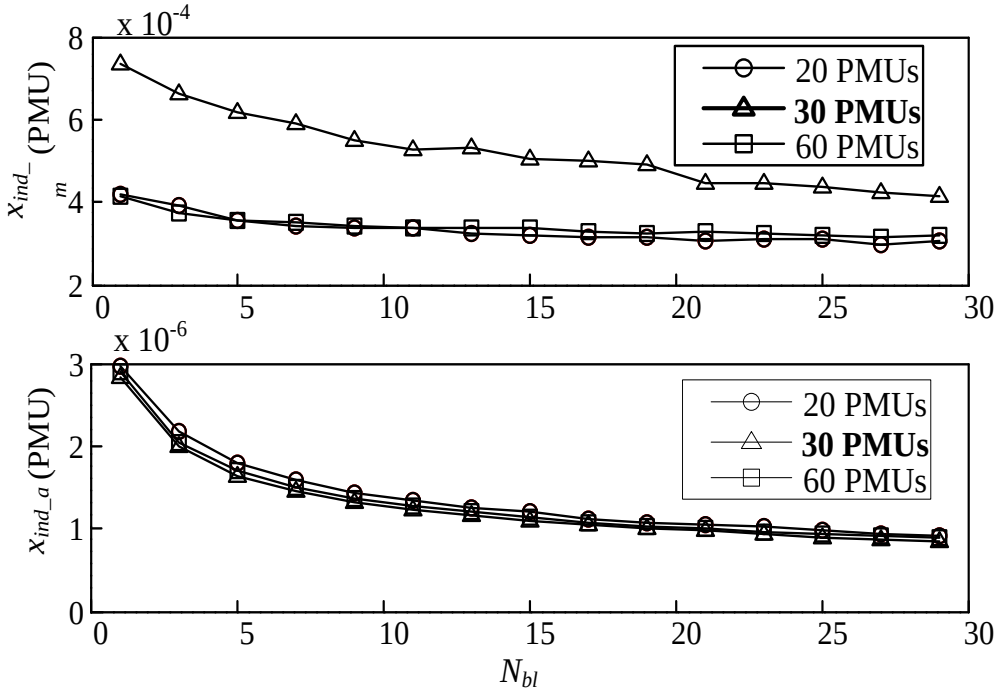

Fig. 7.6 Impact of the buffer length on state estimation error linked to the PMUs buses $x_{ind,n}^{M}$ in the real life based test bed

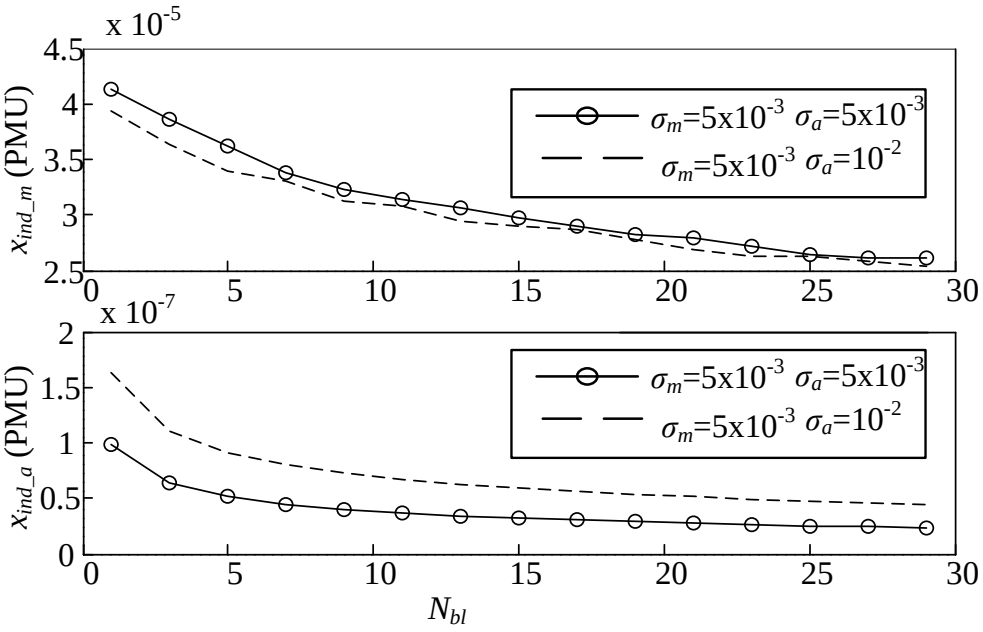

Fig. 7.7 Impact of the buffer length on state estimation error x_{ind}^{M} considering different ratio of the SCADA and PMU standard deviation in the real life based test bed

From these curves, it is concluded that the impact of increasing the buffer length depends on the number of PMUs in the system and the ratio of the SCADA and PMU standard deviation. As more PMUs are introduced, increasing the buffer length improves SE. In conclusion, state estimation improvement is quite a complex problem that depends on different practical factors. Generally in the static case, increasing the buffer length will improve significantly the estimation especially when using the practical real life data. Even in the cases where the buffer length increase does not improve the estimation, it still does not degrade it.

To give some statistical insight about the results, it is noted that if x is estimated in the linear model,

$$Y = Hx + e \tag{7-11}$$

where $Y \in R^m$, $x \in R^l$, $Y(k),...,Y(m)$ are measured by the PMUs series denoted by $\{Y_j^t\}$, for $j = k,...,m$ and $t = 1, ..., n$, then under the assumption that the mean $E(e)= 0$ and $Cov(e) = R$; the Gauss-Markov theorem states that the WLS with weighting matrix R^{-1}, which is the maximum likelihood, is also the best linear unbiased estimator [65] (i.e., it insures the minimum estimator covariance matrix trace among linear unbiased estimators) with,

$$Cov(\hat{x}) = C = (H^T R^{-1} H)^{-1}. \tag{7-12}$$

This means that the variance $var(\hat{x}_i) = E(\hat{x}_i - E(\hat{x}_i))^2 = E(\hat{x}_i - x_i)^2 = C_{ii}$ where C_{ii} is the i^{th} diagonal element of C. Since the observations from k to m are PMUs with n measurements i.e., $m-k$ PMU signals with length n, $Y_j^{PMU} = 1/n \sum_{t=1}^{n} Y_j^t$, $j = k,\ldots,m$; the error matrix R is given by: $R = diag(\sigma_1^2,\ldots,\sigma_{k-1}^2, \sigma_k^2/n,\ldots, \sigma_m^2/n)$. By replacing R in (7-12), it is noticed that when n increases the diagonal variances C_{ii} decrease. It should be noted that the previous model is only a linear approximation of the real non-linear system. Following this development, the error can also be quantified by,

$$E(\|\hat{x} - x\|^2) = E\left[\sum_{j=1}^{m} (\hat{x}(j) - x(j))^2\right] = \sum_{j=1}^{m} \mathrm{var}(\hat{x}(j)) = \sum_{j=1}^{m} C_{ii} \tag{7-13}$$

Furthermore, if all measurements are derived from PMUs then the squared norm of the estimation error will even decrease faster since all the diagonal elements C_{ii} will be proportional to $1/n$. This means that the larger the number of PMUs installed the smaller the bias is.

7.4.4 Adapting to data variation

The impact of changing system state parameters on estimation is shown in this section. Since the system is in practice dynamic and not static, several variables of the electrical network change with time, such variables are: loads, impedances, generators and possibly other parameters. To reach this goal, the previous curve, which corresponds to noise uncertainty, is made horizontal by eliminating the observation noise ε in (7-1). Separating the dynamic effect from the noise uncertainty reduction in a real life system is difficult since they both add together. A system with changing loads after 5 observations is considered. Fig. 8 shows the obtained results for the real-life based test system. In the simulations, only the active parts of loads are changed. Since the active power is closely coupled with voltage angles, only voltage angle error is shown in Fig. 7.8. From this figure, it is clear that when the buffer length increases, the committed estimation error accumulates and increases.

To give further insight into these results, suppose that *n* measurements in the PMUs are considered. This means that

$$Y_j^{PMU} = 1/n \sum_{t=1}^{n} Y_j^t = h_j(x) \tag{7-14}$$

where Y_j^{PMU} is the estimate obtained from the available j^{th} PMU datum. The estimate is equal to the $h_j(x)$ since $\varepsilon = 0$.

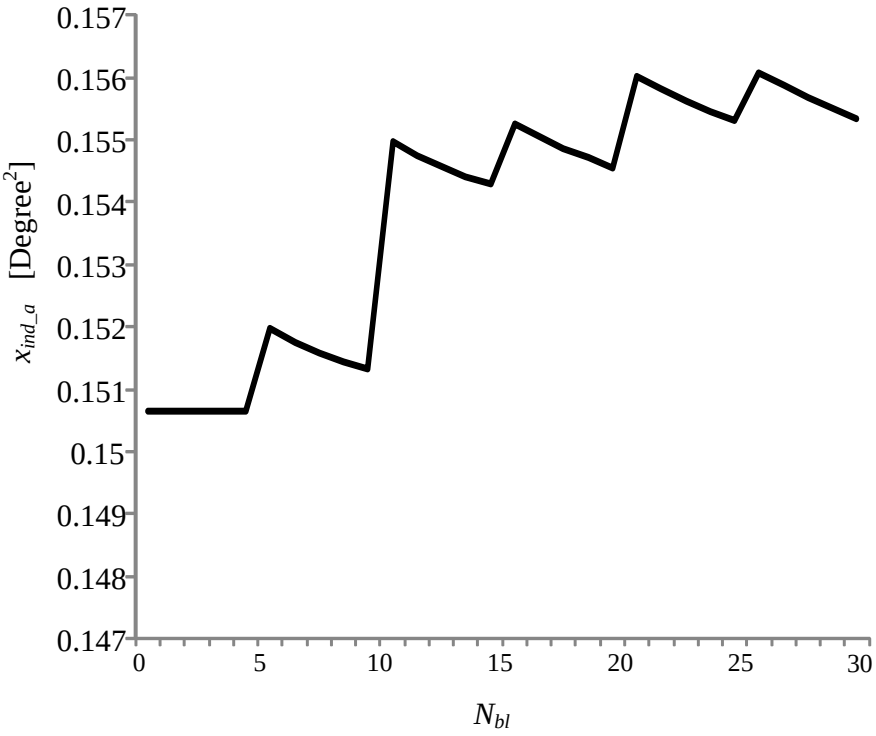

Fig. 7.8 Impact of the buffer length on state estimation error x_{ind}^{M} considering variations of system operating condition in the real life based test bed

Consider now that a jump in the observations has occurred at instant $t = q_1$ which is equal to 5 due to a change in system parameters. If $n = N_{bl} = 8 < 2*5$, for example, the error obtained in this case is

$$Y_j^{PMU} - h_j^{(2)}(x^{(2)}) = \frac{1}{n}(q_1 h_j^{(1)}(x^{(1)}) + (n - q_1)h_j^{(2)}(x^{(2)})) - h_j^{(2)}(x^{(2)}) \quad (7\text{-}15)$$

where $h_j^{(1)}(x^{(1)})$ and $h_j^{(2)}(x^{(2)})$ represent the system before and after the parameter change respectively. This change can be in the state vector x or in other elements in $h(.)$. Finally, the equation is,

$$Y_j^{PMU} - h_j^{(2)}(x^{(2)}) = \frac{q_1}{n}[h_j^{(1)}(x^{(1)}) - h_j^{(2)}(x^{(2)})] \quad (7\text{-}16)$$

It is remarked that when the state changes, the error is different from zero. A better choice would be to insure that $n < q_1$ and commit a null error. This will

split the estimation in two intervals one before the system change and a second after the change.

It is also observed that the smaller q_1 is with respect to n the smaller the committed error is. This is true if after the first change the system stays static for quite a long time. In fact, following the q_1, the error is expected to decrease. In the real case, there could be a second, a third and many other changes until the k^{th} change at step q_k; the error may accumulate and is given by:

$$Y_j^{PMU} - h_j^{(k)}(x^{(k)}) = \sum_{i=1}^{k} \frac{q_i}{n} [h_j^{(i)}(x^{(i)}) - h_j^{(k)}(x^{(k)})] \tag{7-17}$$

An increase in the error in Y_j^{PMU} implies an increase in the state estimation error which explains the results shown in Fig. 7.8. However, the curve is generally quite random; errors can accumulate as shown and then decrease if the system comes back to a previous state for example. For practical systems, the loads would always vary. The continuous increase of load in the simulation would only be one possible case.

There is another simpler way to illustrate the impact of buffer length on state estimation error considering variation of system operation conditions. Consider the instant at the end of one changing interval. Comparison is made based on the system state at that instant. Many PMU measurements prior to this instant are available. Increase the buffer length gradually, and the state estimation errors are shown in Fig. 7.9. It is clearly shown that the state estimation error would increase when neglecting the variations of system operating conditions.

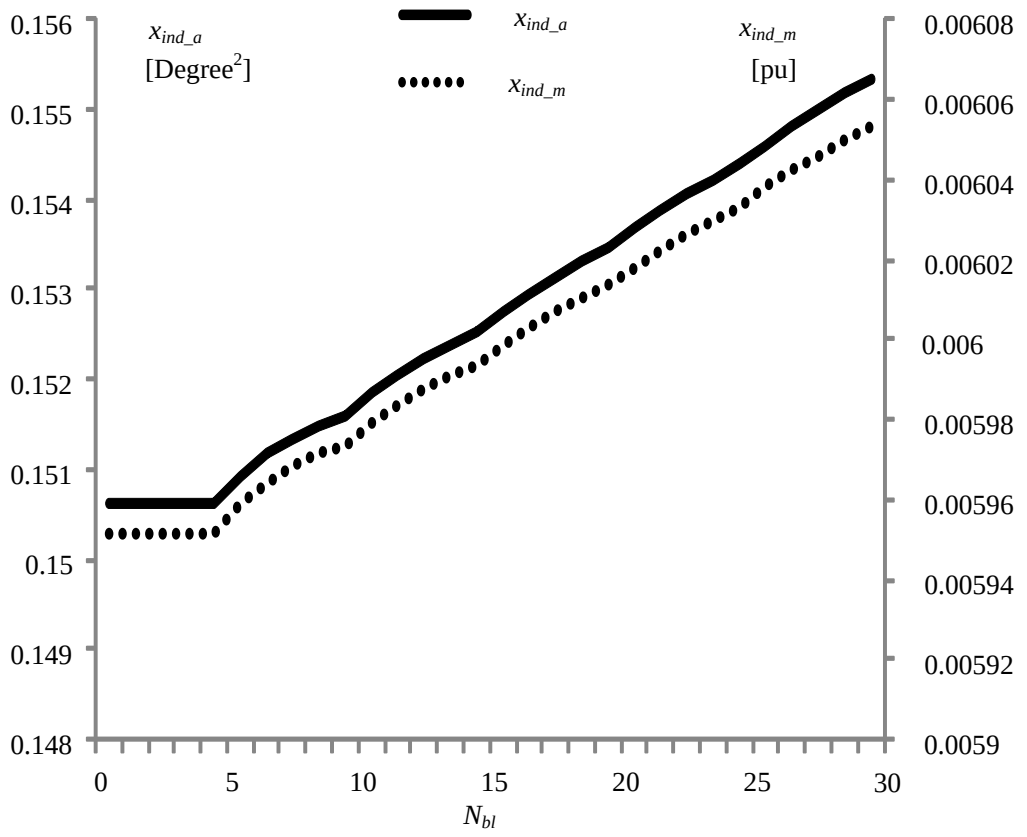

Fig. 7.9 Impact of the buffer length on state estimation error x_{ind}^{M} considering variations of system operating condition in the real life based test bed

7.4.5 Determination of the optimal buffer length

Attention is turned to the design of the optimal input data buffer length. If the variation of PMU measurements due to the change of the system states could be quantified, the optimal buffer length is obtained when the summation of residual due to the uncertainty and variation of measurements is minimum. If the uncertainty level is pre-determined based on preliminary knowledge, similar curves, as shown in Fig. 7.4, could be obtained to display the relationship between the residual index and the buffer length. However, it is difficult to separate the impact of the uncertainty and the variation of the measurements, and it is difficult to

describe the variation of system states in a probabilistic sense. Fig. 7.10 is a pictorial of the possible changing trend of the system states (shown by the dashed curves). It is possible that the system is static as shown by the dashed straight line or varying as shown by the other two dashed curves. As explained previously, it is very important to insure the best possible tradeoff between reducing noise uncertainty impact on estimation and improving system change tracking accuracy. The first objective implies increasing the buffer length is beneficial whereas the second objective implies that it is beneficial to decrease the buffer length. Thus, the goal consists of finding an optimal buffer length. As a result, a method based on hypothesis testing is proposed to solve this problem.

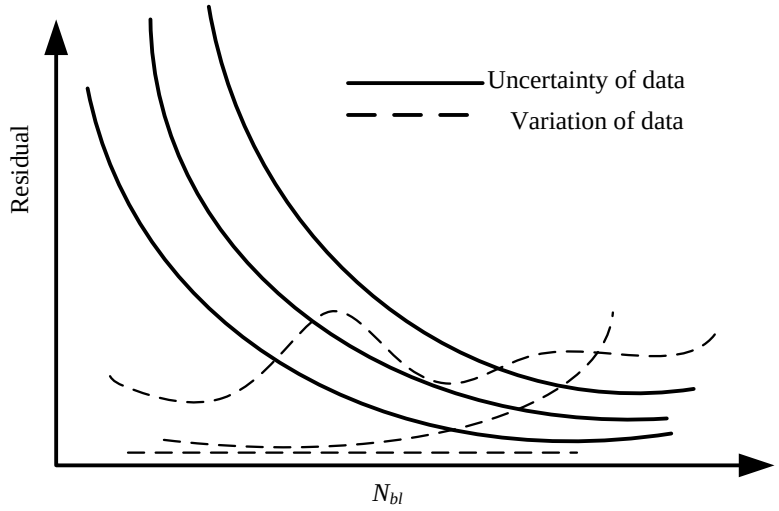

Fig. 7.10 Determination of the optimal buffer length

7.5 Determination of the optimal buffer length by hypothesis testing

7.5.1 The basis of hypothesis testing

As stated in the previous section, it is meaningful to utilize all measurements to extract as much information as possible. In order to find the optimal buffer length, a method based on hypothesis testing is proposed. The basic idea is

to test whether the system is static or not. More importantly, the focus would be on detecting the mean shifts in time. The change in the mean is more challenging than the change of variance since the change in the mean will introduce a bias in estimation and cause the non-consistency of the estimator opposite to the impact of the variance. The stationary is tested by the equality of two means. The means are calculated based on different sections of a random sequence. Reference [63] contains a complete discussion of hypothesis testing. The null and alternate hypothesis are:

H_0 = The two mean values are equal.

H_1 = The two mean values are not equal.

Assume that the reporting rate of a PMU is 30 frames per second. The procedure to determine the optimal buffer length is as follows:

a) Assume that the n_{HT} measurements in t_{HT} second are divided into n_{subset} subsets. Each subset contains n_{meas} measurements. The n_{subset} subsets are denoted by $Z(1)$, $Z(2)$,…, $Z(n_{subset})$.

b) For the latest measurements in $Z(n_{subset})$, determine whether there is a large change in the system state. This could be done by setting a certain threshold for the standard deviation of the five measurements. The threshold is set to guarantee that the change of system states is detected. The choice of the threshold should be tuned in practical implementation. If the standard deviation is less than the threshold, n_{bf1} simply equals n_{meas}. Go to step c). If n_{bf1} is less than n_{meas}, a change of state is detected in the given n_{meas} measurements. In this case, n_{bf1}

equals the number of measurements before the change occurs. If n_{bf1} is less than n_{meas}, the optimal buffer length is n_{bf1} and the procedure is terminated.

c) Conduct the hypothesis testing between subset $Z(n_{subset})$ and $Z(n_{subset}$-1), …, $Z(3)$ and $Z(2)$, $Z(2)$ and $Z(1)$. The testing results are denoted by h_i (i= 1, 2,…, n_{subset}-1). When the null hypothesis H_0 is satisfied, h_i is zero. A simple method is proposed to obtain N_{op_bl} for the purpose of quick execution. The optimal buffer length N_{op_bl} could be calculated by

$$N_{op\_bl} = max(n_{meas},\ 2n_{meas}\,\bar{h}_1,\ 3n_{meas}\,\bar{h}_1\,\bar{h}_2,\ 4n_{meas}\,\bar{h}_1\,\bar{h}_2\,\bar{h}_3,\ \ldots,\ n_{subset}n_{meas}\,(\bar{h}_1\,\bar{h}_2\,\bar{h}_3 \ldots \bar{h}_{n_{subset}-2}\,\bar{h}_{n_{subset}-1})) \quad (7\text{-}18)$$

where the bar over $\bar{h}_i$ denotes the complement of h_i, '*max*' means the maximum value of the vector entry (infinite norm).

Consider a specific example: assume the PMU reporting rate is 30 frames per second, and the thirty measurements are divided into six subsets. Each subset contains 5 measurements. The procedure to determine the optimal buffer length in this case is summarized in Fig. 7.11.

7.5.2 An illustration of the hypothesis testing technique

In this section, a second illustrative example is given. The objective is to illustrate the hypothesis testing technique. In the example, PMU voltage angle measurements from an actual power system are used. Fig. 7.12 shows a time series of measurements over 60 s. The relative voltage angles are with respect to a selected reference PMU. The reporting rate is 30 frames per second. There are 1800 measurements in total. Even though state estimation is not generally run

every second, the hypothesis testing is applied on measurements for all of the 60 seconds to determine the optimal buffer length.

The optimal buffer length of each second is displayed in Fig. 7.13. There are four cases when the optimal buffer length is 10. There are two cases when the optimal buffer length is less than five, which means in the latest measurement subset variation of system state is detected. The variance of the processed PMU measurements is shown in Fig. 7.14. Since a buffer of PMU measurements is processed, the variance could be calculated by (7-3). By observation, the two largest variances in Fig. 7.14 correspond to the two smallest buffer lengths in Fig. 7.13 respectively. According to (7-6), larger variance results in lower weights in state estimation. The matrix R in (7-6) is chosen as being the inverse of the estimated covariance matrix of the errors giving, by the same, the optimal WLS for this case.

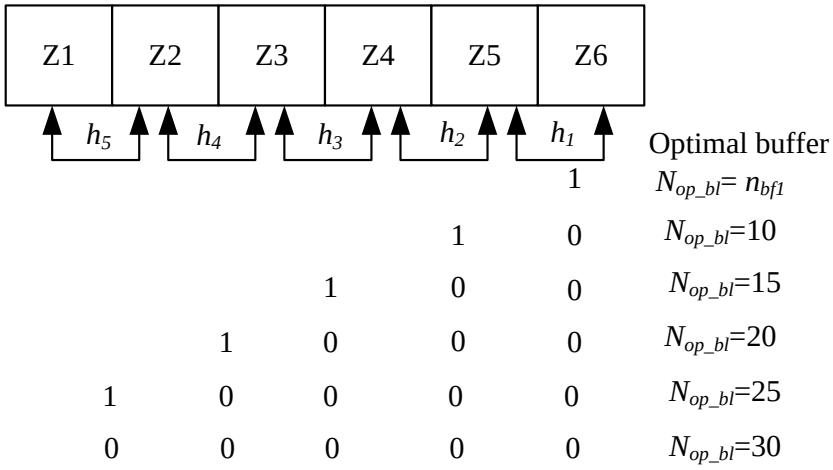

Fig. 7.11 Determination of the optimal buffer length by hypothesis testing

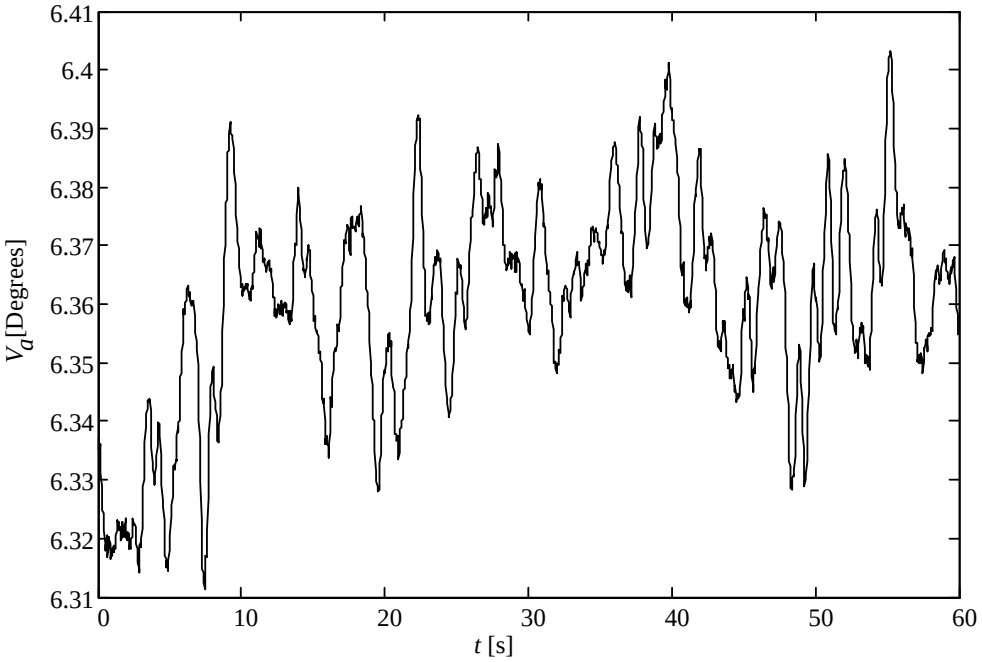

Fig. 7.12 PMU measurements from a practical power system in 60 seconds (PMU 13, data files #4-41, #4-42)

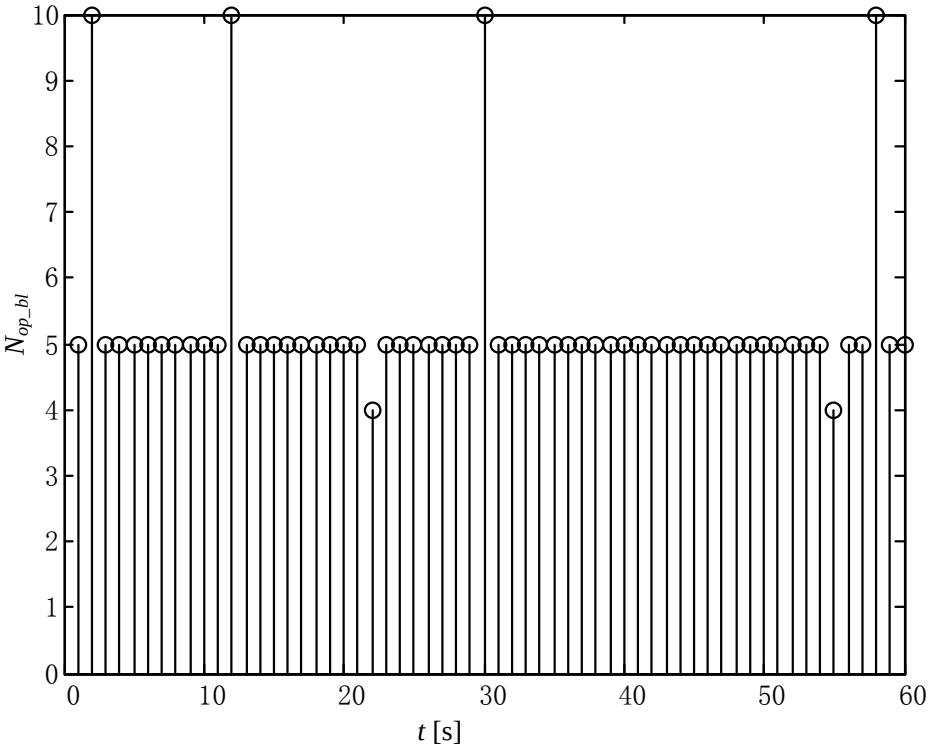

Fig. 7.13 The optimal buffer length of the PMU 13 measurements in 60 seconds

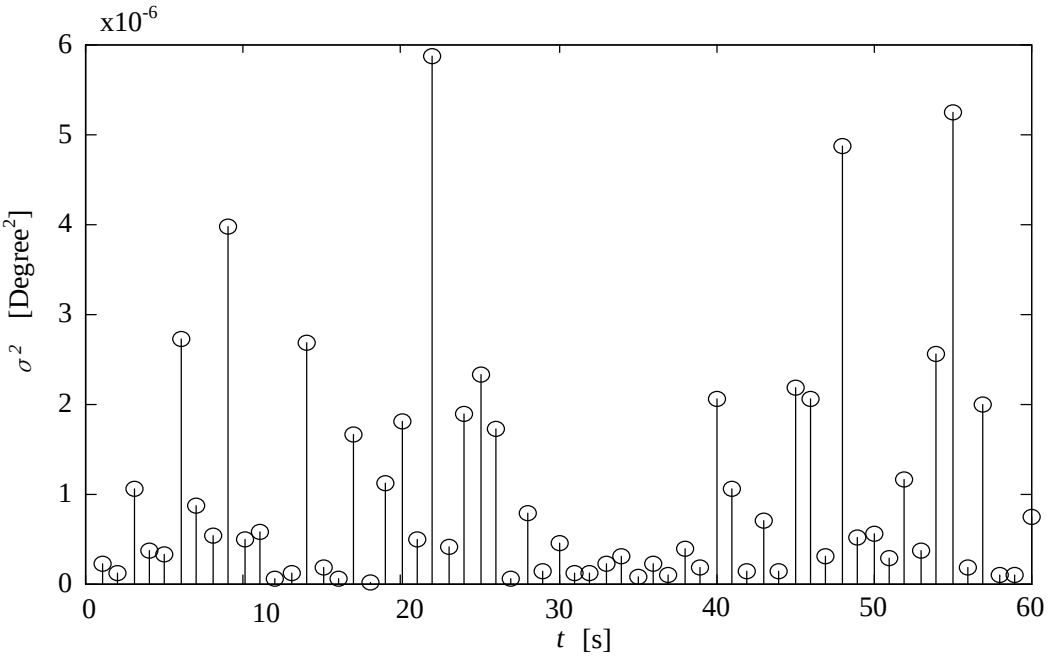

Fig. 7.14 The variances of processed PMU 13 measurements in 60 seconds

7.5.3 Buffer length determination for measurements from multiple PMUs

The buffer length optimization for measurements from a single PMU is implemented following the procedure described in the previous subsection. The question arises as to how to determine the optimal buffer length for measurements from multiple PMUs. The answer to this question is straightforward. Since only the mean of the buffer of measurements is used in the state estimation, the optimal buffer length for individual PMU is not related with the optimal buffer lengths for other PMUs. For example, if the optimal buffer lengths for two PMUs are denoted by N_{bl1} and N_{bl2}. The chance that N_{bl1} is different from N_{bl2} is high, for the impact of changing operating conditions on system states is different from one bus location to the other. Assume N_{bl1} is greater than N_{bl2}. More measurements are recommended to be processed to reduce the impact of noise uncertainty. As a result, the corresponding buffer lengths for the two PMUs are different.

7.6 Conclusions

The research in this chapter deals with an important issue when integrating PMU measurements into state estimation. Due to the different reporting rates of the conventional measurements and the PMU measurements, the question of how to buffer PMU measurements is raised. Two aspects need to be considered. One aspect is the uncertainty with respect to the noise in the measurements. The other is the natural variation of the system state. Simulations are carried out on a real-life based test bed to illustrate the impact of different buffer lengths of PMU measurements on the state estimation residual. When only considering the noise in the measurements, large buffer length of PMU measurements would reduce the state estimation residual and improve the performance of state estimation. However, large buffer length would result in increased state estimation residual when the system states vary. Analytical illustrations are also presented to support the conclusions obtained in the simulations.

The impacts of buffer length on state estimation residual due to the uncertainty of the measurements and the variation of the system states are conflicting. The tradeoff between the uncertainty of the measurements and variation of the system states requires the determination of the optimal buffer length. A method is proposed to determine the optimal buffer length of PMU measurements. Since it is difficult to separate the noise in the measurements and variation of the system states due to the system operating condition change, hypothesis testing is applied to test the stationarity of the system states. A procedure is described to determine the optimal buffer. Furthermore, statistical analysis of these aspects and the buff-

er length impact is provided. The state estimation weights associated with PMU measurements were determined from the developed procedure for the optimal length determination.

Chapter 8

CONCLUSIONS AND FUTURE WORK

8.1 Principal conclusions

Research has been done to explore the potential applications of PMU measurements based on the assumption that high accuracy is obtained both in the quantities and the synchronization feature of PMU measurements. In this work, the research is carried out primarily on real PMU measurements. The following are the main conclusions:

a) A time skew problem is identified from measurements from different PMUs. In other words, the synchronization might not be obtained even though PMU measurements are tagged with the same time stamps. The time skew problem is caused by the inaccuracy of sampling clocks associated with PMUs. Due to the procedural constraints in the field, it may be laborious and expensive to rectify the problem in hardware. A Kalman filter model is proposed to calculate the time skew error. In this way, PMU measurements with time skew error corrected can be used in further applications.

b) PMU measurements constitute a time series which is not free of noise. A Kalman filter is capable of removing the noise from PMU measurements. An adaptive strategy is developed based on the PTDFs to overcome the insensitivity of a regular Kalman filter. Following the strategy, a system state change would be captured in real time. Bad data detection and identification can be implemented at the same time.

c) The accuracy of real PMU measurements is tested in a specific PMU installation scenario. The transmission line parameters can be calculated when both ends are installed with PMUs. Large discrepancies are observed between the calculated results and parameters from the planning case. A method is proposed to calculate the correction factors which indicate possible errors in both voltage and current phasors. An approach using correction factors is also studied. The correction factors can be used to compensate the errors of PMU measurements in real time.

d) A practical issue has been addressed in this work regarding integration of PMU measurements into state estimation. A buffer of PMU measurements is recommended to be processed in order to reduce the impact of random noise. Considering the variation of system states, the buffer length should be carefully selected. Simulations are carried out on a real-life based test bed to illustrate the impact of buffer length when only considering the noise in PMU measurements and variation of system states respectively. Analytical deduction is also provide to support the conclusions obtained through simulations. In order to best improve the performance of state estimation, the tradeoff between the uncertainty of the measurements and the variation of system states requires the determination of an optimal buffer length of PMU measurements. Since it is difficult to separate the noise and variation due to system state change, a method based on hypothesis testing is proposed to obtain the optimal buffer length. The procedure to determine the optimal buffer length is illustrated, and test cases based on *actual* PMU measurements are provided. By processing a buffer of measurements, the variance

could be easily calculated. The measurement weight in state estimation is closely associated with the measurement variance. As a result, processing a buffer of PMU measurements is also helpful for determining the corresponding weights in state estimation.

8.2 Principal contributions of this research

As an innovative study on the accuracy of real PMU measurements has been conducted, the research in this dissertation has made the following contributions:

- Identification of faulty synchronization of PMU measurements

Synchronization is the most important feature of PMU measurements. Many potential applications of PMU measurements are based on the synchronization feature indicated by time stamps. Analysis of real PMU measurements reveals that a time skew problem exists in measurements from different PMUs. The cause of the time skew problem is due to inaccuracy of sampling clocks associated with PMUs. Researchers should be aware of the time skew problem when applying PMU measurements in practical power system applications.

- Novel method to assess the reliability of PMU measurements

When the level of redundancy of PMU measurements is obtained in the network, reliability analysis of PMU measurements can be performed. System state change reflected by the phasor measurements can be distinguished from bad data, since in both cases changes of measurements would be observed. Further, when bad data are detected and identified, it is possible to best correct the bad data based on measurements from other PMUs in the network under study.

- Novel method to calibrate PMU measurements

A study has been conducted to test the accuracy of PMU measurements. Mismatches exist between the voltage and current phasor measurements and transmission line parameters. The possible errors arise from the instrumentation channel comprising the instrument transformer, the A/D converters, and the cables connecting them. Correction factors are calculated to calibrate the phasor measurements.

- Innovative study on integrating PMU measurements into state estimation

Due to the different reporting rates of conventional and PMU measurements, one important issue that needs to be addressed is how to integrate PMU measurements into state estimation. An innovative study has been conducted to resolve this practical problem. A buffer of PMU measurements is recommended to be processed to minimize the impact of noise the measurements. In the meantime, the variance of the PMU measurements could be directly calculated which is helpful for determining the corresponding weight in state estimation.

- Determination of optimal buffer length of PMU measurements in state estimation

Two competing aspects of PMU measurements need be considered when determining the optimal buffer length. The first aspect is referred to as uncertainty due to the noise in the measurements. More measurements should be included to yield the best estimate when the system is static. The second aspect is referred to as variation due to the change in the system states. More measurements that are included would result in larger deviation due to system dynamics. Simula-

tions are carried out on a real-life based test bed. The simulation results illustrate the impact of different buffer lengths on state estimation residual when only considering noise in measurements and variation of system states respectively. Analytical illustrations are also provided. An optimal buffer length needs be determined due to the tradeoff between noise in the measurements and variation due to system state change. Since it is difficult to separate the noise and system state variation, a method to determine the optimal buffer length based on hypothesis testing is proposed. The proposed method is tested on *actual* PMU measurements.

8.3 Future work

The main research in this dissertation focuses on analysis of accuracy of real PMU measurements in practical power systems. The final objective relates to the utilization of PMU measurements in power system monitoring, protection and control. As a result, the effectiveness of methods (i.e. PMU bad data detection and identification, calculation of correction factors, buffer length optimization in state estimation) proposed in the dissertation needs be tested in practical system applications. Work focusing on the following aspects need be conducted in the future:

- Test the effectiveness of the adaptive Kalman filter

Due to insufficient number of PMUs in the practical study, the method proposed in Chapter 4 for system state change detection and identification could not be tested using real PMU measurements. When the requirements of redundancy of PMU measurements are met, the effectiveness of the adaptive Kalman filter can be tested especially under conditions when system states change or bad

data appear in PMU measurements. The processed PMU measurements would reflect the real-time system states more accurately.

- Apply signal processing technologies for 'jump' detection and identification

In this dissertation, 'jump' detection and identification is based on measurements from different PMUs. The redundancy of PMU measurements is used to best estimate the change of system operating conditions. It is meaningful to explore the possibility of applying more advanced and more appropriate modern signal processing technologies to fulfill the same objective in order to lower the requirements of redundancy of PMU measurements.

- Apply the correction factors of PMU measurements in real applications

The correction factors for voltage and current phasor are calculated based on real PMU measurements based on the assumption that the transmission parameters from the planning case are accurate. As a result, further testing in real application needs to done to determine whether the application of the correction factors would improve the performance of PMU measurements.

- Test the effectiveness of the scheme of determining the optimal buffer length in a practical state estimator

The scheme of determining the optimal buffer length is realized based on real PMU measurements. The problem of how to integrate PMU measurements into the state estimation is addressed. The effectiveness of using preprocessed PMU measurements need be tested in a practical state estimator. Another issue that needs be addressed is how to assign proper weights to the processed PMU measurements.

REFERENCES

[1] *IEEE Standard for Synchrophasors for Power Systems*, IEEE Std. C37.118–2005 (Revision of IEEE Std. 1344–1995), Piscataway NJ, 2005.

[2] K. E. Martin, D. Hamai, M. G. Adamiak, S. Anderson, M. Begovic, G. Benmouyal, G. Brunello, J. Burger, J. Y. Cai, B. Dickerson, V. Gharpure, B. Kennedy, D. Karlsson, A. G. Phadke, J. Salj, V. Skendzic, J. Sperr, Y. Song, C. Huntley, B. Kasztenny, E. Price, "Exploring the IEEE Standard C37.118–2005 synchrophasors for power systems," *IEEE Trans. on Power Delivery*, v. 23, No. 4, pp. 1805 – 1811, Oct. 2008.

[3] J. De La Ree, V. Centeño, J. S. Thorp, A. G. Phadke, "Synchronized phasor measurement applications in power systems," *IEEE Trans. on Smart Grid*, vol. 1, No. 1, pp. 20 – 27, June 2010.

[4] A. Abur, A. Gómez-Expósito, *Power system state estimation: theory and implementation*, New-York: Marcel Dekker, 2004.

[5] T. Yang, H. Sun, A. Bose, "Transition to a two-level linear state estimator — part I: architecture," *IEEE Trans. Power Syst.*, vol. 26, no. 1, pp. 46 – 53, Feb. 2011.

[6] T. Yang, H. Sun, A. Bose, "Transition to a two-level linear state estimator — part I: algorithm," *IEEE Trans. Power Syst.*, vol. 26, no. 1, pp. 54 – 62, Feb. 2011.

[7] L. Vanfretti, J. H. Chow, S. Sarawgi, B. Fardanesh, "A phasor-data-based state estimator incorporating phase bias correction," *IEEE Trans. Power Syst.*, vol. 26, no. 1, pp. 111 – 119, Feb. 2011.

[8] A. G. Phadke, J. S. Thorp, R. F. Nuqui, M. Zhou, "Recent developments in state estimation with phasor measurements," *in Proc. Power Systems Conference and Exposition*, pp. 1 – 7, 2009.

[9] S. Chakrabarti, E. Kyriakides, D. Eliades, "Placement of Synchronized Measurements for Power System Observability," *IEEE Trans. Power Delivery*, vol. 24, no. 1, pp. 12 – 19, Jan. 2009.

[10] N. Abbasy, H. Ismail, "A unified approach for the optimal PMU location for power system state estimation," *IEEE Trans. Power Syst.*, vol. 24, no. 2, pp. 806 – 813, May 2009.

[11] R. Emami, A. Abur, "Robust measurement design by placing synchronized phasor measurements on network branches," *IEEE Trans. Power Syst*, vol. 25, no. 1, pp. 38 – 43, Feb. 2010.

[12] F. Aminifar, A. Khodaei, M. Fotuhi-Firuzabad, M. Shahidehpour, "Contingency-constrained PMU placement in power networks," *IEEE Trans. Power Syst*, vol. 25, no. 1, pp. 516 – 523, Feb. 2010.

[13] C. Rakpenthai, S. Premrudeepreechacharn, S. Uatrongjit, N. R. Watson, "An optimal PMU placement method against measurement loss and branch outage," *IEEE Trans. on power delivery,* vol. 22, No. 1, pp. 101 – 107, January 2007.

[14] B. Gou, "Generalized integer linear programming formulation for optimal PMU placement," *IEEE Trans. Power Syst*, vol. 23, no. 3, pp. 1099 – 1104, Aug. 2008.

[15] M. Zhou, V. A. Centeno, J. S. Thorp, A. G. Phadke, "An alternative for including phasor measurements in state estimators," *IEEE Trans. Power Syst.*, vol. 21, no. 4, pp. 1930 – 1937, Nov. 2006.

[16] G. Valverde, S. Chakrabarti, E. Kyriakides, V. Terzija, "A constrained formulation for hybrid state estimation," *IEEE Trans. Power Syst.*, vol. 26, no. 3, pp. 1102 – 1109, Aug. 2011.

[17] S. Chakrabarti, E. Kyriakides, G. Valverde, A. Ghosh, "Inclusion of PMU current phasor measurements in a power system state estimator," *IET Generation, Transmission & Distribution*, vol. 4, no. 10, pp. 1104 – 1115, 2010.

[18] J. Chen, A. Abur, "Placement of PMUs to enable bad data detection in state estimation," *IEEE Trans. Power Syst.*, vol. 21, no. 4, pp. 1608 – 1615, Nov. 2006.

[19] J. Zhu, A. Abur, "Improvements in network parameter error identification via synchronized phasors," *IEEE Trans. Power Syst.*, vol. 25, no. 1, pp. 44 – 50, Feb. 2010.

[20] J. Zhu, A. Abur, "Effect of phasor measurements on the choice of reference bus for state estimation," *in Proc. IEEE PES General Meeting*, June 2007, pp. 1 – 5.

[21] L. Zhao, A. Abur, "Multi area state estimation using synchronized phasor measurements," *IEEE Trans. Power Syst.*, vol. 20, no. 2, pp. 611 – 617, May. 2005.

[22] W. Jiang, V. Vittal, G. Heydt, "A distributed state estimator utilizing synchronized phasor measurements," *IEEE Trans. Power Syst.*, vol. 22, no. 2, pp. 563 – 571, May. 2005.

[23] J. Yan, C. Liu, U. Vaidya, "PMU-based monitoring of rotor angle dynamics," *IEEE Trans. Power Syst.*, vol. 26, no. 4, pp. 2125 – 2133, Nov. 2011.

[24] E. Ghahremani, I. Kamwa, "Dynamic state estimation in power system by applying the extended Kalman filter with unknown inputs to phasor measurements," *IEEE Trans. Power Syst.*, vol. 26, no. 4, pp. 2556 − 2566, Nov. 2011.

[25] E. A. Wan, R. Van Der Merwe, "The unscented Kalman filter for nonlinear estimation," in *Proc. IEEE Adaptive Systems for Signal Processing, Communications and Control Symposium*, pp. 153-158.

[26] E. Ghahremani, I. Kamwa, "Online state estimation of a synchronous generator using unscented Kalman filter from phasor measurements units," *IEEE Trans. Energy Conversion*, vol. 26, no. 4, pp. 1099 – 1108, Dec. 2011.

[27] A. Chakrabortty, J. H. Chow, A. Salazar, "A measurement-based framework for dynamic equivalencing of large power systems using wide-area phasor measurements," *IEEE Trans. Smart Grid*, vol. 2, no. 1, pp. 68 − 81, March 2011.

[28] D. J. Trudnowski, "Estimating electromechanical mode shape from synchrophasor measurements," *IEEE Trans. Power Syst.*, vol. 23, no. 3, pp. 1188 − 1195, Aug. 2008.

[29] N. Zhou, D. J. Trudnowski, J. W. Pierre, W. A. Mittelstadt, "Electromechanical mode online estimation using regularized robust RLS methods," *IEEE Trans. Power Syst.*, vol. 23, no. 4, pp. 1670 – 1680, Nov. 2008.

[30] A. Prince, N. Senroy, R. Balasubramanian, "Targeted approach to apply masking signal-based empirical mode decomposition for mode identification from dynamic power system wide area measurement signal data," *IET Generation, Transmission & Distribution*, vol. 5, no. 10, pp. 1025 − 1032, 2011.

[31] G. Qun, S. M. Rovnyak, "Decision trees using synchronized phasor measurements for wide-area response-based control," *IEEE Trans. Power Syst.*, vol. 26, no. 2, pp. 855 – 861, May 2011.

[32] N. R. Chaudhuri, S. Ray, R. Majumder, B. Chaudhuri, "A new approach to continuous latency compensation with adaptive phasor power oscillation damping controller (POD)," *IEEE Trans. Power Syst.*, vol. 25, no. 2, pp. 939 − 946, May 2010.

[33] M. Zarghami, M. L. Crow, S. Jagannathan, "Nonlinear control of FACTS controllers for damping interarea oscillations in power systems," *IEEE Trans. Power Delivery*, vol. 25, no. 4, pp. 3113 − 3121, Oct. 2010.

[34] S. Corsi, G. N. Taranto, "A real-time voltage instability identification algorithm based on local phasor measurements," *IEEE Trans. Power Syst.*, vol. 23, no. 3, pp. 1271 − 1279, Aug. 2008.

[35] S. Corsi, "Wide area voltage protection," *IET Generation, Transmission & Distribution*, vol. 4, no. 10, pp. 1164 − 1179, 2010.

[36] Y. Wang, I. R. Pordanjani, W. Li, W. Xu, T. Chen, E. Vaahedi, J. Curney, "Voltage stability monitoring based on the concept of coupled single-port circuit," *IEEE Trans. Power Syst.*, vol. 26, no. 4, pp. 2154 − 2163, Nov. 2011.

[37] D. Q. Zhou, U. D. Annakkage, A. D. Rajapakse, "Online monitoring of voltage stability margin using an artificial neural network," *IEEE Trans. Power Syst.*, vol. 25, no. 3, pp. 1566 − 1574, Aug. 2010.

[38] R. Diao, S. Kai, V. Vittal, R. J. O'Keefe, R. Richardson, N. Bhatt, D. Stradford, S. K. Sarawgi, "Decision Tree-Based Online Voltage Security Assessment Using PMU Measurements," *IEEE Trans. Power Syst.*, vol. 24, no. 2, pp. 832 − 839, May 2009.

[39] J. M. Kennedy, B. Fox, T. Littler, D. Flynn, "Validation of fixed speed induction generator models for inertial response using wind farm measurements," *IEEE Trans. Power Syst.*, vol. 26, no. 3, pp. 1454 − 1461, Aug. 2011.

[40] J. F. Hauer, W. A. Mittelstadt, K. E. Martin, J. W. Burns, H. Lee, J. W. Pierre, D. J. Trudnowski, "Use of the WECC WAMS in wide-area probing tests for validation of system performance and modeling," *IEEE Trans. Power Syst.*, vol. 24, no. 1, pp. 250 − 257, Feb. 2009.

[41] J. E. Tate, T. J. Overbye, "Line outage detection using phasor angle measurements," *IEEE Trans. Power Syst.*, vol. 23, no. 4, pp. 1644 – 1652, Nov. 2008.

[42] J. E. Tate, T. J. Overbye, "Double line outage detection using phasor angle measurements," *in Proc. IEEE PES General Meeting*, 2009, pp. 1 − 5.

[43] J. Jiang, J. Yang, Y. Lin, C. Liu, "An adaptive PMU based fault detection/location technique for transmission lines — Part I: Theory and algorithms," *IEEE Trans. Power Delivery*, vol. 15, no. 2, pp. 486 − 493, April 2000.

[44] J. Jiang, J. Yang, Y. Lin, C. Liu, "An adaptive PMU based fault detection/location technique for transmission lines — Part II: PMU implementation and performance evaluation," *IEEE Trans. Power Delivery*, vol. 15, no. 4, pp. 1136 − 1146, Oct. 2000.

[45] C. Yu, C. Liu, S. Yu, J. Jiang, "A new PMU-based fault location algorithm for series compensated lines," *IEEE Trans. Power Delivery*, vol. 17, no. 1, pp. 33 − 46, Jan. 2002.

[46] Y. Lin, C. Liu, C. Chen, "A new PMU-based fault detection/location technique for transmission lines with consideration of arcing fault discrimination— Part I: theory and algorithms," *IEEE Trans. Power Delivery*, vol. 19, no. 4, pp. 1587 − 1593, Oct. 2004.

[47] Y. Lin, C. Liu, C. Chen, "A new PMU-based fault detection/location technique for transmission lines with consideration of arcing fault discrimination— Part II: performance evaluation," *IEEE Trans. Power Delivery*, vol. 19, no. 4, pp. 1594 − 1601, Oct. 2004.

[48] J. Bertsch, C. Carnal, D. Karlsson, J. Mcdaniel, K. Vu, "Wide-area Protection and power system utilization," *Proceedings of the IEEE*, vol. 93, no. 5, pp. 997 − 1003, 2005.

[49] P. V. Navalkar, S. A. Soman, "Secure remote backup protection of transmission lines using synchrophasors," *IEEE Trans. Power Delivery*, vol. 26, no. 1, pp. 87 − 96, Jan. 2011.

[50] J. Ma, J. Li, J. S. Thorp, A. J. Arana, Q. Yang, A. G. Phadke, "A fault steady state component-based wide area backup protection algorithm," *IEEE Trans. Smart Grid*, vol. 2, no. 3, pp. 468 – 475, Sep. 2011.

[51] C. Chen, C. Liu, J. Jiang, "A new adaptive PMU based protection scheme for transposed/untransposed parallel transmission line," *IEEE Trans. Power Delivery*, vol. 17, no. 2, pp. 395 − 404, April 2002.

[52] R. E. Kalman, "A new approach to linear fitering and prediction problems," *Journal of Basic Engineering*, vol. 82, no. 1, pp. 35 – 45, 1960.

[53] P. Stoica, R. Moses, Introduction to spectral analysis, Prentice Hall, 1997.

[54] Institute for Statistics and Mathematics, "The comprehensive R archive network," University of Vienna ("WU"), Vienna, Austria, available at: http://cran.r-project.org/

[55] R. G. Brown, P. Y. C. Hwang, *Introduction to Random Signals and Applied Kalman Filtering: with MATLAB Exercises and Solutions*, John Wiley & Sons, 1997.

[56] T. Overbye, P. Sauer, C. DeMArco, B. Lesieutre, M. Venkatasubramanian, *Using PMU Data to Increase Situational Awareness*, available at: www.pserc.wisc.edu/documents/publications/reports/2010_reports/Overbye_PSERC_S-36_Final_Report_2010.pdf

[57] P. M. Anderson, A. A. Fouad, *Power System Control and Stability*, Wiley – IEEE Press, 2003.

[58] Online resources: http://www.ee.washington.edu/research/psta/, University of Washington.

[59] *IEEE Standard Requirements for Instrument Transformers*, IEEE Standard C57.13-2008, Piscataway NJ, 2008.

[60] I. Dabbaghchi, L. S. VanSlyck, "Inter-utility data exchange for state estimation," *IEEE Trans. Power Syst.*, vol. 3, no. 3, pp. 1254 – 1262, Aug. 1988.

[61] Q. Zhang, V. Vittal, G. Heydt, N. Logic, S. Sturgill, "The integrated calibration of synchronized phasor measurement data in power transmission systems," *IEEE Trans. Power Delivery*, vol. 26, no. 4, pp. 2573 – 2581, Oct. 2011.

[62] L. Zhang, A. Abur, "State estimator tuning for PMU measurements," *in Proc. North American Power Symposium*, Boston, MA, 2011, pp. 1 − 4.

[63] K. S. Shanmugan, A. M. Breipohl, *Random signals: detection, estimation and data analysis*, New York: Wiley, 1988.

[64] DSATools, available at: http://www.dsatools.com/

[65] S. M. Kay, *Fundamentals of statistical signal processing, volume I: estimation theory*, Prentice Hall, 1993.

APPENDIX A

DISCRIPTION OF DATA SOURCE

Most of the study in this dissertation is based on real PMU measurements. In the tables below, the descriptions of PMU names, and file IDs are provided for convenient citations in the dissertation. There are 25 buses involved which are named as ‘S1’, ‘S2’, ⋯, and ‘S25’ subsequently. The PMUs are named corresponding to the bus names at the two ends of a transmission line on which the PMU is installed.

Table A.1 IDs and names of PMUs in a practical system

PMU ID	PMU Name
1	S1-S24
2	S2-S12
3	S3-S16
4	S4-S18
5	S6-S10
6	S6-S21
7	S7-S22
8	S9-S10
9	S10-S6
10	S10-S9
11	S13-S3
12	S13-S16
13	S14-S11

There are 4 sets of data files. In Table A.2, the number of files in each set is listed in the second column, and the time duration of each file in each set is listed in the third column. The file ID is formed by the following rule: ‘file #set number – file number’. For example, file #1-4 denotes the 4^{th} file in data set 1.

Table A.2 Summary of data files

File set	Number of files	Time duration
#1	4	3 minutes
#2	5	3 minutes
#3	2	5 minutes
#4	480	3 minutes

APPENDIX B

SAMPLE OF MATLAB CODES

In this section, a sample of Matlab cods is provided. The codes selected are for the research purpose of calibrating synchronized phasor measurement data in power transmission systems which is illustrated in Chapter 6. It should be noted that the complete program is not shown, and only some functions are selected as examples. In addition, the functions are not shown in detail due to page limitations.

The following is the main function of the program.

```
clc;clear;
close all;
%*****************************************************************
%May 17, 2010, assessment of the accuracy PMU data               *
%Qing Zhang                                                      *
%*****************************************************************
%count the calculation time in seconds
T_start = clock;
%*****************************************************************
%&&&&&&&&&&&&&&&&&&&&&&&&&&&&&&&&&&&&&&&&&&&&&&&&&&&&&&&&&&&&&&&&
LineID=4;
Case_flag =1;%1 one TL; 2 two TL
n_PMU = 16;
n_Data= 5400;%the number of measurements
%20091011-193900000-PosSeq-SRP.csv
%20091101-033600000-PosSeq-SRP.csv
%20091103-184500000-PosSeq-SRP.csv
%20091105-022100000-PosSeq-SRP.csv
filename = '20091101-033600000-PosSeq-SRP.csv';
Date = '(20091101-0336)';
%&&&&&&&&&&&&&&&&&&&&&&&&&&&&&&&&&&&&&&&&&&&&&&&&&&&&&&&&&&&&&&&&
%read topology data from file
Topology_file = 'Set1_PMU.xls';
PMUname = cell(n_PMU,1);
Voltage_level = zeros(n_PMU,1);
[Voltage_level,PMUname] = xlsread(Topology_file,1,'B2:C17');
TL_summary = xlsread(Topology_file,1,'E2:H6');
TwoPMU = xlsread(Topology_file,1,'J2:L6');
TwoLineFourPMU = xlsread(Topology_file,'N2:R2');
Line_parameter = xlsread(Topology_file,2,'E2:I6');

%*****************************************************************
%System base information
Sbase = 100000000; %MVA
Sbaseplot = 1000000;
%Constants in calculation
D2R = pi/180;
R2D = 180/pi;
```

```
tstep = .0333333;
T =1/30*n_Data;
%****************************************************************
%read measurement from datafile
t = 0:tstep:T-tstep;
n_row = 1;
n_col = 1;
M = csvread(filename, n_row, n_col);
[M_row,M_col] = size(M);
Voltage =[];
VAngle = [];
for i = 1:M_col
    if rem(i+1,4)==0
        Voltage =[Voltage M(:,i)];
    end
    if rem(i,4)==0
        VAngle =[VAngle  M(:,i)];
    end
end
save voltage Voltage
save vangle VAngle

[t_row,t_col] = size(t);
if(M_row ~= t_col)
    disp('Checking the file');
end
switch Case_flag
    case 1
Frombus = TL_summary (LineID,2);
Tobus =TL_summary(LineID,3);
LineType = TL_summary(LineID,4);


Vbase = Line_parameter(LineID,5)*1000;%kv
Zbase = Vbase^2/Sbase;
Vbase_str = num2str(Vbase);
PMU_str = char(PMUname(Frombus));
TL_name = [Vbase_str, ' kV ', PMU_str];
TL_name = [TL_name, ' ', Date];
output_file = ['Summary_',PMU_str,Date,'.dat'];

%****************************************************************
R = Line_parameter(LineID,1)*Zbase;
X = Line_parameter(LineID,2)*Zbase;
if(Frombus<Tobus)
B1 = Line_parameter(LineID,3)/Zbase;
B2 = Line_parameter(LineID,4)/Zbase;
end
if(Frombus>Tobus)
B2 = Line_parameter(LineID,3)/Zbase;
B1 = Line_parameter(LineID,4)/Zbase;
end
Line_ZB = [R X B1 B2];
Base =[Vbase Sbase];
%****************************************************************
```

```
switch LineType
    case 1
        temp = [M(:,(Frombus-1)*4+1:1:Frombus*4) M(:,(Tobus-
1)*4+1:1:Tobus*4)];
        anglediff=temp(:,4)-temp(:,8);
TL_TypeOne(t,temp,Frombus,Tobus,Line_ZB,output_file,filename,PMU_
str,TL_name,n_Data,Base);
    case 2
        temp = [M(:,(Frombus-1)*4+1:1:Frombus*4) M(:,(Tobus-
1)*4+3:1:Tobus*4)];

TL_TypeTwo(t,temp,Frombus,Tobus,Line_ZB,output_file,filename,PMU_
str,TL_name,n_Data,Base);
end
    case 2
%%%%%%%%%%%%%%%%%%%%%%%%%%%%%%%%%%%%%%%%%%%%%%%%
%! Tobus should be the bus with two PMUs
Frombus1 = TwoLineFourPMU (LineID,2);
Tobus1 =TwoLineFourPMU(LineID,3);
Frombus2 = TwoLineFourPMU (LineID,4);
Tobus2 =TwoLineFourPMU(LineID,5);

%finding LineID in  TL summary
[m,n]=size(TL_summary);
for i=1:m
    if(Frombus1>Tobus1)
    if(TL_summary(i,2)==Tobus1&&TL_summary(i,3)==Frombus1)
        LineID1 = TL_summary(i,1);
    end
    else
    if(TL_summary(i,3)==Tobus1&&TL_summary(i,2)==Frombus1)
        LineID1 = TL_summary(i,1);
    end
    end
end
for i=1:m
    if(Frombus2>Tobus2)
    if(TL_summary(i,2)==Tobus2&&TL_summary(i,3)==Frombus2)
        LineID2 = TL_summary(i,1);
    end
    else
    if(TL_summary(i,3)==Tobus2&&TL_summary(i,2)==Frombus2)
        LineID2 = TL_summary(i,1);
    end
    end
end

Vbase = Line_parameter(LineID1,5)*1000;%kv
Zbase = Vbase^2/Sbase;
Vbase_str = num2str(Vbase);

PMU_str1 = char(PMUname(Frombus1));
TL_name1 = [Vbase_str, ' kV ', PMU_str1];
TL_name1 = [TL_name1, ' ', Date];
output_file1 = ['Summary_',PMU_str1,Date,'2.dat'];
```

```
PMU_str2 = char(PMUname(Frombus2));
TL_name2 = [Vbase_str, ' kV ', PMU_str2];
TL_name2 = [TL_name2, ' ', Date];
output_file2 = ['Summary_',PMU_str2,Date,'2.dat'];

%*****************************************************************
R1 = Line_parameter(LineID1,1)*Zbase;
X1 = Line_parameter(LineID1,2)*Zbase;
if(Frombus1<Tobus1)
B11 = Line_parameter(LineID1,3)/Zbase;
B12 = Line_parameter(LineID1,4)/Zbase;
end
if(Frombus1>Tobus1)
B12 = Line_parameter(LineID1,3)/Zbase;
B11 = Line_parameter(LineID1,4)/Zbase;
end
Line_ZB1 = [R1 X1 B11 B12];
%*****************************************************************
R2 = Line_parameter(LineID2,1)*Zbase;
X2 = Line_parameter(LineID2,2)*Zbase;
if(Frombus2<Tobus2)
B21 = Line_parameter(LineID2,3)/Zbase;
B22 = Line_parameter(LineID2,4)/Zbase;
end
if(Frombus2>Tobus2)
B22 = Line_parameter(LineID2,3)/Zbase;
B21 = Line_parameter(LineID2,4)/Zbase;
end
Line_ZB2 = [R2 X2 B21 B22];
%*****************************************************************
temp1 = [M(:,(Frombus1-1)*4+1:1:Frombus1*4) M(:,(Tobus1-
1)*4+1:1:Tobus1*4)];
temp2 = [M(:,(Frombus2-1)*4+1:1:Frombus2*4) M(:,(Tobus2-
1)*4+1:1:Tobus2*4)];
temp=[temp1 temp2];
Frombus=[Frombus1; Frombus2];
Tobus=[Tobus1; Tobus2];
Line_ZB = [Line_ZB1;Line_ZB2];
Base =[Vbase Sbase];
output_file = cell(2,1);
output_file(1)=cellstr(output_file1);
output_file(2)=cellstr(output_file2);
PMU_str = cell(2,1);
PMU_str(1) = cellstr(PMU_str1);
PMU_str(2) = cellstr(PMU_str2);
TL_name = cell(2,1);
TL_name(1) = cellstr(TL_name1);
TL_name(2) = cellstr(TL_name2);
TL_TypeThree(t,temp,Frombus,Tobus,Line_ZB,output_file,filename,PM
U_str,TL_name,n_Data,Base);
end
%count the calculation time in seconds
Simulation_time = etime(clock,T_start)
```

The purpose of the function 'TL_TypeOne' is dealing with 'Case 1' which is illustrated in Chapter 6.

```
function
TL_TypeOne(t,M,Frombus,Tobus,Line_ZB,output_file,filename,PMU_str
,TL_name,n_meas,Base)
%*************************************************************
D2R = pi/180;
R2D = 180/pi;
Sbaseplot = 1000000;
R = Line_ZB(1);
X = Line_ZB(2);
B1 = Line_ZB(3);
B2 = Line_ZB(4);
% seperate magnitude and angle of current and voltage
I1_m = M(:,1);
I1_a = M(:,2);
V1_m = M(:,3);
V1_a = M(:,4);
I2_m = M(:,5);
I2_a = M(:,6);
V2_m = M(:,7);
V2_a = M(:,8);
I1 = I1_m.*exp(1i*I1_a*D2R);
I2 = I2_m.*exp(1i*I2_a*D2R);
V1 = V1_m.*exp(1i*V1_a*D2R);
V2 = V2_m.*exp(1i*V2_a*D2R);
%filter bad measurements
M_filtered = FilterBadMeasurement(M);
I1_filtered = M_filtered(:,1).*exp(1i*M_filtered(:,2)*D2R);
I2_filtered = M_filtered(:,5).*exp(1i*M_filtered(:,6)*D2R);
V1_filtered = M_filtered(:,3).*exp(1i*M_filtered(:,4)*D2R);
V2_filtered = M_filtered(:,7).*exp(1i*M_filtered(:,8)*D2R);
%*************************************************************
**********
temp = AngleNorm(V1_a-I1_a);
phi1=mean(temp);
temp = AngleNorm(V2_a-I2_a);
phi2=mean(temp);
S1=mean(V1_m.*I1_m);
S2=mean(V2_m.*I2_m);
PF=[phi1 phi2 S1 S2];
%*************************************************************
%calculate TL impedance from voltage and current
[Impedance_calculated]
=CalImepedance(I1_filtered,I2_filtered,V1_filtered,V2_filtered);
disp('Impedance checking completed!');
%*************************************************************
%calculate current from voltage and TL impedance
[Cur-
rent_cal,Current_diff]=CalCurrent(Line_ZB,I1_filtered,I2_filtered
,V1_filtered,V2_filtered);
Current_diff_ave = mean(Current_diff);
disp('Current checking completed!');
```

```
%*************************************************************
%calculate correction factor
%voltage, current, PQ, Pmismatch, cf magnitude.
[Meas_After,CF,Vin]=NR_New(Line_ZB,I1_filtered,I2_filtered,V1_fil
tered,V2_filtered,Base,n_meas);
disp('Correction factor calculation completed!');

%*************************************************************
%comparison before and after
%Calculate P Q using measurements
[err_bf,err_info_bf,Power_bf,Power_info_bf]=PowerMismatch(Line_ZB
,V1_filtered,V2_filtered,I1_filtered,I2_filtered);
I1_af = Meas_After(:,1).*exp(1i*Meas_After(:,2)*D2R);
I2_af = Meas_After(:,5).*exp(1i*Meas_After(:,6)*D2R);
V1_af = Meas_After(:,3).*exp(1i*Meas_After(:,4)*D2R);
V2_af = Meas_After(:,7).*exp(1i*Meas_After(:,8)*D2R);

[err_af,err_info_af,Power_af,Power_info_af]=PowerMismatchAfter(Li
ne_ZB,V1_af,V2_af,I1_af,I2_af,Vin);
save CFmat CF Meas_After M_filtered Line_ZB
CF_V = mean(CF(:,5:8));
CF_V_std = std(CF(:,5:8));
CF_I = mean(CF(:,1:4));
CF_I_std = std(CF(:,1:4));
vcf_diff=CF(:,6)-CF(:,8);
icf_diff=CF(:,2)-CF(:,4);
Va_diff_bf = AngleNorm(M_filtered(:,4)-M_filtered(:,8));
Va_diff_af = AngleNorm(Meas_After(:,4)-Meas_After(:,8));
A_diff_sum =[mean(Va_diff_bf) std(Va_diff_bf);
    mean(Va_diff_af) std(Va_diff_af);
    mean(vcf_diff) std(vcf_diff);
    mean(icf_diff) std(icf_diff);];
%*************************************************************
%output to file
% output correction factor to data file
CF_M=[Frombus CF_I(1,1) CF_I(1,2) CF_V(1,1) CF_V(1,2);
    Frombus CF_I_std(1,1) CF_I_std(1,2) CF_V_std(1,1)
CF_V_std(1,2);
    Tobus CF_I(1,3) CF_I(1,4) CF_V(1,3) CF_V(1,4);
    Tobus CF_I_std(1,3) CF_I_std(1,4) CF_V_std(1,3)
CF_V_std(1,4);];
CF_file = [TL_name,'.csv'];
csvwrite(CF_file,CF_M);
Adiff_file = [TL_name,'Adiff.csv'];
csvwrite(Adiff_file,A_diff_sum);
```

.....

The purpose of the function ‘NR_New’ is to calculate the correction factors.

```
function
[Meas_After,CF_M,Vin_M]=NR_New(Line_ZB,I1,I2,V1,V2,Base,n_meas)
Meas_After =[];
CF_M=[];
Vin_M=[];
D2R = pi/180;
R2D = 180/pi;
%n_Var ==10 consider Vinduce
%n_Var ==8 not consider Vinduce
n_Var =8;
%for NR method
n_M = n_meas;
n_meas =1;

%just consider Ti1=Ti2=1
dimension =[1:16 19 20];

%%%%%%%%%%%%%%%%%%%%%%%%%%%%%%%%%%%%%%%%
%p.u. all measurements
Meas = [I1 I2 V1 V2];
V_Base = Base(1); %kV
S_Base = Base(2); %MVA
Z_Base = V_Base^2/S_Base;
Line_ZB(1,1)=Line_ZB(1,1)/Z_Base;
Line_ZB(1,2)=Line_ZB(1,2)/Z_Base;
Line_ZB(1,3)=Line_ZB(1,3)*Z_Base;
Line_ZB(1,4)=Line_ZB(1,4)*Z_Base;

I_Base =S_Base/V_Base;
I1_M = I1/I_Base;
I2_M = I2/I_Base;
V1_M = V1/V_Base;
V2_M = V2/V_Base;
Meas_M(:,1:2)=Meas(:,1:2)/I_Base;
Meas_M(:,3:4)=Meas(:,3:4)/V_Base;
%%%%%%%%%%%%%%%%%%%%%%%%%%%%%%%%%%%%%%%%

for n=1:n_M
    if(rem(n,100)==0)
        n
    end
step=1;
delta = Inf;
endsgn = 0.001;
n_loop =0;
%%%%%%%%%%%%%%%%%%%%%%%%%%%%%%%%%%%%%%%%
I1=I1_M(n,1);I2=I2_M(n,1);
V1=V1_M(n,1);V2=V2_M(n,1);
Meas = Meas_M(n,:);
%the start point of correction factor
```

```
CF_zero = [1 0*D2R 1  0*D2R 1 0*D2R 1 0*D2R]';

X_zero = zeros(n_Var*n_meas,1);
for i =1:n_meas
    X_zero(n_Var*(i-1)+1)=abs(I1(i,1));
    X_zero(n_Var*(i-1)+2)=angle(I1(i,1));
    X_zero(n_Var*(i-1)+3)=abs(I2(i,1));
    X_zero(n_Var*(i-1)+4)=angle(I2(i,1));
    X_zero(n_Var*(i-1)+5)=abs(V1(i,1));
    X_zero(n_Var*(i-1)+6)=angle(V1(i,1));
    X_zero(n_Var*(i-1)+7)=abs(V2(i,1));
    X_zero(n_Var*(i-1)+8)=angle(V2(i,1));
    if(n_Var==10)
        X_zero(n_Var*(i-1)+9)=0;
        X_zero(n_Var*(i-1)+10)=0;
    end
end
X_zero =[X_zero;CF_zero];
X = X_zero;

%%%%%%%%%%%%%%%%%%%%%%%%%%%%%%%%%%%%%%%%%%%%%%%%%%%%%%%%%%%%%%%%%%%%%%%
%NR method
while (delta>endsgn&&n_loop<100)
    Fx = NRvalue_rate_New(Meas,X,Line_ZB,n_Var,n_meas);
    J=NRformJacobian_New(X,Line_ZB,n_Var,n_meas);
    J_used =J(dimension,:);
    Fx_used = Fx(dimension,:);
    temp = pinv(J_used);
    deltaX = pinv(J_used)*Fx_used ;
    deltaCF = deltaX(n_Var*n_meas+1:n_Var*n_meas+8,1);
    delta = max(abs(deltaX));
    temp = cond(J_used);
    X = X-step*pinv(J_used)*Fx_used;
    n_loop = n_loop+1;
end


CF_inv = X(n_Var*n_meas+1:n_Var*n_meas+8,1);

for i=1:4
    CF_inv(2*i,1)=CF_inv(2*i,1)*R2D;
end
for i=1:4
    CF(2*(i-1)+1,1)=1/CF_inv(2*(i-1)+1,1);
    CF(2*i,1)=rem(-CF_inv(2*i,1),360);
end

CF_M=[CF_M;CF'];
      ……
```

The purpose of the function 'NRformJacobian_New' is to form the jacobian matrix which is used in the process of correction factor calculation.

```
function [J]=NRformJacobian_New(X,Line_ZB,n_Var,n_meas)
%There are 9 equations for each set of measurements
n_J = 18;
%Transmission line constants
R = Line_ZB(1);
Xx = Line_ZB(2);
B1 = Line_ZB(3);
B2 = Line_ZB(4);
Z = R+1i*Xx;
a = -(1i*B1+1/Z);a_m = abs(a);a_a = angle(a);
b = 1/Z;b_m = abs(b);b_a = angle(b);
c = -1/Z;c_m = abs(c);c_a = angle(c);

d = b; d_m = abs(d);d_a = angle(d);
e = -(1i*B2+1/Z);e_m = abs(e);e_a = angle(e);
f = d;f_m = abs(f);f_a = angle(f);

g = 1i*B1-1/conj(Z); g_m = abs(g); g_a = angle(g);
h =1/conj(Z); h_m = abs(h); h_a = angle(h);
j = -h; j_m = abs(j);j_a =angle(j);

k = 1i*B2-1/conj(Z); k_m = abs(k); k_a = angle(k);
l =1/conj(Z); l_m = abs(l); l_a = angle(l);
m = h; m_m = abs(m);m_a =angle(m);

Ti1_m = X(n_Var*n_meas+1,1);
Ti1_a = X(n_Var*n_meas+2,1);
Ti2_m = X(n_Var*n_meas+3,1);
Ti2_a = X(n_Var*n_meas+4,1);
Tv1_m = X(n_Var*n_meas+5,1);
Tv1_a = X(n_Var*n_meas+6,1);
Tv2_m = X(n_Var*n_meas+7,1);
Tv2_a = X(n_Var*n_meas+8,1);
for i = 1:n_meas
    I1_m=X(n_Var*(i-1)+1);
    I1_a=X(n_Var*(i-1)+2);
    I2_m=X(n_Var*(i-1)+3);
    I2_a=X(n_Var*(i-1)+4);
    V1_m=X(n_Var*(i-1)+5);
    V1_a=X(n_Var*(i-1)+6);
    V2_m=X(n_Var*(i-1)+7);
    V2_a=X(n_Var*(i-1)+8);
    if (n_Var==10)
        Vin_m=X(10*(i-1)+9);
        Vin_a=X(10*(i-1)+10);
    else
        Vin_m=0;
        Vin_a=0;
    end
%%%%%%%%%%%%%%%%%%%%%%%%%%%%%%%%%%%%%%%%%%%%%%%%%%%%%%%%%%%%%%%%%%%%%%%%%%%%
```

```
T_m = Ti1_m; T_a = Ti1_a; M_m = I1_m;M_a = I1_a;
theta = T_a+M_a;
%delt I1_m delt I1_a
J(n_J*i-n_J+1,n_Var*(i-1)+1) = T_m*cos(theta);
J(n_J*i-n_J+1,n_Var*(i-1)+2) = -T_m*M_m*sin(theta);
J(n_J*i-n_J+2,n_Var*(i-1)+1) = T_m*sin(theta);
J(n_J*i-n_J+2,n_Var*(i-1)+2) = T_m*M_m*cos(theta);
%delt Ti1_m delt Ti1_a
J(n_J*i-n_J+1,n_Var*n_meas+1) = M_m*cos(theta);
J(n_J*i-n_J+1,n_Var*n_meas+2) = -T_m*M_m*sin(theta);
J(n_J*i-n_J+2,n_Var*n_meas+1) = M_m*sin(theta);
J(n_J*i-n_J+2,n_Var*n_meas+2) = T_m*M_m*cos(theta);

T_m = Ti2_m; T_a = Ti2_a; M_m = I2_m;M_a = I2_a;
theta = T_a+M_a;
%delt I2_m delt I2_a
J(n_J*i-n_J+3,n_Var*(i-1)+3) = T_m*cos(theta);
J(n_J*i-n_J+3,n_Var*(i-1)+4) = -T_m*M_m*sin(theta);
J(n_J*i-n_J+4,n_Var*(i-1)+3) = T_m*sin(theta);
J(n_J*i-n_J+4,n_Var*(i-1)+4) = T_m*M_m*cos(theta);
%delt Ti2_m delt Ti2_a
J(n_J*i-n_J+3,n_Var*n_meas+3) = M_m*cos(theta);
J(n_J*i-n_J+3,n_Var*n_meas+4) = -T_m*M_m*sin(theta);
J(n_J*i-n_J+4,n_Var*n_meas+3) = M_m*sin(theta);
J(n_J*i-n_J+4,n_Var*n_meas+4) = T_m*M_m*cos(theta);

T_m = Tv1_m; T_a = Tv1_a; M_m = V1_m; M_a = V1_a;
theta = T_a+M_a;
%delt V1_m delt V1_a
J(n_J*i-n_J+5,n_Var*(i-1)+5) = T_m*cos(theta);
J(n_J*i-n_J+5,n_Var*(i-1)+6) = -T_m*M_m*sin(theta);
J(n_J*i-n_J+6,n_Var*(i-1)+5) = T_m*sin(theta);
J(n_J*i-n_J+6,n_Var*(i-1)+6) = T_m*M_m*cos(theta);
%delt Tv1_m delt Tv1_a
J(n_J*i-n_J+5,n_Var*n_meas+5) = M_m*cos(theta);
J(n_J*i-n_J+5,n_Var*n_meas+6) = -T_m*M_m*sin(theta);
J(n_J*i-n_J+6,n_Var*n_meas+5) = M_m*sin(theta);
J(n_J*i-n_J+6,n_Var*n_meas+6) = T_m*M_m*cos(theta);
T_m = Tv2_m; T_a = Tv2_a; M_m = V2_m; M_a = V2_a;
theta = T_a+M_a;
%delt V2_m delt V2_a
J(n_J*i-n_J+7,n_Var*(i-1)+7) = T_m*cos(theta);
J(n_J*i-n_J+7,n_Var*(i-1)+8) = -T_m*M_m*sin(theta);
J(n_J*i-n_J+8,n_Var*(i-1)+7) = T_m*sin(theta);
J(n_J*i-n_J+8,n_Var*(i-1)+8) = T_m*M_m*cos(theta);
%delt Tv2_m delt Tv2_a
J(n_J*i-n_J+7,n_Var*n_meas+7) = M_m*cos(theta);
J(n_J*i-n_J+7,n_Var*n_meas+8) = -T_m*M_m*sin(theta);
J(n_J*i-n_J+8,n_Var*n_meas+7) = M_m*sin(theta);
J(n_J*i-n_J+8,n_Var*n_meas+8) = T_m*M_m*cos(theta);
```

……